CIRCADIAN AND CIRCATIDAL RHYTHMS OF PROTEIN ABUNDANCE IN THE INTERTIDAL MUSSEL *MYTILUS CALIFORNIANUS*

A Thesis
presented to
the Faculty of California Polytechnic State University,
San Luis Obispo

In Partial Fulfillment
of the Requirements for the Degree
Master of Science in Biological Sciences

by
Cory Robinson Elowe
December 2016

COMMITTEE MEMBERSHIP

TITLE:	Circadian and Circatidal Rhythms of Protein Abundance in the Intertidal Mussel *Mytilus californianus*
AUTHOR:	Cory Robinson Elowe
DATE SUBMITTED:	December 2016
COMMITTEE CHAIR:	Lars Tomanek, Ph.D. Associate Professor of Biology
COMMITTEE MEMBER:	Nikki Adams, Ph.D. Professor of Biology
COMMITTEE MEMBER:	Ulric Lund, Ph.D. Professor of Statistics

ABSTRACT

Circadian and Circatidal Rhythms of Protein Abundance in the Intertidal Mussel *Mytilus californianus*

Cory Robinson Elowe

The intertidal zone is a dynamic environment that fluctuates with the 12.4-h tidal and 24-h light/dark cycle to predictably alter food availability, temperature, air exposure, wave action, oxygen partial pressure, and osmotic conditions. Intertidal sessile bivalves exhibit behavioral or physiological changes to minimize the persistent challenges of fluctuating environmental conditions, such as adjusting gaping behavior and heart rate. At the cellular level, transcriptomic studies on mussels' baseline circadian and circatidal rhythms have determined that the circadian rhythm is the dominant transcriptional rhythm. However, as proteins reflect the basic molecular phenotype of an organism and their abundance may differ greatly from that of mRNA, these methods could fail to detect important cyclical changes in the proteome that cope with the regular stress of tidal rhythms. For this study, we acclimated intertidal *Mytilus californianus* to circadian (12:12 h light/dark cycle) and circatidal (6:6 h tidal cycle) conditions in a tidal simulator and sampled gill tissue from mussels every 2 h for 48 h for proteomic analysis. Approximately 86% of the proteins that were detected exhibited rhythmicity over the time course. The circadian cycle primarily determined the cyclic abundance of energy metabolism proteins, pivoting around the transition to the nighttime high tide. The tidal cycle contributed to alterations in cytoskeletal components, ER protein processing and vesicular trafficking, extracellular matrix and immune proteins, and oxidative stress and chaperoning proteins. We also found evidence that post-translational modifications may

be important for driving these rhythms, as acetylation and phosphorylation motifs were enriched in the rhythmic proteins and we identified rhythms in elements of methylation, mitochondrial peptide processing, and acylation. These dynamic changes in proteins across numerous functional categories indicate that the combination of circadian and tidal cycles drive complex cellular changes to coordinate processes in a changing environment. This variation clearly shows that differential expression studies and biomonitoring efforts cannot assume a static baseline of cellular conditions in intertidal mussels.

Keywords: Proteomics, circadian, circatidal, *Mytilus californianus*

ACKNOWLEDGMENTS

Donations from the following companies contributed to the construction of the tidal simulator for this experiment: Drain Master, Irrigation Direct, Coastal Aquariums, Glass-Holes, Tinned Marine Wire, Current USA, and Fibox Enclosures. Other donated materials came from FiltersFast.com, Fisher Bag Company, and Reed Mariculture. This work was funded by the CSU COAST Graduate Research Award, Sigma Xi Grants-in-Aid of Research, and the Myers Ocean Trust, as well as the NSF-IOS 1145840 to Lars Tomanek and Cal Poly College Based Fees.

For support throughout this experience I would like thank my committee members, Nikki Adams and Ulric Lund, along with all the members of the Environmental Proteomics Lab (EPL) at Cal Poly. I would especially like to thank my advisor Lars Tomanek for guiding me with enthusiasm and shared philosophical ambitions, and Christina Vasquez for her wit and wisdom during this undertaking, which kept me afloat when my best laid plans would go awry. My work would also have been incomplete without the tutelage and camaraderie of the following lab members/friends: Marcus Zuzow, Joshua Mier, Aubrie Fowler, Jackie Campbell, Talia Head, Melissa Voisinet, Daniela Martinez, Maritza Luquin, Mark Hamer, and Lauren Linsmayer. I would also like to thank the Summer 2015 STAR fellows Kristina Koster and Andrea Reider for their help in the enormous sample-processing effort.

Numerous individuals outside of the EPL were also vital to the execution of this study. Rob and Doug Brewster, as well as Ted Johansen, were instrumental in the planning, assembly, and programming of the tidal simulator. Tom Moylan and Jason

Felton at the Cal Poly Pier were extremely helpful for planning, monitoring, and maintaining this experiment. The support staff in the Cal Poly Biology Department were essential to my success, especially Ellen Calcagno, Melanie Gutierrez, and Alice Hamrick.

Last but not least, I would like to thank my wife, Emily Tong, for her unconditional support (both emotional and financial) during my time at Cal Poly. Thank you for showing interest in my work, even when it seemed like cryptic nonsense; for encouraging my mental health through countless Californian adventures; and for your divine patience in allowing me to pursue this immense undertaking.

TABLE OF CONTENTS

LIST OF FIGURES

Page

CHAPTER I. INTRODUCTION

Overview

Coastal marine ecosystems are undergoing vast changes due to anthropogenic effects, forcing organisms to shift biogeographic ranges or adapt (Harley et al., 2006). Rapid environmental changes test the physiological tolerance of organisms, and a current focal point of climate change research is to identify the plasticity and adaptability of organisms' physiological responses to these changes (Harley, 2008; Lesser, 2016; Todgham and Stillman, 2013; Tomanek, 2008; Tomanek, 2012). Studies of physiological responses to environmental changes typically attempt to isolate one or two causative factors, comparing a control group at stable conditions while the factors of interest are adjusted for experimental groups (Dowd and Somero, 2013; Fitzgerald-Dehoog et al., 2012; Halpin et al., 2004; Tomanek et al., 2012). The responses are then attributed to the altered factors and extrapolated to natural conditions to predict an organism's response to future environmental changes.

In many cases, the controlled conditions of an experiment may not accurately translate to natural conditions. Dynamic environments regularly influence organisms' physiology and behavior. Any inference about the natural effects of environmental changes on these organisms can potentially be skewed due to a study's assumption of a static, oversimplified baseline (Tessmar-Raible et al., 2011). This problem is particularly apparent in biomonitoring programs that consider specific markers of environmental stress in sentinel organisms. Understanding how natural environmental variability affects specific diagnostic markers for pollutants in these programs is essential for generating a baseline for marker fluctuations to avoid false-positive detection of pollution stress

(Garcia-March et al., 2016; Hagger et al., 2006; Livingston, 1976; Luedeking and Koehler, 2004).

The intertidal zone is a particularly dynamic environment that regularly influences the physiology of its inhabitants. The 12.4-hour tidal cycle and the 24-hour light/dark cycle predictably alter food availability, temperature, aerial emersion, pressure changes, water current, dissolved oxygen, and salinity (Tessmar-Raible et al., 2011). The limited mobility of sessile intertidal mussels (*Mytilus* spp.) in the intertidal zone requires that they cope with the environmental fluctuations to which they are exposed through behavioral (Bayne et al., 1976) and physiological changes (Connor and Gracey, 2012; Place et al., 2012; Shick et al., 1986; Tagliarolo et al., 2012). These changes may be internally synchronized between the organism and the environment to minimize the predictable dangers of high temperatures, hypoxia and oxidative stress, and desiccation as tides change and the sun illuminates the intertidal zone.

The transcriptomic and metabolomic methods used to study the circadian and circatidal rhythms in these intertidal mussels have provided invaluable information about cellular-level changes in a dynamic environment (Connor and Gracey, 2011; Connor and Gracey, 2012; Gracey et al., 2008). However, mRNA expression may fail to predict up to half of the variation in the proteome—the complete pool of proteins in a tissue (Feder and Walser, 2005). Likewise, a recent study on circadian rhythms in the mouse liver have shown that 20% of cycling proteins showed no corresponding rhythm to the transcript, and half of those proteins with a matching rhythmic transcripts showed a delayed cycle of over six hours (Robles et al., 2014). Given that proteins reflect the basic functional level of the molecular phenotype, there is a great need to characterize the proteomic changes

that parallel the transcriptome in an organism that is regularly exposed to both circadian and circatidal cycles.

This study addresses the rhythmic changes in the abundance of proteins in the intertidal California mussel (*Mytilus californianus*) during a simulation of predictable circadian and circatidal rhythms. Characterizing the proteome of this species through circadian and circatidal cycles is an important step for establishing a realistic baseline that considers natural variations in molecular expression patterns that extrapolate from laboratory studies to field conditions (Connor and Gracey, 2011; Tomanek, 2011). Furthermore, experimental design for stress response studies will benefit from evaluating the importance of environmental cues in generating biological rhythms. I will begin with a summary of research constituting three important aspects of this study design: (1) *Mytilus californianus* as a study species, (2) the characterization and analyses of biological rhythms, and (3) the proteomic study approach.

Mytilus californianus **as a study organism**

Natural history of Mytilus *spp.*

Intertidal mussels are a vital feature of the intertidal community around the world (Suchanek, 1981; Ricciardi and Bourget, 1999; Gaitán-Espitia et al., 2016). Within the *Mytilus* genus, seven species are distributed throughout coastal ecosystems from warm- to cold- temperate waters and these species play an important role in shaping the surrounding communities (Gutiérrez et al., 2003; Borthagaray and Carranza, 2007). The dense beds of *Mytilus* in the intertidal provide microhabitats for numerous fauna, substrate for epibionts, refuge from predation and physiological stress, and altered fluid

dynamics controlling solutes and suspended algae (Dolmer, 2000; Gutiérrez et al., 2003; Smith et al., 2006).

Mussels in the genus *Mytilus* are filibranch bivalves, preferably forming dense beds on solid substrates in the low- to high-intertidal zone where they feed on suspended algae and detritus (Seed and Suchanek, 1992). As dioecious broadcast spawners, gametes are released by both males and females into the water column where fertilized eggs rapidly begin developing into planktonic larvae. In *Mytilus californianus,* this larval stage lasts up to 45 days, allowing for significant dispersal of up to 50 km (Addison et al., 2008), though this dispersal time and distance varies with species and habitat preferences. Larval settlement involves descent from the water column followed by a period of mobility while finding suitable location for attachment, during which the larvae are sensitive to substrate type and chemical cues from conspecifics (Carl et al., 2012; Gosling, 2015). At this point, the larvae (known at this stage as pediveligers) secrete byssal threads that adhere mussels strongly to the substrate, potentially for the duration of their lives in species with no secondary mobility (Gosling, 2015; Paine, 1974).

Mytilus *gill physiology*

As suspension feeding bivalves, *Mytilus* show remarkable responsiveness to available algae and detritus in the water column (Riisgård et al., 2003; Riisgård et al., 2013; Robson et al., 2010a). *Mytilus* utilize a specialized set of gills (ctenidia) for both respiration and feeding, making this metabolically active, vital organ for their survival (Dahlhoff et al., 2002). The gills are comprised of numerous W-shaped filaments that are reinforced internally by collagen-rich structures and connected loosely by ciliary

junctions (Gómez-Mendikute et al., 2005; Gosling, 2015). Lateral cilia beat continuously to move water and suspended particles between gill filaments while laterofrontal cilia transfer particles to the frontal cilia and bind them in mucous. Epithelial mucous cells secrete heavily glycosylated mucin glycoproteins as well as bioactive molecules to lubricate, prevent desiccation, form a physical immune-recognition barrier, and transport food particles (Pales Espinosa et al., 2016). Mucous-bound particles are moved to a ventral food groove where cilia move the string of aggregated particles toward the labial palps. Here, particles are either passed to the mouth or rejected as pseudofeces (Gosling, 2015; Riisgård et al., 2011).

The large surface area for particle processing also allows for efficient gas exchange through the thin filament walls to the hemolymph circulating within (Gosling, 2015). The rhythmic beating of the lateral cilia on the ctenidia drive the filter-pump that draws oxygenated and particle-laden water into the valves through an inhalant opening in the mantle tissue. After passing this water between the gill filaments, the deoxygenated filtered water is expelled through the exhalant opening formed by the mantle tissue (Gosling, 2015). Filtration rate varies by species, season, particle concentration, and individual, but studies have found that *Mytilus californianus* is capable of filtering at a rate of 50 – 3000 mL/min (Bayne et al., 1976). This unique and important organ, serving a dual purpose for bivalve feeding and respiration, makes it a common focal tissue for studies of *Mytilus* stress physiology (Dahlhoff et al., 2002; Dowd et al., 2013; Jaafar et al., 2015; Letendre et al., 2009; McDonagh et al., 2006; Rocher et al., 2015; Tomanek and Zuzow, 2010). Furthermore, the direct interaction between the gill tissue of sessile bivalves and their environment leaves them acutely exposed to pollutants, making this

organ of great interest for research supporting ecotoxicological monitoring programs (Gómez-Mendikute et al., 2005).

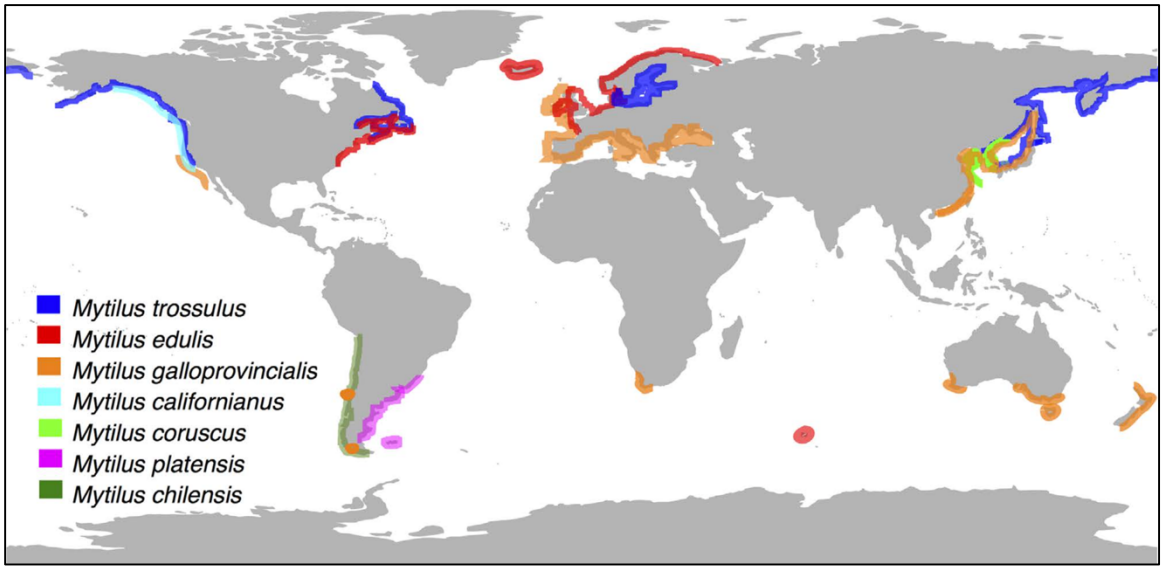

Figure 1. Worldwide distribution of *Mytilus* spp. as reviewed by Gaitán-Espitia et al. (2016). See publication for figure and details on data sources and sampling.

Sensory systems in Mytilus

Sensory systems in the phylum Mollusca vary widely, and within the class Bivalvia there is still a great amount of differentiation. The nervous system is broadly connected by three sets of ganglia—the pedal ganglia, cerebral pleural ganglia, and the visceral ganglia—lying along the ventral hinge of the valves. Activity of the cilia in each gill is under dopaminergic and seratonergic nervous system control from a branchial nerve from the visceral ganglion (Stefano and Aiello, 1975) and a circumpallial nerve follows the mantle margin along the edges of the valves (Gosling, 2015). The nervous system of bivalves also includes an incredibly diverse array of photoreceptors (Morton, 2008; Wilkens, 2008). One set of photoreceptors senses light through rudimentary cephalic eyes. In the genus *Mytilus*, two "eyes" are located on the inside base of the gill

filament, forming a simple invagination about 50 μm in width and containing ciliated pigment cells in close proximity to approximately 37 photoreceptor cells with axons leading directly to the cerebral ganglion (Northrop, 2000). The greatest spikes detected in the optic nerve fibers in *Mytilus edulis* occurred in blue light (490 nm wavelength) and green light (520 nm) (LaCourse, 1981). The ability for the mussels to sense light has been shown in responses to changing the timing of light conditions and a particularly strong "shadow reflex" of valve closure following a sudden switch to darkness (Gnyubkin, 2010; Wilkens, 2008). No image is possible to discern with such a rudimentary eye structure as that which has been described, and following the destruction of the photoreceptor cells in *Mytilus edulis* the shadow reflex remained, suggesting that there may be additional photoreceptors or photoreceptive molecules in other organs (LaCourse, 1981).

In addition to light-sensing, mussels receive numerous cues associated with tidal cycles. For food sensing, the osphradium and abdominal sense organs may sense food in the inhalant water current, acting as a cue for feeding activity (Thompson and Bayne, 1972). Feeding activity is closely regulated by both the type (Espinosa et al., 2016), size (Riisgård et al., 2014), and concentration (Riisgård et al., 2003) of food in the water, indicating that filter-feeders can adjust activity to respond to ideal feeding conditions. Mussels have also been shown to respond to short-term aerial emersion with the upregulation of the oxygen-sensing pathway signaled by hypoxia-inducible factor 1 α (HIF1α) and HIF prolyl hydroxylase (PHD) (Giannetto et al., 2015). This may be a peripheral mechanism for cells to sense the depletion of oxygen during air exposure.

California mussel Mytilus californianus *as a study species*

The California mussel (*Mytilus californianus* Conrad, 1837) is a common intertidal bivalve native to the northeastern Pacific Ocean (Morris et al., 1980; Harbo, 1996). It is most closely related to the Korean mussel *M. coruscus*, forming a sister clade to the other *Mytilus* congeners (Gaitán-Espitia et al., 2016). This mussel is frequently dominant in the mid-intertidal zone throughout its range from Baja in northern Mexico to the Aleutian Islands in Alaska (Abbott and Haderlie, 1980), overlapping in range with native *M. trossulus,* invasive *M. galloprovincialis,* and occasionally introduced *M. edulis* (Shields et al., 2008; Gaitán-Espitia et al., 2016). However, *M. californianus* colonizes turbulent rocky intertidal habitats while *M. galloprovincialis* and *M. trossulus* are typically found in protected bays (Harbo, 1996; Morris et al., 1980). Additionally, *M. californianus* preferentially settles areas where other mussels and barnacles already exist (Dayton, 1971) and will successfully outcompete these other sessile species over time (Dayton, 1971; Paine, 1974).

The main predators for *M. californianus* include birds (*Larus* spp. and *Haematopus bachmani*), marine mammals (pinnipeds and *Enhydra lutris*), gastropods (*Nucella* spp.), and sea stars (primarily *Pisaster* spp.) (Paine, 1974; Seed and Suchanek, 1992). After settling, other major sources of mortality beyond predation include desiccation, salinity stress, sedimentation, and wave exposure causing large scale population disturbances (Seed and Suchanek, 1992; Dahlhoff and Menge, 1996; Harley, 2008; Gosling, 2015). Each of these sources of mortality, including *Pisaster* predation,

have been proposed as mediating the upper and lower extent of *M. californianus* ranges within the intertidal zone

M. californianus is an ideal study species due to its range-wide homogeneity in both stress tolerance (Mislan et al., 2014) and population connectivity (Addison et al., 2008). Furthermore, reciprocal transplants of mussels between locations at vertical tidal ranges (Halpin et al., 2004) and latitudinal ranges (Dahlhoff, 2004) have shown a high degree of plasticity in *M. californianus* responses to environmental variations, though certain aspects of temperature threshold responses may reflect population level adaptations to sites (Logan et al., 2012).

Intertidal mussels are also increasingly used for biomonitoring purposes. In California, the Environmental Protection Agency State Water Resources Control Board runs a Mussel Watch Program (SMW), as well as a Regional Monitoring Program and a NOAA sampling program with the National Mussel Watch Program (NMW) (State of California, 2016). Because sessile, filter-feeding bivalves will be exposed to any changes in the water quality, they may be monitored for behavioral (AquaDect) or molecular (Luedeking and Koehler, 2004) signs of stress. For this reason, researchers are increasingly seeking to fine-tune our understanding of how intertidal mussels respond to varying environmental stressors (Benedetti et al., 2015; Campos et al., 2012) and how natural environmental changes may influence biomonitoring markers (Luedeking and Koehler, 2004).

Biological Rhythms

Overview of biological rhythms

Biological clocks allow an organism to anticipate predictable changes in the environment that can have important implications for survival, such as food availability, temperature, and light (Reinke and Gatfield, 2006; Roenneberg and Merrow, 2014), as well as coordinating temporal niche selection to reduce interspecies competition (Paranjpe and Sharma, 2005). The ability to anticipate and coordinate biological processes with the environment appears to be incredibly important to life. The initial evolution of circadian rhythms may have arisen to reduce the risk of photo-oxidative damage on light-sensitive reactions (Pittendrigh, 1993). Endogenous circadian timing in early cyanobacteria would have coordinated metabolic processes with the light/dark cycle to protect sensitive metabolic reactions from harmful oxidative stress (Huang et al., 1990). This protective nature of temporal separation of cellular processes is clear in several cases. Some cyanobacteria reduce the risk of oxidative damage by evolving specialized, segregated structures called heterocysts that isolate damaging processes while others achieve the same result through temporal compartmentalization (Stal and Krumbein, 1985). Beyond prokaryotes, a study on the oscillation of transcripts in yeast (*Saccharomyces cerevisiae*) found a distinct separation of potentially harmful oxidative metabolism and the replication of DNA in the cell cycle (Klevecz et al., 2004; Reinke and Gatfield, 2006). Numerous other studies have also uncovered the adaptive importance of synchronizing an organism's behavior and physiology with the external environment, showing that there is indeed a competitive advantage for individuals with

intact rhythms over those without (Emerson et al., 2008; Jones et al., 2015; Wang et al., 2015; Yerushalmi and Green, 2009).

Circadian Rhythms

The daily light-dark cycle influences organisms from nearly every studied life form (Bell-Pedersen et al., 2005). This daily rhythm of approximately 24 hours is known as the circadian (Latin: *circa* – "about", *diem* – "day") rhythm. Circadian rhythms typically follow a self-sustaining, or endogenous, mechanism that continues even in the absence of an exogenous environmental cues, or Zeitgeber (German: "time giver"), that synchronizes the rhythm with the environment (Dunlap, 1999; Paranjpe and Sharma, 2005). However, these environmental cues typically entrain the rhythms by resetting them on a regular basis, ensuring the synchrony of the biological clock with the surroundings (Reddy and Rey, 2014).

The typical molecular model for the cellular clock mechanism involves a transcription/translation feedback loop (TTFL) with a core set of timekeeping molecules that function similarly in multiple organisms despite utilizing different components (Bell-Pedersen et al., 2005; Dunlap, 1999; Reddy and Rey, 2014). Briefly, the typical oscillators are comprised of a set of positive and negative regulating elements. In the mammalian model, these positive elements are the transcription activators CLOCK and BMAL1. Together, positive regulating elements activate clock-controlled gene expression, which in the mammalian model includes the target regions *Per* and *Cry* among many other products that regulate biological processes. The products of the clock genes (PER and CRY) act as negative regulators that eventually inhibit the activity of the

positive elements (with some time delay), and the positive elements are only allowed to restart their cycle after the gradual phosphorylation and degradation of the negative elements (Bell-Pedersen et al., 2005). The specific components of the molecular clock in bivalves are currently uncharacterized (Mat et al., 2016), though in *M. californianus* gill tissue orthologs were identified for the mammalian clock genes CLOCK, BMAL, CRY1, and RORB (Connor and Gracey, 2011).

While the core TTFL mechanism behind circadian rhythms has been explored thoroughly in mammalian models, research continuously uncovers new complications to the basic model. The circadian control of transcription has been found to be sensitive to methylation (Fustin et al., 2013), miRNA control (Wang et al., 2016), rhythmic polyadenylation (Kojima et al., 2012; Kojima et al., 2015), epigenetic modification (Martelot et al., 2012), as well as other unknown factors that result in differences between the levels of nascent transcription and mRNA abundance (Janich et al., 2015; Menet et al., 2012). Furthermore, multiple other alternative or additional clock mechanisms have been proposed in addition to the traditional TTFL model. Additional clocks that have been reported include post-translational modifications through phosphorylation (Jolley et al., 2012) or acetylation (Masri et al., 2013; Ramsey et al., 2013; Rey and Reddy, 2013a), protein degradation (Lück et al., 2014), and oxidation (Hoyle and O'Neill, 2015; Kil et al., 2015), as well as nutrient sensing and metabolic control (Nakahata et al., 2009; Peek et al., 2012; Wang et al., 2016). Theoretically, there may be an underlying mechanism by which the TTFL timekeeping model is tightly coupled to the post-transcription/translation mechanisms (McClung, 2011; Nakahata et al., 2009).

Interestingly, the core TTFL model has been most studied in light-receptive organs containing photoreceptors (Block and Colwell, 2014; Blumenthal et al., 2001; Muñoz et al., 2011; Pairett and Serb, 2013; Wilkens, 2008), which then coordinates the whole-organism response through a central network such as the suprachiasmatic nucleus (SCN) or efferent optic nerve activity. However, research has also shown that circadian rhythms can persist in peripheral tissues independently (Kaneko et al., 2006). Interestingly, a light-sensitive family of molecules known as cryptochromes (cry) are thought to be involved in the coordination of these peripheral tissues with light/dark entrainment. However, cryptochromes are extremely diverse and may serve a variety of different functions depending on the organism. For example, the cry transcript oscillated with a circadian rhythm in the gill tissue of both *M. californianus* (Connor and Gracey, 2011) and *Crassostrea gigas* (Tran et al., 2015), while the transcript appeared to follow a tidal rhythm in *Crassostrea gigas* striated adductor muscle (Mat et al., 2016).

Circatidal Rhythms

The significance of biological rhythms as an adaptive coordinator of physiological and behavioral activity in a fluctuating environment reaches beyond that of light/dark cycles. Many organisms reside in environments where additional rhythms in the environment alter the conditions in such a way that anticipation of the predictable changes becomes advantageous (Tessmar-Raible et al., 2011). Tidal cycles constitute predictable environmental fluctuations that make coastal intertidal zones uniquely challenging.

Tides are generated by the combined effects of the gravitational pull of the moon and the centrifugal force of Earth's rotation, resulting in a cycle where tides (high or low) occur approximately every 12.4 h (Fig. 2). With these changes in tides come changes in food availability, temperature, aerial emersion, wave exposure, pressure changes, water current, dissolved oxygen, and salinity (Dowd and Somero, 2013; Harley, 2008; Place et al., 2012; Riisgård et al., 2006; Saurel et al., 2007; Tessmar-Raible et al., 2011). Organisms that live in this habitat can either respond to or anticipate these extreme environmental fluctuations to which they are exposed (Chabot and Watson III, 2014; Zhang et al., 2013). Free-running circatidal rhythms of activity have been recorded for numerous marine species, including horseshoe crabs (*Limulus polyphemus*), green crabs (*Carcaenus maenus*), speckled sea-louse (*Eurydice pulchra*), and several bivalve species (*Crassostrea gigas, Mytilus* spp., *Austrovenus stutchburyi*) (Chabot and Watson III, 2014; de la Iglesia and Johnson, 2013).

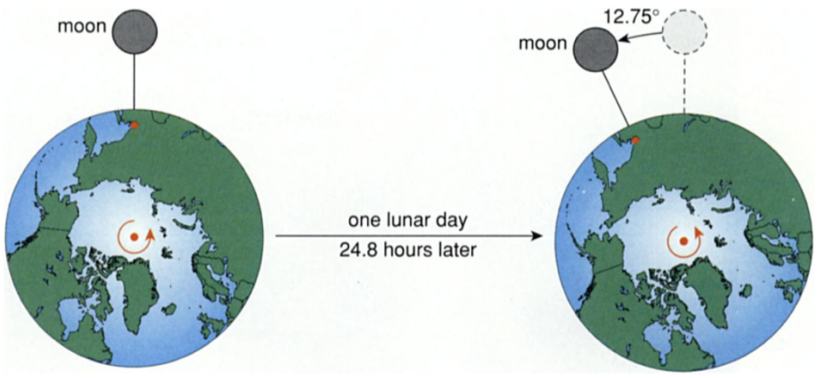

Figure 2. The influence of the relative movements of the earth and moon drive the 24.8 h tidal cycle. The timing of tides occurs due to the non-synchronous counter-clockwise movement of the rotating earth and orbiting moon. One full rotation of the earth plus an another 12.75^{o} is required for a single location on earth to catch up to the orbit of the moon in the same direction. The tides are driven by the gravitational pull of the moon on

the water below while a tidal bulge on the opposite side of the earth is generated by centrifugal force. Figure from (Palmer, 1996).

The challenges of an intertidal environment are particularly pertinent for sessile intertidal organisms, such as mussels, that lack the mobility to avoid exposure to tidal fluctuations and instead exhibit other behavioral (Shick et al., 1986; Tran et al., 2011; Widdows and Shick, 1985) and physiological (Connor and Gracey, 2012; Gracey et al., 2008; Han et al., 2013; Place et al., 2012; Zaldibar et al., 2004) mechanisms to endure the environmental changes. The existence of a persistent, endogenous tidal rhythm of valve gaping behavior in the Pacific oyster *Crassostrea gigas* has been known for some time (Tran et al., 2011), and a tidal environment has been found to induce physiological plasticity in mussels, making individuals that experience tidal cycles more resilient and responsive to stress than those that remain in subtidal zones (Altieri, 2006; Demers and Guderley, 1994; Letendre et al., 2009; Moon and Pritchard, 1970; Petes et al., 2008; Place et al., 2012; Tagliarolo et al., 2012; Widdows and Shick, 1985). The most pronounced response of intertidal mussels to aerial exposure during low tide is metabolic depression and decreased heart rate (Bayne et al., 1976) accompanied by a clear switch to anaerobic metabolism (Bayne et al., 1976; Connor and Gracey, 2012; Moon and Pritchard, 1970; Shick et al., 1986; Tagliarolo et al., 2012).

The studies mentioned above suggest that the aerial exposure presents a strong Zeitgeber for behavioral and physiological entrainment to tidal cycles. However, the large magnitude of environmental changes during a tidal cycle makes pinpointing the specific Zeitgeber for circatidal entrainment extremely difficult (Tessmar-Raible et al.,

2011). Previous studies have found that food ability can also entrain persistent circatidal valve gaping behavior in filter-feeding bivalves (Higgins, 1980; Williams and Pilditch, 1997). Furthermore, studies on cell renewal in the digestive epithelium in *M. galloprovincialis* demonstrated a perfect circatidal rhythm, with cells proliferating just after high tide hours (Zaldibar et al., 2004). In an effort to isolate the importance of food entrainment in establishing biological rhythms, studies have found that restricted food timing can establish rhythmicity in gene expression and metabolites even when the genetic circadian clock mechanism is absent in mice (Atger et al., 2015). The rhythmicity associated with food availability may be related to the energetic costs to synthesize rhythmic genes, which was supported in yeast when researchers were able to increase the number and degree of cycling genes by manipulating nutrient availability (Wang et al., 2015). While intertidal mussels experience variations in food availability simply due to the limited feeding ability during high tide submersion (Dowd et al., 2013; Thompson and Bayne, 1972), studies have also found that the amounts of suspended particulate matter in the nearshore environment also fluctuated with the tides, which would implicate food in circatidal entrainment of subtidal mussels as well (Hill et al., 2008; Saurel et al., 2007). Other implicated cues include salinity changes, temperature, water depth, hydrostatic pressure, or water flow and turbulence (de la Iglesia and Johnson, 2013; Mat et al., 2014).

While the Zeitgebers entraining the circatidal clock are varied, the cellular mechanisms driving endogenous circatidal rhythms are currently unknown (Mat et al., 2016). There are multiple theories about the clocks behind tidal entrainment, ranging from discrete circatidal and circadian clocks to antiphase-coupled lunar clocks (Mat et al.,

2014; Palmer, 1996). The existence of two discrete clocks is supported in the marine isopod *Eurydice pulchra* (Zhang et al., 2013) and in the marine annelid *Platyneris dumerilii* (Zantke et al., 2013). There is evidence of a "masking" effect of one rhythm, circadian or circatidal, over another, suggesting (1) a potentially shared mechanism for the two rhythms and that (2) the relative importance of the dominant rhythm may be reflective of the most prominent rhythm in the organism's environment (Chabot and Watson III, 2014; Connor and Gracey, 2011; de la Iglesia and Johnson, 2013; Mat et al., 2012; Mat et al., 2014; Tran et al., 2011). For instance, in some marine organisms, one of the two clocks drives behavior in the presence of the Zeitgeber for that specific clock, but with both sets of cues there is a clear masking of a competing clock (Mat et al., 2012; Robson et al., 2010b). To reinforce how rudimentary our current knowledge of circatidal mechanisms remains, the light-sensitive cytochrome 1 that is involved in the circadian clock in many organisms showed exogenous (not free-running) circadian expression in the adductor muscle of *C. gigas* under light/dark conditions but followed a circatidal expression when exposed only to tidal cycle (Mat et al., 2016). This type of competing information demonstrates the general absence of evidence concerning the molecular mechanisms driving circatidal rhythms, making the prominence of circadian and circatidal rhythms appear both taxa- and habitat-specific.

Analysis of Biological Rhythms

The analysis and detection of biological rhythms requires a sampling regime with proper replicates, time intervals, duration, and under carefully controlled conditions to determine whether, if any, entrainment to environmental fluctuations has occurred

(Refinetti et al., 2007). Studies of circadian or circatidal behaviors are often longitudinal, with frequent or constant observations on the same individuals over a long duration of time (Higgins, 1980; Williams and Pilditch, 1997). Transverse, or cross-sectional, studies are frequently used when tissue collection requires many individuals that are sampled only once as representatives of the population (Connor and Gracey, 2012; Robles et al., 2014). With acclimation to routine, controlled conditions, a longer time series, and many individuals sampled randomly from the population at frequent, discrete time points there is a greater opportunity to detect not only whether rhythms exist but also to estimate the features of an oscillating rhythm such as the period, phase, and amplitude (Refinetti et al., 2007).

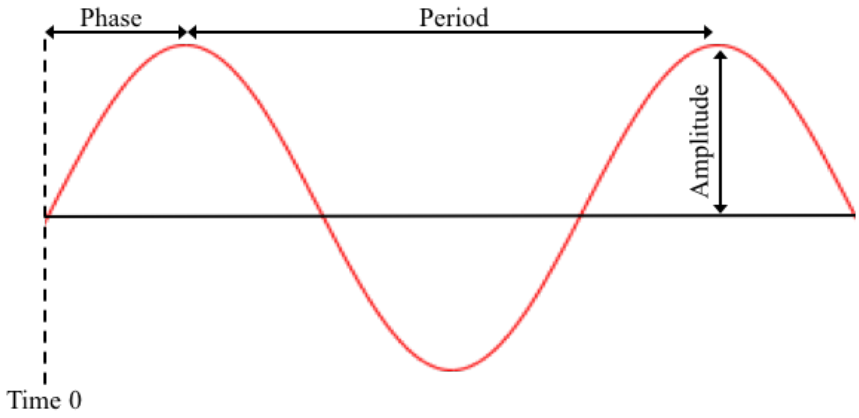

Figure 3. Visualization of the attributes of biological rhythms. The phase indicates the delay of the initial peak with regards to a reference point (Time 0 in this example). The period is the regular length of an oscillation from one peak to the next. The amplitude is the difference between a peak and the average value for the oscillation. Finally, the waveform is a description of the shape of the oscillation (in this case a cosine waveform).

Statistical detection of rhythmicity requires statistical analysis to confirm the existence of rhythms that may or may not be apparent to the eye. Evaluation of rhythmicity has amassed a wealth of methods for various situations, including ANOVA, Fourier analysis, autocorrelation, cosinor and cosine fit, Rayleigh test, periodograms, and harmonic regression (Deckard et al., 2013; Hughes et al., 2010; Refinetti et al., 2007). For large transverse datasets such as microarray data from transcriptomic studies, a major challenge has been to develop a statistical method that is (1) robust with noisy data, (2) powerful and computationally efficient, and (3) provides measurements of period, phase, and amplitude (Hughes et al., 2010). One particularly effective algorithm that has been applied to numerous studies is the JTK_CYCLE algorithm (Connor and Gracey, 2011; Connor and Gracey, 2012; Eckel-Mahan et al., 2012; Hughes et al., 2010; Kojima et al., 2012; Lück et al., 2014; Masri et al., 2013; Robles et al., 2014; Schick et al., 2016; Wang et al., 2015). This algorithm uses the nonparametric Jonckheere-Terpstra (JT) test to detect monotonic data ordering and applies Kendall's τ measurement of rank correlation to optimize the period and phase combination that minimizes the Kendall's τ correlation p-value between experimental data and a reference waveform (Hughes et al., 2010). As a result, the script is able to run large datasets very quickly in the statistical program R (R Core Team, 2016) to provide a conservative p-value, period, phase, and estimated amplitude. However, one significant shortcoming for the use of JTK_CYCLE to analyze biological data is that it assumes a symmetric waveform, with the rising and falling

portions being the same on both sides of the peak (Hutchison et al., 2015; Thaben and Westermark, 2014).

A recent method was developed to address this shortcoming using Rhythmicity Analysis Incorporating Nonparametric methods (RAIN) (Thaben and Westermark, 2014). This test groups data by either a rising or falling part of an oscillation period using a K-sample rank test for umbrella alternatives (Mack and Wolfe, 1981; Thaben and Westermark, 2014). By allowing for asymmetries in the rising and falling portions of the oscillation, such as a sawtooth-shape waveform, RAIN nearly doubled the number of detectable circadian rhythms in transcriptomic and proteomic datasets (Mauvoisin et al., 2014; Robles et al., 2014; Schick et al., 2016; Thaben and Westermark, 2014). Furthermore, RAIN was able to detect almost all of the cycling proteins and transcripts from the datasets that had been previously identified by other methods, such as JTK_CYCLE, making it adequate for detecting symmetric waveforms as well as asymmetric (Thaben and Westermark, 2014). The authors of RAIN caution against using its estimates of period and phase, however, since it is not designed to accurately approximate the parameters. Furthermore, increased flexibility also leads to slower computation when evaluating for multiple periods and expanded rising/falling phases (Thaben and Westermark, 2014).

For both JTK_CYCLE and RAIN there is the added complication of correcting for multiple tests. In hypothesis testing, an alpha value indicates the cutoff for significance testing using a standard p-value. However, in large datasets involving the analysis of hundreds of data series the chance of making a Type I statistical error (falsely

rejecting the null hypothesis) in any single test increases (Refinetti et al., 2007; Storey and Tibshirani, 2003). By adjusting the alpha value threshold for the family-wise error rate researchers can conservatively control the likelihood of detecting true significance, the false positive rate (FPR) (Refinetti et al., 2007; Storey and Tibshirani, 2003). However, if the threshold is set too low, which is often the case with a Bonferroni correction, then many biologically important true positives may be excluded (Refinetti et al., 2007). For biological rhythms, this error may appear in (1) conducting multiple statistical tests to evaluate each possible period length in a single data series and/or (2) evaluations of multiple data series for rhythmicity (Refinetti et al., 2007). Most tests for oscillation features are automatically corrected in the output p-value (Thaben and Westermark, 2014). However, the problem of false positives in evaluations of data series (hundreds to thousands in many –omics studies) requires additional attention.

A solution to the problem of false positives in genome-size datasets was proposed by Benjamini and Hochberg (1995). While the FPR represents the probability of a false positive among the large collection of multiple comparisons, a false discovery rate (FDR) is calculated for each series to denote the probability that the feature is a false positive (Benjamini and Hochberg, 1995; Storey and Tibshirani, 2003). This FDR, represented by the q-value, is now widely implemented in circadian analyses and allows statistical testing to be biologically relevant by remaining conservative but not constricting (Refinetti et al., 2007). Both JTK_CYCLE and RAIN provide this q-value as an

alternative test statistic for the analysis of rhythmicity in large datasets (Hughes et al., 2010; Thaben and Westermark, 2014).

Proteomics

Overview

The proteome comprises the complete array of proteins expressed in a given tissue, generating a snapshot of the functional cellular phenotype of the organism's tissue. This offers an extremely dynamic and responsive examination of the ever-changing molecular response to internal and external stimuli (Campos et al., 2012; Lovrić, 2011; Rabilloud, 1999; Rocher et al., 2015). However, the proteome is subject to extreme variability, ranging from subcellular location of proteins, protein-protein interaction, and post-translational modification (Baltz et al., 2012; Lovrić, 2011; Mata et al., 2005; Wallach et al., 2013; Walsh et al., 2005). For this reason, proteomics broadly encompasses the study of protein abundance patterns as well as the numerous modifications that can alter protein interactions and activity.

The study of the genomics has a vital place in the "-omics" family, but its scope for describing physiologically important functions is limited by the incredible downstream variability. As previously mentioned, the proteome represents the basic functional phenotype of an organism. In humans, a genome consisting of 23,000 genes results in a proteome of 100,000 proteins (or proteoforms) to reflect the overwhelming diversity and complexity that arises from a relatively simple set of genetic instructions (Salway, 2012; Smith et al., 2013). This makes the genome an important tool for

exploring evolutionary relationships and predicting downstream functionality, but there is an incredible amount of molecular variation between a gene and its corresponding protein, including mRNA splicing, localization, silencing, and degradation (Evans, 2015; Feder and Walser, 2005; Lovrić, 2011).

Another level of the "-omics" research approach is transcriptomics, which assesses the pool of transcribed mRNA in a given tissue (Evans, 2015; Feder and Walser, 2005). This is a powerful tool that addresses much of the previously mentioned variability between a transcribed gene and a functional product. However, mRNA levels do not inherently have a physiological function and do not necessarily correspond with a functional protein product, thus their scope for informing fitness consequences may fall short in many cases (Evans, 2015). The relative expression levels and degradation rates of mRNA and their corresponding proteins clearly differ in many cases, making mRNA transcript levels inaccurate predictors of protein abundance (Feder and Walser, 2005; Janich et al., 2015; Kojima et al., 2012; Menet et al., 2012). This is due to the multi-step process leading from mRNA to functional protein during which polypeptides undergo subcellular localization, assembly into complexes, silencing, degradation, or aggregation (Feder and Walser, 2005). Furthermore, a single mRNA may be translated numerous times to yield upwards of 23,000 proteins (Feder and Walser, 2005)

However, working with proteins poses several challenges, especially with respect to the study of less abundant proteins (Rabilloud, 2000). This shortcoming is further emphasized by the absence of an amplification tool equivalent to PCR for protein processing (Rabilloud, 2000). Therefore, while measuring protein abundance may be

more difficult than assessing levels of mRNA transcripts, it provides advantages in that it allows for deeper insight into biological systems (Abbott, 1999). Given their sensitivity to intrinsic regulation, external perturbations, and fast response time, proteins are ideal biochemical indicators of metabolic stress and are thus the focus of many ecological studies (Dahlhoff, 2003; Tomanek and Zuzow, 2010).

Proteomics addresses these shortcomings of genomics and transcriptomics to examine the protein content in a tissue at a given time, thus depicting the molecular content of the cell that typically comprises the functional phenotype (Lovric, 2011). The holistic examination of this biochemical machinery allows researchers to explore the dynamic and complex connections between proteins that are likely to have fitness consequences for the organism (Tomanek, 2011; Tomanek, 2014). The complexity of this network of related proteins with diverse functions provides a snapshot of cellular functions under unique circumstances (Tomanek and Zuzow, 2010). Upon assessing the array of proteins expressed in varying abundances under different conditions, proteomics typically generates specific hypotheses that describe the changes in the system, thus providing a focal point for future experimentation (Dowd, 2012). Unfortunately, the importance of the proteome is matched by the difficulties associated with comprehensive and reliable detection on a large scale (Abbott, 1999).

The proteomic workflow falls into three main parts: separation, quantification, and identification (Lovrić, 2011; Tomanek, 2011). In the typical gel-based approach, proteins are extracted from tissues, separated by isoelectric point and molecular weight, digested, identified via mass spectrometry, and assessed using relevant statistics (Abbott,

1999; Berth et al., 2007; Rabilloud and Lelong, 2011). The refinement of gel-based methods for large proteomics projects over the past few decades as made 2D gels far more affordable, easier to handle and reproduce, and more of effective separation of up to thousands of proteins on a single gel (Rabilloud and Lelong, 2011). Meanwhile, software advances allow for more efficient and accurate analysis of large sample sizes (Berth et al., 2007). Using 2DGE also allows for the separation of protein isoforms with multiple posttranslational modifications, allowing researchers to not only examine changes in protein abundance but also track the relevant posttranslational modifications that may occur under experimental conditions (Görg et al., 2004; Michel et al., 2003). While gel-free proteomic systems exist and are widely used, these methods typically supplement shortcomings of gel-based methods such as poor detection of low abundance proteins, basic or acidic proteins, or proteins that are poorly soluble (Lovrić, 2011). However, gel-based methods are still the most commonly used and therefore the methods for this approach will be addressed here.

Protein Separation

The protein separation step falls into three main parts: sample preparation, isoelectric focusing (IEF, or 1st dimension separation) using an immobilized pH gradient (IPG) strip, and 2D gel electrophoresis (2DGE, or 2nd dimension separation). No single method of sample preparation applies to all experimental questions, tissue types, or technologies, so protocols must be optimized for every study (Görg et al., 2004). Sample preparation generally must (1) retain most of the original proteins, (2) remove

contaminants, (3) preserve protein modifications, and (4) retain compatibility with subsequent analytical steps (Lovrić, 2011).

Because the proteome is a snapshot of the protein content in a tissue at a given time, tissue samples must be flash frozen in liquid nitrogen to prevent subsequent aggregation and degradation of proteins (Berth et al., 2007; Lovrić, 2011). The first step following dissection is cell disruption to release intracellular proteins, which can be accomplished through mechanical homogenization in a lysis buffer (Görg et al., 2004). Mechanical force helps to accelerate membrane decomposition while buffer chaotropes (urea and thiourea) disrupt hydrophobic interactions and hydrogen bonds to denature protein structures, which simultaneously prevents the activity of proteases in the sample (Shaw and Riederer, 2003). Membrane proteins must be disrupted using a zwitterionic detergents (surfactants) such as amidosulfobetaine (ASB-14) (Lovrić, 2011; Shaw and Riederer, 2003). Reducing agents such as dithiothreitol (DTT) maintain proteins in their unfolded primary structure by breaking disulfide bonds within the proteins (Shaw and Riederer, 2003). Finally, a mixture of carrier ampholytes (IPG buffer) enhances protein solubility, helps to prevent nucleic acid contamination, and ultimately improves 2DGE resolution (Shaw and Riederer, 2003). A pH range of 4-7 for the IPG buffer allows efficient separation of physiologically relevant cellular proteins without confronting the challenges of separating highly acidic or alkaline proteins (Görg et al., 2009).

After full homogenization of the tissue, the unwanted cellular components (such as lipids, nucleic acids, polysaccharides, and salts) need to be inactivated or removed (Görg et al., 2004). The negative charge of nucleic acids makes them easily interfere with

isoelectric focusing by strongly binding to proteins, while both nucleic acids and polysaccharides can interact with ampholytes and impair 2DGE resolution (Rabilloud and Lelong, 2011; Shaw and Riederer, 2003). Salts can impair protein separation by precipitating proteins from IEF strips and increasing electrical conductivity in the 1st dimension separation (Görg et al., 2009; Shaw and Riederer, 2003). Lipids can also bind to proteins through hydrophobic interactions, both affecting the uptake of the proteins into gels during IEF strip rehydration and affecting the charge of the protein and altering 2DGE resolution (Shaw and Riederer, 2003).

Many large cellular components are removed following centrifugation of the homogenate, but the sensitive contaminants mentioned above require additional steps to purify the protein sample. Trichloroacetic acid (TCA)/acetone precipitation followed by an acetone wash to remove remaining TCA works in most cases to purify a protein mixture, though some protein is typically lost during the process (Görg et al., 2004; Lovrić, 2011). The protein in this case is preserved as a pellet separate from the contaminants and subsequently re-solubilized in a salt-free rehydration buffer. This buffer contains chaotropes and ampholytes similar to homogenization buffer as well as octylphenoxypolyethoxyethanol (Nonidet P- 40), a non-ionic detergent that solubilizes membrane proteins and prevents protein aggregation (Lovrić, 2011). Additionally, the buffer contains 3-[(3-cholamidopropyl) dimethylammonio]-1-propanesulfonate (CHAPS), a non-denaturing zwitterionic detergent to solubilize proteins, and

dithioerythritol (DTE), another reducing agent to prevent disulfide bonds (Görg et al., 2004; Lovrić, 2011).

Quantification of the purified protein sample is vital to ensure that the same amount of protein is loaded for each gel, allowing for comparison of the altered composition of the proteome without the confounding effect total protein differences. The Lowry method of protein quantification utilizes the spectrophotometric analysis of protein-catalyzed reduction of Cu^{2+} to Cu^{+} (Weist et al., 2008). The 2-D Quant Kit (GE Heathcare Bio-Sciences) was developed to overcome the challenge of quantifying protein alongside rehydration buffer components like reducing agents, chaotropes, and detergents. As Cu^{2+} ions bind to proteins in a copper-sulfate solution, the absorbance reading (measured at 480nm) of unbound Cu^{2+} in a colorimetric agent provides an inverse measurement of protein concentration (2-D Quant Kit, GE Healthcare). Based on the protein concentration assay, the gel size, and the type of stain being used, samples are diluted in working IPG rehydration buffer to load a total of 400 μg of protein on each IPG strip.

Once diluted, the protein solution is added to a ready-made IPG strip to separate the proteins by their isoelectric point (pI), the pH at which a protein's charge is neutralized. IPG strips are dehydrated polyacrylamide gels containing acrylamide derivatives with the general structure CH_2=CH-CO-NH-R, where R contains either an amino or a carboxyl group forming a stable, immobilized pH gradient between pH 1 and 13 (Görg et al., 2009; Righetti and Bossi, 1997). The strips come in a variety of lengths (e.g. 7 cm, 11 cm, 24 cm) and pH ranges (e.g. pH 3-10, pH 4-7, pH 4.7-5.9) that can be

selected based on the target proteins for the experiment (Görg et al., 2009). A narrower pH range typically increases the retention of protein in the gel but with reduced protein resolution (Righetti and Bossi, 1997). When the protein solution rehydrates the IPG strip, a charge is applied that allows the proteins to migrate through the strip. Proteins are amphoteric molecules that contain a unique combination of side chains that are either charged or may become charged depending on the surroundings (Lovrić, 2011). The electric field applied in IEF moves the proteins toward the anode or cathode depending on the charge of their side chains until the immobilized pH gradient neutralizes the charge (Görg et al., 2009; Lovrić, 2011). Once completed, the strips are stably frozen at -80^{o}C until the proteins are separated in the 2nd dimension.

To separate proteins in the 2nd dimension by molecular weight, the proteins must be charged proportionally to their size. To do so, IPG gels strips are equilibrated with sodium dodecylsulfate (SDS), a negatively charged detergent with a hydrophilic sulfate group that gives the denatured peptide backbone a negative charge (Lovric, 2011). The equilibration buffer also consists of Tris-HCl (pH 8.8), urea, glycerol, and the reducing agent DTT to cleave disulfide bonds (Görg et al., 2004). This equilibration step is followed by a second step using the same buffer, except with iodoacetamide (IAA) instead of DTT. IAA binds covalently with both free DTT and reduced cysteine residues to act as a permanent cap preventing disulfide bridges from reforming (Görg et al., 2004).

Now that the proteins are charged proportionally to their size and equilibrated for the pH conditions of the 2nd dimension, the proteins are separated using sodium-dodecyl-sulfate polyacrylamide gel electrophoresis (SDS-PAGE). An SDS-PAGE gel is mesh

matrix of acrylamide and “cross-linking” bisacrylamide monomers that forms pores though which the proteins migrate (Lovrić, 2011). By altering the percentage of acrylamide and bisacrylamide for casting the gels, pore sizes can be altered to separate higher or lower molecular weight proteins (Lovrić, 2011). The equilibrated IPG strips are placed on top of the polyacrylamide gel and exposed to an electric current that forces the negatively charged proteins to leave the strip and migrate through the pores of the polyacrylamide gel towards the positive cathode (Lovrić, 2011). Smaller molecular weight proteins move easily through matrix and larger proteins move slowly and as a result, when the electric current is stopped, the smaller proteins are found near the bottom of the gel and larger proteins closer to the top where they originated in the IPG strip (Lovrić, 2011).

Because the polyacrylamide gel is translucent and the proteins are not visible, a stain must be to bind to the proteins and highlight them within the gel (Berth et al., 2007). Different staining methods are available depending on the amount of protein in the gel and the protein identification procedure (Görg et al., 2004). Several protein stains rely on visual fluorescence (e.g. SYPRO Ruby, LavaPurple) while others are colorimetric (e.g. Colloidal Coomassie Blue, Silver Stain) (Ball and Karuso, 2007). Colloidal coomassie Blue (CCB) is a common staining method that binds reversibly to tyrosine residues on proteins (Lovrić, 2011). It is easy to use, specific to proteins, and is the most compatible method with mass spectrometry (Lovrić, 2011). However, CCB requires a fair amount of protein to bind (10 ng of protein/spot) so lower quantity proteins may be missed (Lovrić, 2011). While other methods, such as silver staining, may be more sensitive and bind to lower quantities of protein, they lack the reproducibility of CCB and tend to be

incompatible with ionization during mass spectrometry (Görg et al., 2004). Meanwhile, fluorescent stains, while comparable to the sensitivity of silver stains and compatible with mass spectrometry, are generally more expensive both in the stains and visualization methods (Ball and Karuso, 2007; Lovrić, 2011).

Protein Quantification

Once proteins are separated and stained in the gels, digitized images are analyzed using one of the gel image analysis software packages, such as Delta2D (DECODON, Greifswald, Germany), the software used in this project. One important attribute of current software is the ability to warp the digitized gel image to account for imperfections and variations amassed during 2DGE due to differences in pH, temperature, air bubbles in the gel, and uneven gel polymerization (Berth et al., 2007). Because these differences require subsequent image processing, it is essential that the protein separation be executed with care to minimize the differences in the protein samples (Berth et al., 2007).The gel images for experimental replicates are grouped together and each corresponding protein spot with a variable location on the gel is warped to ensure that proteins are matched (Berth et al., 2007). The gel images are manually warped to one another using match vectors that connect corresponding points in an obvious spot pattern to a master gel image (Berth et al., 2007; Lovrić, 2011). With corresponding spots carefully overlaid, spot matches can be compared for differences between treatment groups, making this a vital aspect of the proteomic analysis (Berth et al., 2007).

After warping each gel in the project, overlapping spots are integrated into a composite fusion image that shows the average 2D distribution and volume of proteins across all gels (Berth et al., 2007). Using the fusion image, Gaussian models/algorithms

are used to determine spot boundaries and intensities (Berth et al., 2007). These spots are then edited manually to ensure proper boundaries around true spots and eliminate false spots around artifacts (bubbles, dust, fingerprints, etc.) and labeled before transferring to each gel image used to generate the fusion image (Berth et al., 2007). To determine the relative protein quantity, image processing software enacts background subtraction to correct for the saturation of the gel surrounding each spot, then the area and pixel density of each spot is used as a proxy for protein amount. One assumption to be made when comparing protein spots across gels is that most of the differences in spot volume will be due to factors such as protein loss during IEF, SDS-PAGE, staining, or differences in staining efficiency and gel scanning (Berth et al., 2007). To account for these inherent differences between gel images, image analysis software typically normalizes the volume of each individual spot against the total volume of all spots on the gel (Berth et al., 2007). The result of this adjustment is to provide a quantitative measurement of a relative subject; thus, the normalized spot volume of one gel can be compared to all others across treatment groups to draw conclusions about the relative amount of protein under differing conditions (Berth et al., 2007). Using these normalized spot volumes, statistical analyses can be performed and expression profiles can be made to show statistically significant differences in protein abundance for a given protein across treatment groups.

Protein Identification

Mass spectrometry (MS) is typically used to identify proteins as the last step in proteomic analysis. MS relies on the ionization of analytes to measure both the mass-to-charge ratio (m/z) and the number of ions detected at a given m/z methods, thus generating a list of masses for fragmented proteins that can then be compared to DNA or

RNA sequence databases for identification (Aebersold and Mann, 2003; Lovrić, 2011). Consistently improving technologies allow researchers to detect post-translational modifications (PTMs) on protein isoform, detect proteins in extremely low concentrations, and accomplish high-throughput, automated detection of proteins (Aebersold and Mann, 2003; Lovrić, 2011; Suckau et al., 2003).

As previously mentioned, the first step to MS analysis is to ionize the sample. Two common ionization methods are electrospray ionization (ESI) and matrix-assisted laser desorption ionization (MALDI) (Aebersold and Mann, 2003). Both methods reduce the fragmentation of the sample during ionization, which is particularly important for the preservation of peptide masses for identification (Aebersold and Mann, 2003; Lovrić, 2011). While both ESI and MALDI generate gas-phase ions, ESI ionizes peptides in solution and will often be paired with high-performance liquid chromatography (HPLC) for analysis of complex protein mixtures (Aebersold and Mann, 2003). On the other hand, MALDI accomplishes sample ionization using a solid crystalline dried-droplet technique, making it ideal for the identification of isolated proteins from 2DGE (Lovrić, 2011). The MS method utilized for protein identification from 2DGE in this research was MALDI tandem time-of-flight (TOF/TOF), so this method will be the focus of the review.

To prepare samples for MALDI TOF/TOF MS, protein spots of interest are excised from 2D gels and digested using proteases to cleave proteins at known locations (Aebersold and Mann, 2003). Trypsin is a commonly used enzyme that cleaves proteins at the C-terminal of lysine and arginine, leaving a mixture of peptide fragments of a unique, predictable size and sequence for a given protein (Lovrić, 2011). Using the dried

droplet technique for MALDI analysis, this small volume of digested protein is plated along with a matrix solution (including the commonly used α-hydroxycyano-cinnamic acid) that integrates the peptides into a dried crystalline spot on a target plate (Lovrić, 2011). Once this target plate is loaded into the mass spectrometer under a high vacuum (approximately 5 x 10^7 millibar), a laser fires on the sample to form a gas plume of peptides (Lovrić, 2011). The matrix serves to both keep the peptides intact following the laser pulse and confer a positive charge to the peptide fragments, which are then accelerated toward the mass analyzer by voltage plates (Lovrić, 2011).

Once the ions are accelerated in the vacuum, a mass analyzer measures the mass-to-charge ratio (m/z) of the ionized peptides (Lovrić, 2011). There are four different mass analyzers typically used, including ion trap, linear time-of- flight (TOF), Fourier transform ion cyclotron (FT-MS), and quadrupole analyzers (Aebersold and Mann, 2003). TOF analyzers are typically used with MALDI and are based on the simple premise that peptide fragments that carry the same charge will be accelerated by the voltage plates at different speeds based on their mass, with heavier ions traveling more slowly than lighter ions (Lovrić, 2011). As ionized peptides move to the detector, the mixture of peptide fragments in the sample appears as a unique spectral output, with m/z ratio values displaying the peptide size and the height of the peak (intensity) indicating the abundance of a given peptide fragment (Lovrić, 2011). This spectral output is a peptide mass fingerprint (PMF) for a sample, which can be compared to databases of theoretical PMFs for proteins based on known cleavage sites for trypsin-digested proteins (Aebersold and Mann, 2003). To confirm matches to theoretical PMF databases, individual peaks from a sample PMF can be selected for further fragmentation using

tandem mass spectrometry (MS/MS) to generate a peptide fragment fingerprints (PFF) (Lovrić, 2011). These provide additional information regarding the amino acid composition of each peptide (Tomanek, 2011).

The MALDI-TOF/TOF mass spectrometer used in this study includes two TOF analyzers separated by a collision cell (Suckau et al., 2003). A single peak in the PMF is selected by the first TOF analyzer (high abundance peptides of one m/z ratio) and fragmented using collision-induced dissociation (CID) (Suckau et al., 2003). Fragmented ions are separated in the second TOF analyzer to determine the amino acid sequence of the selected peptide fragment (PFF) (Suckau et al., 2003). Using these two steps, protein identifications are more accurate due to the unlikely occurrence of both a shared PMF and PFF (Aebersold and Mann, 2003).

With both PMFs and PFFs for a given sample, experimental data are compared to theoretical tryptic digestions (Lovrić, 2011). Typically, protein or expressed sequence tag (EST) databases are searched using a program (MASCOT, Matrix Science Inc., Boston, MA, USA) that compares experimental data to determine whether an existing protein or nucleic acid shares peptide matches with the sample (Aebersold and Mann, 2003). The likelihood of detecting a positive match within sequence databases depends in a large part on the extent to which the organism's genome has been sequenced (Dowd, 2012). Using a quality sequence database, a pure sample, and broad search parameters that accommodate m/z differences due to certain PTMs or sequence differences, probability-based matching calculates the highest score for a significant match between the search spectra and the available sequence databases (Aebersold and Mann, 2003). Together,

MS/MS spectra comprised of both the PMF and PFFs typically provide high resolution for discriminating a truly significant match from one due to random chance (Aebersold and Mann, 2003).

To determine a protein identification with a high level of confidence, the MASCOT search software uses a molecular weight search engine (MOWSE) algorithm to determine the likelihood that a match is found due to chance alone (Perkins et al., 1999). A sequence match with a MOWSE score above a significance threshold (p-value < 0.05) and matching two or more peptide fragments typically indicates a high probability of a correctly matched sequence (Perkins et al., 1999). In this experiment, databases used in the MASCOT search included the following: *Mytilus* protein (7,844 sequences), *Mytilus* EST (409,254 sequences), *Mytilus edulis* EST (447,720 sequence), Mollusca EST (1,147,871 sequences), and NCBI Metazoa (last update: April 2016; 9,560,026 sequences). Since many databases searched by MASCOT contain sequences that are not fully annotated, the sequence matches are typically run through NCBI Basic Local Alignment Search Tool (BLAST) to identify proteins based on homology with previously annotated and reviewed sequences.

Study objectives

Intertidal mussels are increasingly used for biomonitoring purposes (AquaDect; Benedetti et al., 2015; Campos et al., 2012) and as sentinel species for climate change effects in coastal ecosystems (Helmuth et al., 2011; Lesser, 2016; Lesser et al., 2010; Tomanek, 2008). For this reason, it is vital that research establishes an understanding of

how these organisms respond to a consistently fluctuating environment with predictable modulations of behavior and physiology (Connor and Gracey, 2011; Tomanek, 2011). Proteomics has emerged as a useful tool for exploring the mechanistic underpinnings of the cell that relate to whole-organism physiology (Tomanek, 2014). Given the variable results of studies documenting the relative importance of circadian (Connor and Gracey, 2011; Mat et al., 2012) and circatidal (Connor and Gracey, 2012; Gracey et al., 2008; Zaldibar et al., 2004) cycles on intertidal bivalves, it is important to address this question using proteomics to characterize these rhythms at the level of the functional cellular phenotype. Due to the importance of gill tissue for both feeding and respiration in *M. californianus*, we hypothesize that the tidal cycle exerts a larger influence on the rhythmic fluctuations of the proteome in this tissue than has been previously suggested by transcriptomic studies (Connor and Gracey, 2011). This rhythmic variation in the proteome is expected to contain elements of the anaerobic response to aerial emersion (Connor and Gracey, 2012; Shick et al., 1986), an anticipatory response to oxidative stress during rapid reoxygenation (Ellington, 1983; Hermes-Lima et al., 2015; Rivera-Ingraham et al., 2013), a drastic response of aerobic metabolism to reoxygenation and food availability (Saurel et al., 2007; Thompson and Bayne, 1972), and temporal compartmentalization of redox-sensitive processes (Connor and Gracey, 2011; Gracey et al., 2008; Reinke and Gatfield, 2006).

CHAPTER II. MANUSCRIPT

Abstract

The intertidal zone is a dynamic environment that fluctuates with the 12.4-h tidal and 24-h light/dark cycle to predictably alter food availability, temperature, air exposure, wave action, oxygen partial pressure, and osmotic conditions. Intertidal sessile bivalves exhibit behavioral or physiological changes to minimize the persistent challenges of fluctuating environmental conditions, such as adjusting gaping behavior and heart rate. At the cellular level, transcriptomic studies on mussels' baseline circadian and circatidal rhythms have determined that the circadian rhythm is the dominant transcriptional rhythm. However, as proteins reflect the basic molecular phenotype of an organism and their abundance may differ greatly from that of mRNA, these methods could fail to detect important cyclical changes in the proteome that cope with the regular stress of tidal rhythms. For this study, we acclimated intertidal *Mytilus californianus* to circadian (12:12 h light/dark cycle) and circatidal (6:6 h tidal cycle) conditions in a tidal simulator and sampled gill tissue from mussels every 2 h for 48 h for proteomic analysis. Approximately 86% of the proteins that were detected exhibited rhythmicity over the time course. The circadian cycle primarily determined the cyclic abundance of energy metabolism proteins, pivoting around the transition to the nighttime high tide. The tidal cycle contributed to alterations in cytoskeletal components, ER protein processing and vesicular trafficking, extracellular matrix and immune proteins, and oxidative stress and chaperoning proteins. We also found evidence that post-translational modifications may be important for driving these rhythms, as acetylation and phosphorylation motifs were enriched in the rhythmic proteins and we identified rhythms in elements of methylation,

mitochondrial peptide processing, and acylation. These dynamic changes in proteins across numerous functional categories indicate that the combination of circadian and tidal cycles drive complex cellular changes to coordinate processes in a changing environment. This variation clearly shows that differential expression studies and biomonitoring efforts cannot assume a static baseline of cellular conditions in intertidal mussels.

Introduction

Coastal marine ecosystems that are of vital importance for human food supply and for maintaining biodiversity face increasing pressure from anthropogenic climate change altering levels of dissolved oxygen, pH, temperature, and oxygen-minimum zones (Harley et al., 2006; IPCC, 2015; Somero et al., 2016). These drastic environmental changes are forcing organisms to shift biogeographic ranges, adapt, or disappear (Harley et al., 2006; Tomanek, 2012). The unprecedented rates of these environmental changes test the physiological tolerance of organisms, and a current focal point of climate change research is to identify the resilience of organisms to changes across multiple levels of biological organization (Bernhardt and Leslie, 2013; Harley, 2008; Lesser, 2016; Somero et al., 2016; Todgham and Stillman, 2013; Tomanek, 2008; Tomanek, 2012). The characterization of physiological responses to climate change are important for (1) understanding the mechanisms of physiological resilience, (2) helping to develop accurate projections for population responses to different scenarios, and (3) developing a knowledge base of population status indicators and stress threshold values (Somero et al., 2016).

Typically, stress response experiments attempt to isolate one or two causative factors in the environment, comparing a control group at stable conditions while the factors of interest are adjusted for experimental groups (Dowd and Somero, 2013; Fitzgerald-Dehoog et al., 2012; Halpin et al., 2004; Tomanek et al., 2012). The physiological responses of the organisms are then attributed to the experimental alterations and extrapolated to natural conditions to predict an organism's response to future environmental changes.

Often times, the controlled conditions of an experiment may not accurately translate to natural conditions. Dynamic environments regularly influence organisms' physiology and behavior. Any inference about the natural effects of environmental changes on these organisms can potentially be skewed due to a study's assumption of a static, oversimplified baseline (Tessmar-Raible et al., 2011). The natural variations seen in organisms, particularly in a field setting, can limit the interpretation of results collected at only one time point (Logan et al., 2012). This problem is particularly apparent in biomonitoring programs that consider specific markers of environmental stress in sentinel organisms. Understanding how natural environmental variability affects specific diagnostic markers for pollutants in these programs is essential for generating a baseline for marker fluctuations to avoid false-positive detection of pollution stress (Garcia-March et al., 2016; Hagger et al., 2006; Livingston, 1976; Luedeking and Koehler, 2004; Vidal-Liñán and Bellas, 2013). For example, *Mytilus galloprovincialis* are commonly used to monitor water quality, but the baseline enzyme activities for the biomarkers glutathione S-transferase (GST) and catalase (CAT) in their gill tissue were shown to vary between individuals sampled from different tidal heights (Vidal-Liñán and Bellas, 2013).

The intertidal zone is a particularly dynamic environment that regularly influences the physiology of its inhabitants. The 12.4-hour circatidal cycle of high and low tides and the 24-hour circadian light/dark cycle predictably alter food availability, temperature, aerial emersion, pressure changes, water current, dissolved oxygen, and salinity (Naylor, 2010; Tessmar-Raible et al., 2011). The limited mobility of sessile intertidal mussels (*Mytilus* spp.) in the intertidal zone requires that they cope with the environmental fluctuations to which they are exposed through behavioral (Bayne et al., 1976) and physiological changes (Connor and Gracey, 2012; Place et al., 2012; Shick et al., 1986; Tagliarolo et al., 2012). The *Mytilus* gill is particularly sensitive as the interface with the environment where the ciliated organ pulls water through the mantle cavity across the gills, simultaneously extracting oxygen and food particles from the water (Doeller et al., 1993). This metabolically active organ consumes up to half of the total oxygen for the mussel, with 90% of the oxygen supporting the ATP demand of the ciliated cells (Doeller et al., 1993). For this reason, the gill tissue is particularly important for synchronization with the tidal environment to both minimize the predictable dangers of high temperatures, hypoxia, oxidative stress, and desiccation and to maximize the energetic gains during limited feeding opportunities.

The transcriptomic and metabolomic methods used to study the circadian and circatidal rhythms in these intertidal mussels have provided invaluable information about cellular-level changes in a dynamic environment (Connor and Gracey, 2011; Connor and Gracey, 2012; Gracey et al., 2008). However, mRNA expression may fail to predict up to half of the variation in the proteome—the complete pool of proteins in a tissue (Feder and Walser, 2005). Likewise, a recent study on circadian rhythms in the mouse liver have

shown that 20% of cycling proteins showed no corresponding rhythm to the transcript, and half of those proteins with a matching rhythmic transcripts showed a delayed cycle of over six hours (Robles et al., 2014). Proteomics studies in intertidal mussels have explored responses to numerous stressors, including oxidative stress (McDonagh et al., 2006; Tomanek, 2015), hypoxia (Fields et al., 2014), hyposalinity (Tomanek et al., 2012), and high temperature (Fields et al., 2012; Tomanek and Zuzow, 2010). Given that proteins reflect the basic functional level of the molecular phenotype, there is a great need to characterize the proteomic changes that parallel the transcriptome in an organism that is regularly exposed to both circadian and circatidal cycles.

This study sought to uncover these rhythmic changes in protein abundance in the California Mussel (*Mytilus californianus* Conrad, 1837) during a simulation of circadian and circatidal rhythms. *M. californianus* is a native, sessile bivalve of the mid-intertidal zone that ranges from northern Mexico to the Aleutian Islands (Morris et al., 1980) and is frequently used as a subject for intertidal stress response studies (Dowd et al., 2013; Fitzgerald-Dehoog et al., 2012; Harley, 2008; Logan et al., 2012). Multiple studies have presented results assessing the relative importance of circadian (Connor and Gracey, 2011; Mat et al., 2012) and circatidal (Connor and Gracey, 2012; Gracey et al., 2008; Zaldibar et al., 2004) cycles on intertidal bivalves, making it important to address the contribution of the proteome to the functional cellular phenotype. Due to the importance of gill tissue for both feeding and respiration in *M. californianus*, we hypothesized that the tidal cycle exerts a larger influence on the rhythmic fluctuations of the proteome in this tissue than has been previously suggested by transcriptomic studies (Connor and Gracey, 2011). This rhythmic variation in the proteome was expected to contain elements

of the anaerobic response to aerial emersion (Connor and Gracey, 2012; Shick et al., 1986), signs of metabolic depression and ATP-saving regulation during emersion (Ivanina et al., 2016; Shick et al., 1986; Storey and Storey, 2004), an anticipatory response to oxidative stress during rapid reoxygenation (Ellington, 1983; Hermes-Lima et al., 2015; Rivera-Ingraham et al., 2013), an activation of aerobic metabolism in response to reoxygenation and food availability (Saurel et al., 2007; Thompson and Bayne, 1972), and temporal compartmentalization of redox-sensitive processes (Connor and Gracey, 2011; Gracey et al., 2008; Reinke and Gatfield, 2006).

Results and discussion

Protein detection and rhythmicity analysis

This study characterized the rhythmic fluctuation of protein abundances in the gill tissue of *M. californianus* following a four-week acclimation to a 12 h light/dark cycle and 6 h cycle of alternating high and low tides. Gill tissue samples were collected during a continuation of the acclimation regime from six individuals every two hours for 48 h beginning one hour after the simulated switch to high tide and daylight. This resulted in 24 sampling time points and 144 individual samples encompassing four high/low tide series and two light/dark cycles. Samples were processed for proteomic analysis using 2D gel electrophoresis and image analysis followed by protein identification using tandem mass spectrometry. A total of 606 protein spots were detected on the fusion image, which includes all 144 2D gels.

Using the mean normalized spot volume as a quantitative measurement of relative protein abundance, each of the 606 spots were evaluated for rhythmic patterns across the 48 h time series (Fig. 4) using the JTK_CYCLE algorithm (Hughes et al., 2010) with a false discovery rate cutoff of $q < 0.05$, resulting in 279 proteins with a significant rhythm (Benjamini and Hochberg, 1995). A second rhythmicity analysis using the program RAIN (Thaben and Westermark, 2014) evaluated protein abundance rhythms with asymmetrical rising and falling phases around the peaks identified 479 proteins (Fig. 4A; $q < 0.05$). Of these, 234 were shared with the JTK_CYCLE analysis, leaving 45 proteins that were uniquely deemed significant using JTK_CYCLE. Between the two analyses, a total of 524 (86%) of the total 606 proteins delineated on the fusion image were found to show rhythmic abundance patterns (Fig. 6A). Of these 524 significant proteins, 406 (77%) were successfully identified using mass spectrometry (Fig. 5A and 5B; Table S1).

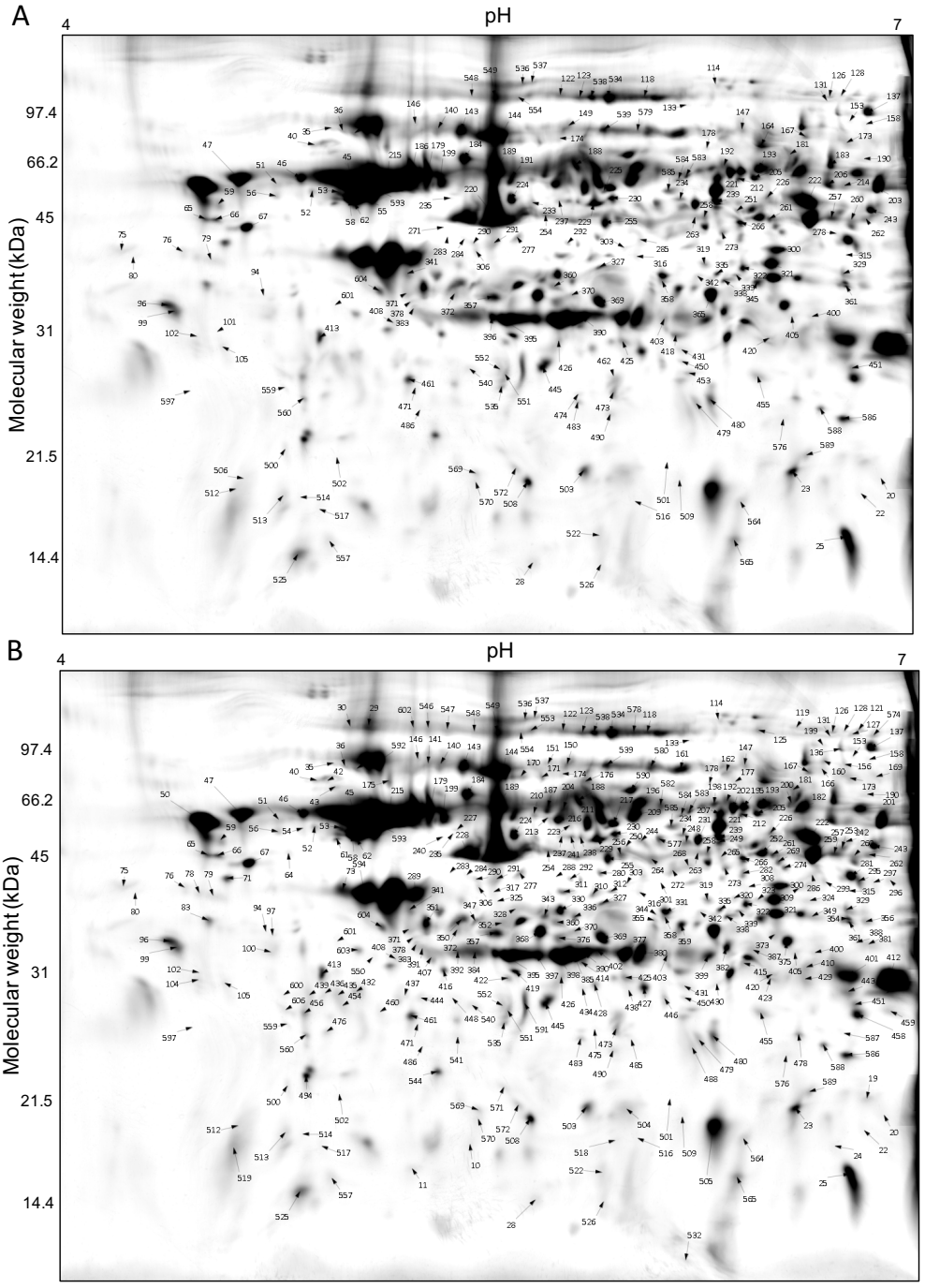

Figure 4. 2D GE fusion image composite of 144 individual gill tissue samples. Labels show significantly identified rhythmic protein spots from (A) JTK_CYCLE (212 spots) and (B) RAIN (379 spots).

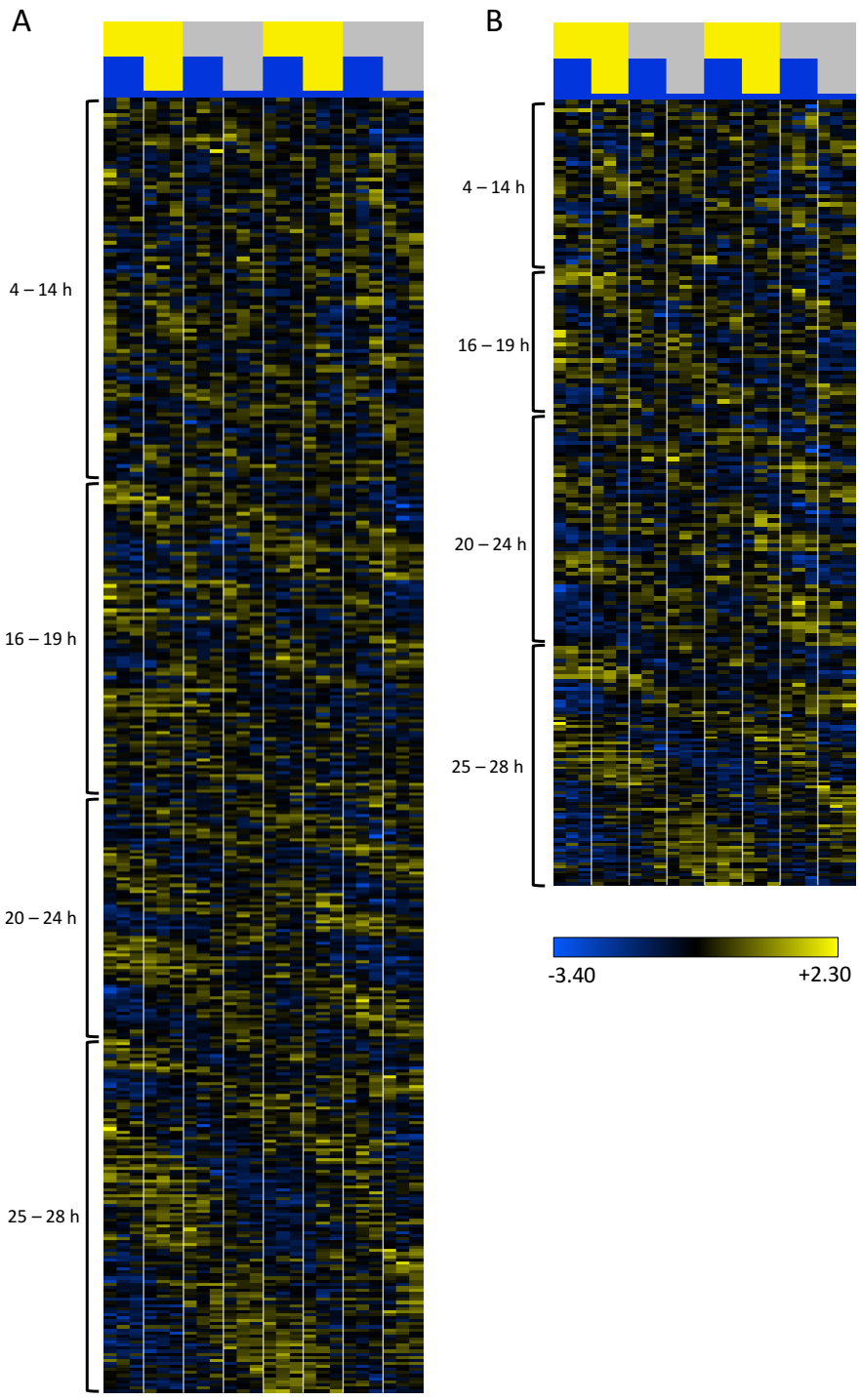

Figure 5. Oscillations in the proteome were identified with period lengths ranging from 4 – 28 hours. Heat maps for significantly identified rhythmic proteins using (A) RAIN and (B) JTK_CYCLE ordered first by period length then by phase. Period length ranges are

shown to the left of the heat map and tank conditions over the 48 h sampling time course are shown above, with tidal height shown in blue and light/dark shown in yellow and gray, respectively. Each row depicts an individual protein and columns represent the mean standardized Log_2 ratio of the normalized spot volume for a time point (6 individuals included per column). Increased protein abundance is shown in yellow and decreased abundance in blue.

Focusing on the proteins with positive identifications, the period and phase parameters estimated by the JTK_CYCLE algorithm provide insight into the timing patterns in these cycling proteins. The period length (h) approximates the time span between recurring peaks in the cycling abundance pattern while the phase (h) indicates when the initial abundance peak occurs in the time course. Both analyses searched period lengths ranging from 4 – 28 h for rhythmicity. Based on the period length alone, both RAIN and JTK_CYCLE were enriched for period lengths around 8 h, 18 h, 24 h, and a substantial number of cycling proteins with a 28 h period (Fig. 6B and 6C). This distribution of period lengths differs somewhat from the transcriptomic evaluation of *M. californianus* gill in a similar tidal and light/dark simulation, where the predominant period lengths were 12 h and 24 – 28 h (Connor and Gracey, 2011). However, a study evaluating rhythmic transcripts in mouse liver across all period lengths uncovered the typical circadian period length of approximately 24 h along with two previously undocumented sub-circadian period lengths around 8 h and 12 h (Hughes et al., 2009). Furthermore, a recent study of protein half-lives across subcellular compartments in

HeLa cells found that overall protein turnover showed a bimodal distribution around 7 – 12 h and 18 – 28 h (Boisvert et al., 2012). Therefore, the overall distribution of period lengths for this proteomic dataset may share more in common with existing rhythms documented in terrestrial organisms than with the tidal environment.

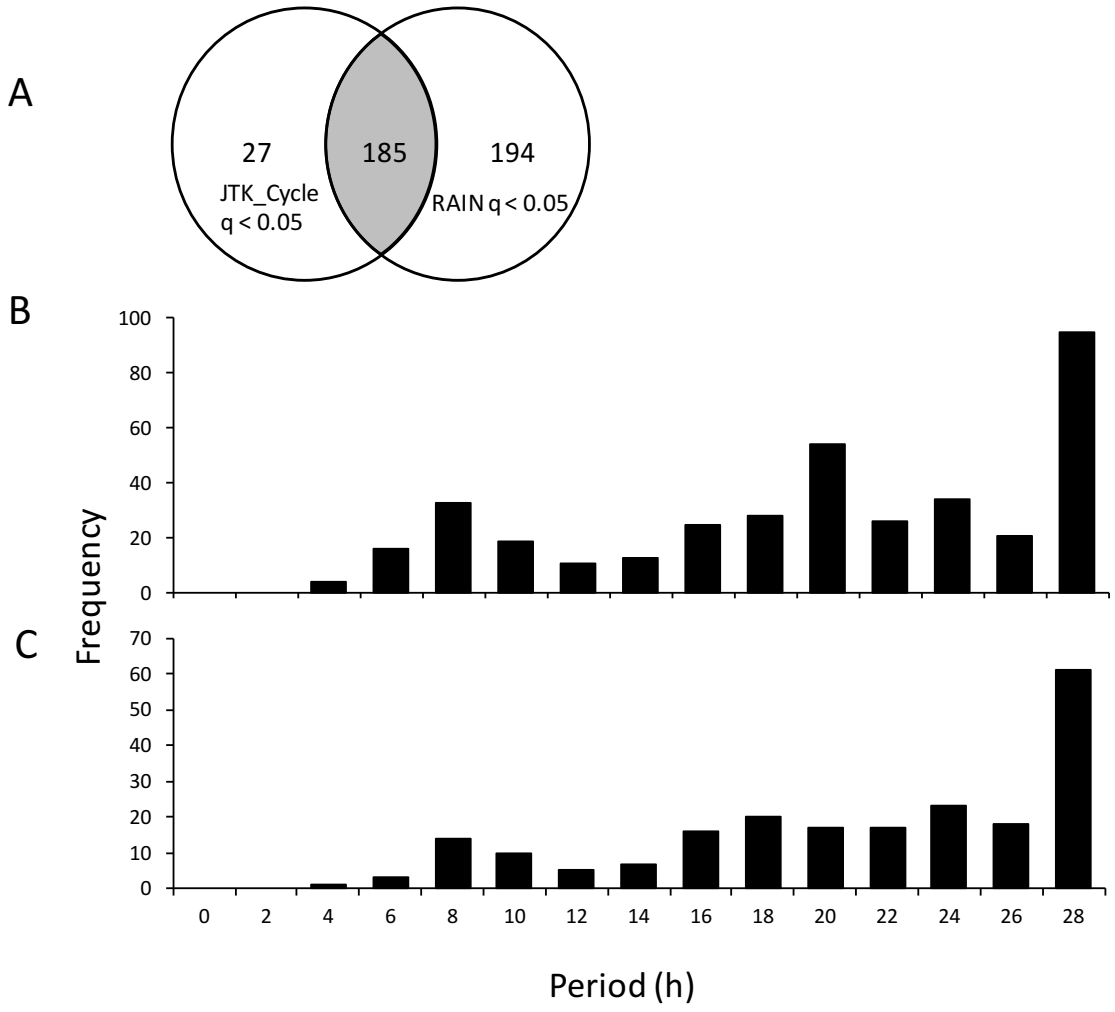

Figure 6. Comparison of rhythmicity analyses using JTK_CYCLE and RAIN. (A) Out of the total 406 significantly rhythmic and identified proteins, 194 were uniquely detected by RAIN and 27 by JTK_CYCLE, with 185 shared between the two. (B) Distribution of JTK_CYCLE estimates of period lengths (h) for significantly cycling proteins identified by RAIN and (C) JTK_CYCLE.

To discern the timing of the phase peaks in cyclic protein abundance, periods can be binned by three discrete categories: tidal (4 – 14 h period), intermediate (16 – 19 h), and daily (20 – 28 h). RAIN detected additional tidal proteins that were not included in JTK_CYCLE corresponding with a peak phase around 2 h (in the middle of the first high tide) and around 8 h (middle of the first low tide) (Fig. 7A). For the intermediate period lengths, both programs identified a minor phase peak at 2 h and a prominent peak at 12 h, corresponding with the shift to high tide and darkness (Fig. 7B). However, the intermediate period length means that the following peak would occur 5 to 8 h earlier in the second day than the initial phase peak. The phases for the daily period proteins were more widely distributed, but peaks occurred in both analyses from 4 – 8 h (midday) and 18 h (midnight). RAIN detected an additional phase peak at 12 h (beginning of nighttime high tide) (Fig. 7C).

The phase enrichment of circadian proteins agreed with current literature on the circadian timing of peaks in protein abundance. Mauvoisin et al. (2014) found a similar enrichment of circadian phases in the mouse liver proteome around 5 h and 18 h using the same 12:12 h L:D entrainment conditions. An 18 h phase peak enrichment for circadian proteins is also predicted by a model using rhythmic protein degradation to account for cyclic protein abundances (Lück et al., 2014). This generally bimodal distribution of circadian phases was further supported by a coordinated study of the mouse liver transcriptome and proteome (Robles et al., 2014). Studies of the circadian mouse liver proteome agree that a large majority of the cyclic protein abundances could be explained by a 5 – 6 h delay between the corresponding transcript and protein peaks (Mauvoisin et al., 2014; Robles et al., 2014). This relationship may also be evident in *M. californianus*

gill tissue, where a transcriptomic analysis using the same experimental time course as this proteomic study showed a circadian transcripts oscillating with bimodal phases between 2 – 5 h and 12 – 14 h (Connor and Gracey, 2011). Meanwhile, circadian proteins in this study showed phase bimodality around 4 – 8 h and 16 – 20 h, agreeing with a 5 – 6 h delay between peak transcript and protein abundance (Fig. 7C).

As previously mentioned, the period length distribution for tidal proteins (4 – 14 h) did not appear to align closely with those for transcripts identified in the Connor and Gracey (2011) study. The tidal transcripts were found to follow a bimodal phase distribution around 2 h and 9 h, corresponding with the middle of the high tide submergence and middle to late low tide (Connor and Gracey, 2011). In this study, proteins with tidal period lengths showed similar phase enrichment, but phase peaks were more evenly distributed across 0 – 10 h (Fig. 7A).

An intermediate period length for rhythmic proteins was found ranging from 16 to 19 h. The phase enrichment for these proteins showed a similarly moderate peak around 2 h between JTK_CYCLE and RAIN. Both analyses also uncovered a large phase peak at 12 h, with RAIN doubling the number of rhythmic proteins detected with a 12 h phase (Fig. 7B). This 12 h phase peak was preferentially detected by RAIN in the intermediate period length as well as in the daily period lengths (Fig. 7B and 7C). This intermediate period length may indicate the presence of responsive abundance peaks rather than cyclical predictive rhythms, resulting in peaks that pivot around transitions such as the day-night interphase. Furthermore, Connor and Gracey (2011) found that numerous tidal transcripts were susceptible to the influence of higher temperatures, suggesting that these

intermediate rhythms could arise based on the degree of heating experienced by the mussels during the midday aerial exposure.

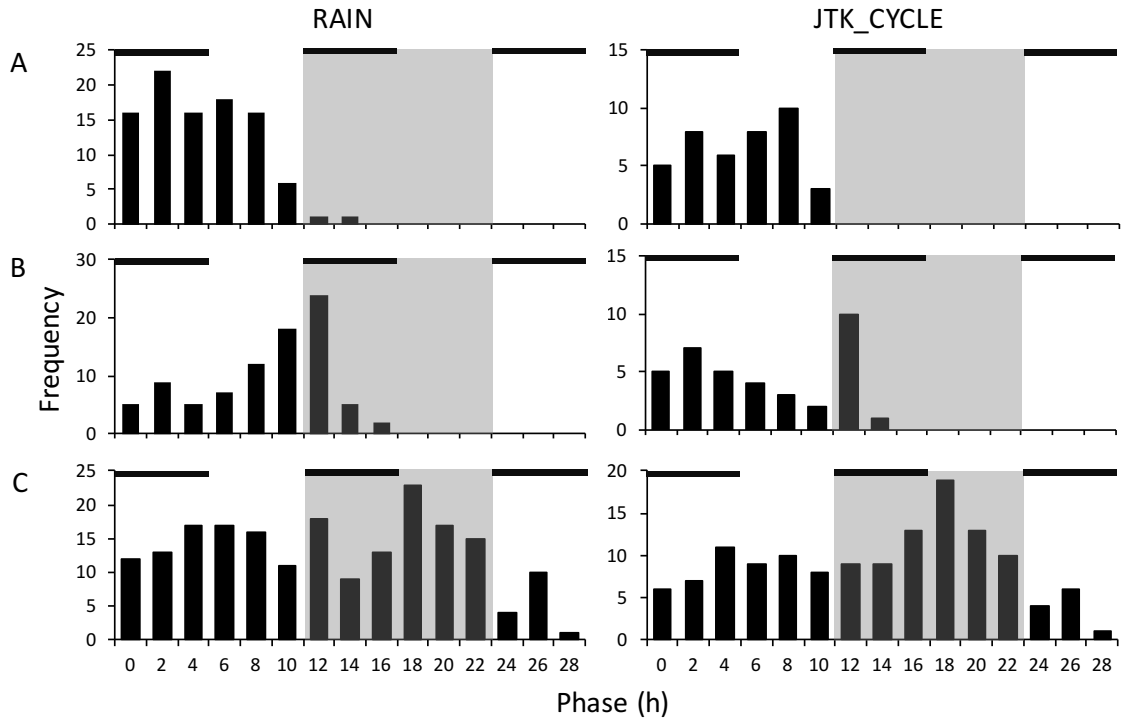

Figure 7. Phase distributions of significantly identified cycling proteins using the JTK_CYCLE and RAIN analyses. Simulated conditions at each time point are shown with high tide as black bar above and darkness as gray shading behind. Phase distributions are separated by period length of (A) 4 – 14 h, (B) 16 – 19 h, (C) and 20 – 28 h.

The similarity in the overall distributions of the rhythmic proteins identified by JTK_CYCLE and RAIN support previous examples of their compatibility (Thaben and Westermark, 2014; Wang et al., 2015). RAIN effectively doubled the detection of rhythmically expressed proteins in the data that may encompass important biological functions (Thaben and Westermark, 2014). However, the 26 proteins that were uniquely

identified using JTK_CYCLE demonstrate a slight advantage for this program when evaluating a data series with symmetrical rising and falling abundance around the peak (Thaben and Westermark, 2014). Furthermore, the period, phase, and amplitude parameter estimates using JTK_CYCLE help to organize, categorize, and evaluate the rhythmicity output (Hughes et al., 2010; Wang et al., 2015). Meanwhile, the inclusive and adaptable analysis used by RAIN greatly enhances the ability to detect rhythms in proteomic data, which typically suffer from lower accuracy and lower amplitude changes relative to transcript abundance changes (Mauvoisin et al., 2014; Thaben and Westermark, 2014).

Functional categories

Aerobic metabolism

Proteins involved in oxidative phosphorylation primarily followed a circadian cycle peaking at night. Multiple F1 domain subunits of ATP synthase followed a general circadian cycle peaking during and after the day-night transition, particularly the δ (506, 512, 519) and α (206) subunits. Likewise, both complex II (succinate dehydrogenase flavoprotein subunit (539)) and complex III (cytochrome b-c1 reductase subunit 2 (UQCRC2; 224)) of the electron transport system (ETS) peaked during the evening submersion (Fig. 8A). However, some ATP synthase subunits deviated from this pattern. For example, two ß subunits showed a trend toward a midday peak (53, 58) along with one α subunit (203). Most subunits showed a high degree of noise with minor abundance spikes correlating with tidal shifts, such as one ß subunit (62) peaking with low tides while others (53, 206, 437) spiked during high tides (Fig. 8B). The responsiveness of these ATP synthase subunits may reflect the importance of controlling the proton

gradient during hypoxia. Because ATP synthase may act in reverse during hypoxia, hydrolyzing ATP to pump H^+ into the intermembrane space and maintain the proton motive force (St-Pierre et al., 2000), the reorganization of subunits seen in this study may reflect a functional change to limit the occurrence of the ATP-consuming process during metabolic depression (Brand, 2000). Interestingly, the average JTK_Cycle period and phase outputs for all components of oxidative phosphorylation show a predominant circadian (24.7 h) period and a phase peak of 10.8 h, at the shift to the evening high tide. This likely reflects the timing of greatest activity in these intertidal mussels, as *Mytilus* exhibit primarily nocturnal valve gaping activity (Gnyubkin, 2010; Robson et al., 2010b).

The reducing equivalents (NADH and $FADH_2$) for the ETS are primarily generated during the tricarboxylic acid (TCA) cycle. Many proteins in this pathway were found to follow a circadian rhythm of peak abundance matching oxidative phosphorylation, just prior to the evening high tide shift. These proteins included aconitase (158), NAD^+-dependent isocitrate dehydrogenase (IDH; 292), 2-oxoglutarate dehydrogenase (119, 126), succinate dehydrogenase (539), and malate dehydrogenase (273). These TCA cycle proteins peaked alongside the glycolytic proteins phosphoglycerate kinase (222) and enolase (585) (Fig. 8C). This circadian peak timing for proteins involved in oxidative metabolism corresponds closely with the finding that most mitochondrial proteins tended to peak during the evening-night interphase in the liver of nocturnally active mice (Robles et al., 2014).

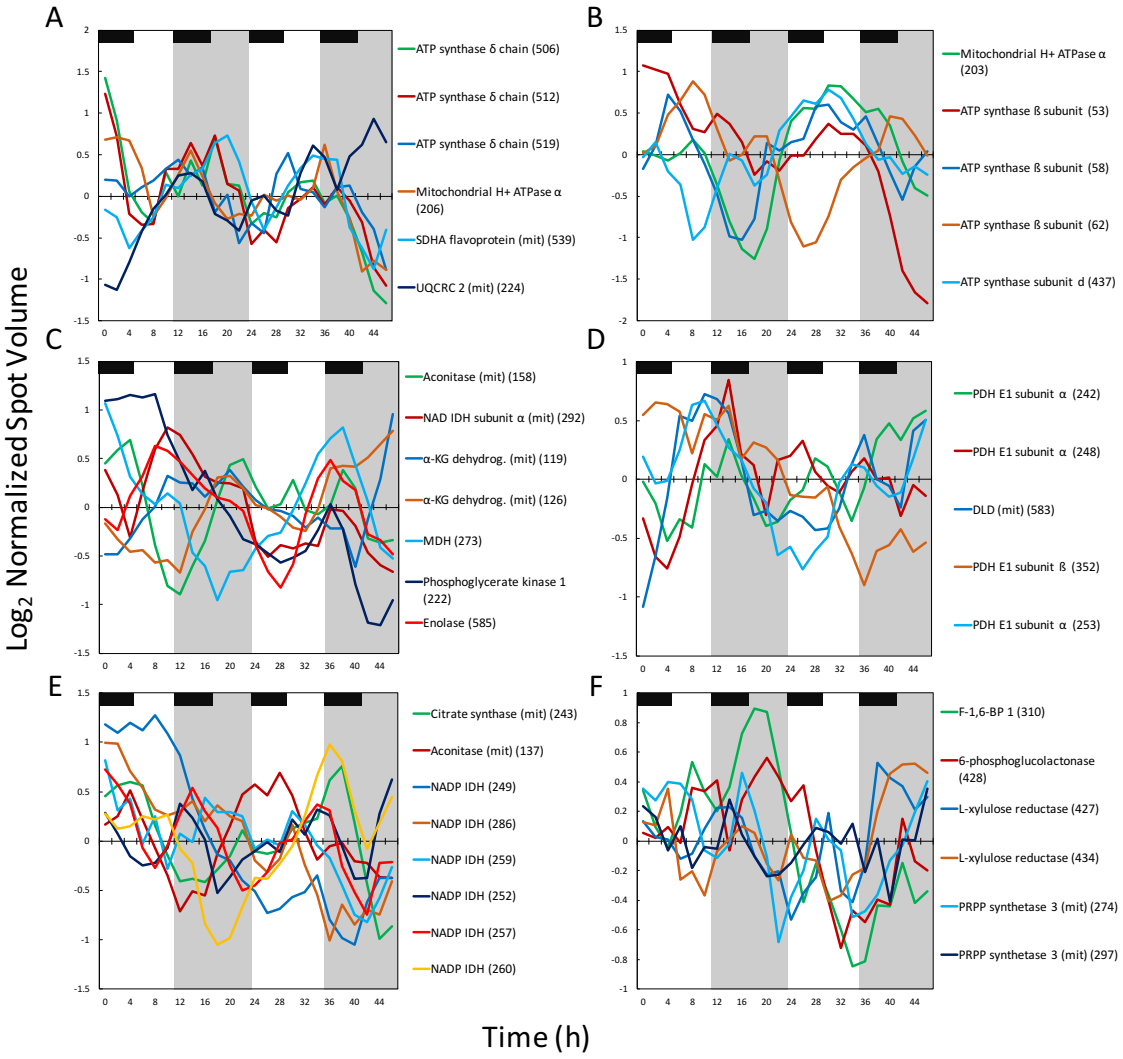

Figure 8. Moving average expression profiles for individual protein data across the 48 h time series for identified aerobic metabolism proteins. Simulated conditions at each time point are shown with high tide as black bar above and darkness as gray shading behind.

Pyruvate dehydrogenase (PDH) transcript abundance has been shown to follow oxygen consumption rates, demonstrating a close link between active feeding and the integration of pyruvate into the TCA cycle (Manoogian and Panda, 2016). In the presence

of food, *Mytilus* oxygen consumption rates rapidly increase to accommodate the feeding activity and this metabolic rate remains elevated even after the removal of food in order to process the nutrients (Riisgård et al., 2003; Thompson and Bayne, 1972). In this study, some PDH E1 α subunits (242, 248) followed high-tide cycles while others followed the circadian day-night transition, including dihydrolipoyl dehydrogenase (DLDH; 583) and two PDH isoforms (352, 253) (Fig. 8D). This pattern agrees with previous research on responses to metabolic depression in bivalves (Russell and Storey, 1995). The multiple PDH isoforms seen in this study could be due to the reversible phosphorylation that inactivate the enzyme to both reduce metabolic flux and divert metabolites toward anaerobic pathways (Russell and Storey, 1995). Interestingly, in mouse liver, cyclic protein abundance for PDH was found to be dependent on the presence of intact PER1/2 genes (Neufeld-Cohen et al., 2016). Therefore, while the tidally fluctuating isoforms may reflect a short-term response to intervals of metabolic depression and feeding in *Mytilus* gill tissue, the connection of circadian isoforms to clock gene oscillations may reflect findings that nocturnal activity of *Mytilus* occurs regardless of food entrainment (Gnyubkin, 2010; Robson et al., 2010b).

In the present study, we detected circadian daytime peaks in peroxisomal fatty acid binding protein 6 (516), acyl-CoA oxidase (173) and long-chain acyl-CoA ligase (166), suggesting a preparatory timing for the early oxidation and entry of long-chain fatty acids into the mitochondria prior to the evening activity (Fig. 9A). Following the transition to darkness, there was a distinct circadian peak during submersion in medium-chain acyl-CoA dehydrogenase (251) and electron transfer flavoprotein subunit α (359) (Fig. 9B). This suggests that the evening submersion, like glycolytic, TCA, and ETS

proteins, is also the peak time for fatty acid oxidation (FAO). This timing of FAO during an active feeding period appears in direct opposition to previous studies on circadian timing in lipid use.

In mouse liver studies, certain lipid metabolic proteins exhibit a distinct circadian rhythm, such as the rate-limiting carnitine palmitoyl transferase (CPT) that determines the transport of fatty acids into the mitochondria (Neufeld-Cohen et al., 2016). By isolating mitochondria and assessing rhythmic protein abundances and respiration rates with different substrates, Neufeld-Cohen et al. (2016) found that the oscillations in the rate-limiting enzymes PDH and CPT were dependent on functional PER1/2 genes. The strong circadian cycle of CPT, which peaked in the middle of the night around Zeitgeber Time (ZT) 17 (or 17 hours after the lights-on stimulus), indicates that the carnitine conjugation of long-chain fatty acids to transport them into the mitochondria occurs during this evening time period. However, several components of β-oxidation, such as acyl-CoA dehydrogenases (ACADS) peaked around midday at ZT 4 (Neufeld-Cohen et al., 2016). The authors suspected that this rhythm of fatty acid transport at night and oxidation during the day was coordinated with activity of mice, temporally separating lipid oxidation during the daytime "rest" period and carbohydrate use during the active nighttime period (Neufeld-Cohen et al., 2016). On the other hand, the plasticity of this process may be visible in contrasting findings that fatty acid oxidation (FAO) peaked along with NAD^+ levels at the end of the rest period in mice, just prior to nighttime (Peek et al., 2013).

Peek et al. (2013) found that NAD^+-dependent SIRT3 deacetylation of multiple enzymes, including medium chain acyl-CoA dehydrogenase, drives the late-daytime rhythm of FAO found in their study, with increased levels of acetylation at night decreasing the enzyme's activity. In mussels, Connor and Gracey (2012) found a prominent pattern of carnitine conjugates accumulating during low tide, indicating that tidal cycles may exert an influence on the rate-limiting enzyme CPT. This poses interesting questions as to why the timing of proteins across multiple metabolic pathways in *M. californianus* coincides so closely with the evening high tide despite the clear separation of substrate use seen in these nocturnal mice, including an opposite pattern of FAO to that seen in this study. The limited feeding opportunities in tidally-acclimated mussels may provide a clue, as a recent lipidomics analysis compared mice fed *ad libitum* to those with nighttime-restricted feeding to find a complete inversion of the peak time of mitochondrial lipid accumulation (Aviram et al., 2016).

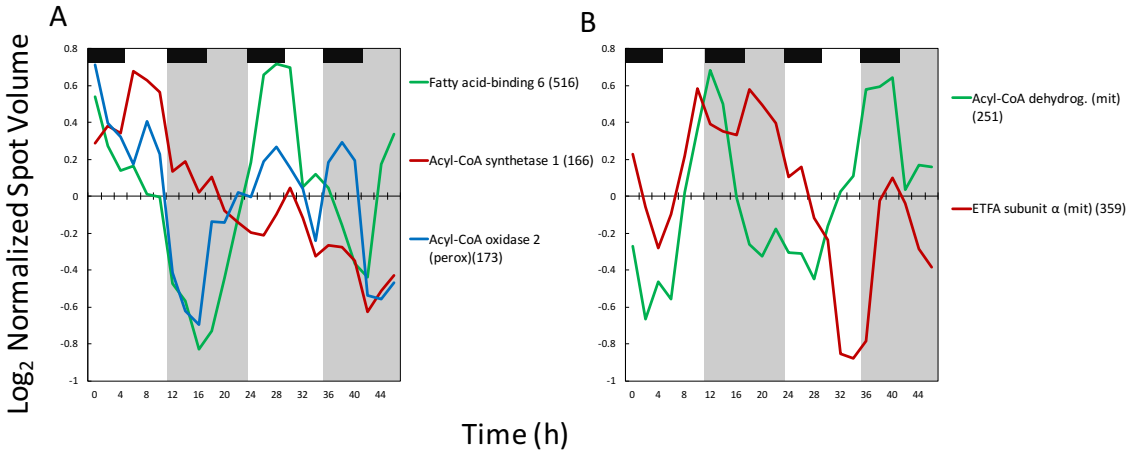

Figure 9. Moving average expression profiles across the 48 h time series for proteins involved in fatty acid metabolism. Simulated conditions at each time point are shown with high tide as black bar above and darkness as gray shading behind.

A subset of TCA cycle proteins show peaks in the middle of the day, often in addition to evening peaks as seen with the rest of the TCA cycle proteins. These proteins appear to be involved in the early TCA cycle reactions to generate 2-oxoglutarate while forming the anabolic reducing equivalent NADPH. These midday peaks are visible in citrate synthase (243), aconitase (158, 137), and $NADP^+$-dependent IDH (249, 286, 259), as well as two PDH E1 subunits (248, 242). These daytime peaks occur in addition to the evening peaks, either resulting in shorter period lengths, as with PDH and citrate synthase, or through the interchange of isoforms peaking at different times, as with IDH (252, 257, 260) (Fig. 8E).

The coordination between glycolytic and TCA cycle proteins in the early evening submersion as well as minor daytime peaks indicates at least a partial reliance on carbohydrate metabolism at these times. However, evening also appeared to be the primary time for anabolic processes, as suggested by the changes to the pentose phosphate pathway (PPP). This pathway serves multiple purposes, such as generating ribose-5-phosphate for nucleotide synthesis and NADPH for anabolic reactions and a reducing equivalent to scavenge reactive oxygen species (ROS). The diversion of metabolites from glycolysis to the PPP instead of towards the TCA cycle is most apparent in the matching peaks of fructose-1,6-bisphosphatase (310) and 6-phosphoglucolactonase (428) during the evening low tide. Two isoforms of L-xylulose reductase (427, 434) also peaked during daytime and nighttime high tides (Fig. 8F). While this enzyme generates NADPH and L-xylulose for the PPP, it may peak during high tide to catabolize the sugar alcohol xylitol that is documented in marine algae (Chu et al., 1982). The evening contribution to the PPP is an intuitive use of favorable energetic conditions for anabolic

pathways as NADPH is used for the synthesis of fatty acids, nucleic acids, and proteins. The peaks in phosphoribosyl pyrophosphate synthetase 3 (PRPP synthetase 3; 274, 297) during daytime and evening high tides suggests a siphoning of ribose-5-phosphate for nucleotide synthesis, potentially to accommodate the increased need for the carbohydrate unit of adenosine to meet increasing ATP demand during submersion (Dudognon et al., 2013) (Fig. 8F). However, the daytime peak in NADPH synthesis may primarily supply a reducing equivalent for scavenging ROS accumulated during the potentially stressful midday low tide.

Oxidative stress

Evidence for a rhythmic abundance pattern occurred for several ROS scavenging proteins. The daytime peak in NADPH synthesis was also accompanied by predominantly daily peaks in S-formylglutathione hydrolase (FGH; 375), which produces glutathione and formate. Glutathione is an important antioxidant and relies on NADPH to restore its reduced form following ROS-scavenging reactions (Tomanek, 2015). Other circadian antioxidants included manganese superoxide dismutase (Mn SOD; 485), which catalyzes the transformation of the superoxide radical to hydrogen peroxide (H_2O_2) in mitochondria, and mitochondrial peroxiredoxin 5 (589), which reduces the potentially reactive H_2O_2 to H_2O. These daytime peaks in ROS-scavenging proteins were complemented with the peaks of the chaperone heat shock cognate 71 (Hsc71; 144), suggesting a demand for increased stabilization of protein structure, possibly due to ROS damage (Fig. 10A).

The tidal cycles also correlated with multiple antioxidant proteins, including copper-zinc SOD (Cu-Zn SOD; 504, 505), nucleoredoxin, a thioredoxin-homolog (565), and thioredoxin peroxidase (458). Oxidative damage following aerial exposure, accompanied in most cases by ischemia-type damage due to the rapid influx of oxygen following immersion (reoxygenation), has been well-documented in studies of bivalve respiration under tidal regimes and hypoxia exposure (Dudognon et al., 2013; Ellington, 1983; Ivanina et al., 2016; Place et al., 2012; Widdows and Shick, 1985). The clearest evidence of oxidative damage in this study was the strong high-tide cycling of methionine-R-sulfoxide reductase (572), which repairs the oxidation of methionine residues on proteins (Cui et al., 2011) (Fig. 10B). Remarkably, the gradual oxidation of proteins has been shown to impair function over time, and rhythms of decreasing protein activity being offset with the synthesis of new proteins has been proposed as an explanation for rhythms in enzyme activity when total abundance remains relatively constant (Atger et al., 2015; Cui et al., 2011).

The fluctuating abundance of prohibitin (419) during low tides, particularly at night, offers interesting prospects about its role in maintaining mitochondrial integrity (Fig. 10B). Prohibitins reside in the inner mitochondrial membrane and show multiple chaperoning and signaling functions for mitochondrial proteins, as well as regulating apoptosis in response to ROS (Thuaud et al., 2013). Prohibitin 2 is also subject to regulation by sphingosine-1-phosphate (S1P), generated from sphingosine 1 by sphingosine kinase (SK1) (Strub et al., 2011). The complex of prohibitin and S1P functions in the assembly and function of cytochrome c oxidase (COX), complex IV of the ETS (Strub et al., 2011). This function has been shown to have a cytoprotective role

during ischemia/reperfusion in the heart (Gomez et al., 2011). This may be an important function in tidally-acclimated *Mytilus*, as Connor and Gracey (2012) found that sphingosine 1 was depleted during low tide, which they speculated was due to the binding of HIF-1α to SK1 leading to increased conversion of sphingosine to S1P. The prohibitin abundance changes in this study may indicate a role for the complex with S1P in preparing the gill tissue for ischemia/reperfusion injury following submersion.

Two isoforms of dimethylarginine dimethylaminohydrolase (DDAH; 322, 308) peaked during the evening (Fig. 10B). This enzyme is involved in the degradation of methylarginine, a product of protein catabolism that is known to be a potent inhibitor of nitric oxide synthase (NOS) (Cooke, 2004). The role of nitric oxide (NO) in *Mytilus* gill tissue is currently unclear. Recent evidence shows that NO formation is partially concentrated around the longitudinal endothelial muscle cells surrounding the hemolymph (Rivera-Ingraham et al., 2013). The primarily evening peaks of DDAH may indicate that an increase in the products of protein degradation during feeding and metabolic activity may risk accumulating and inhibiting the NO formation that is required for proper function of endothelial muscle cells and oxygenation of the hemolymph (MacAllister et al., 1996; Rivera-Ingraham et al., 2016).

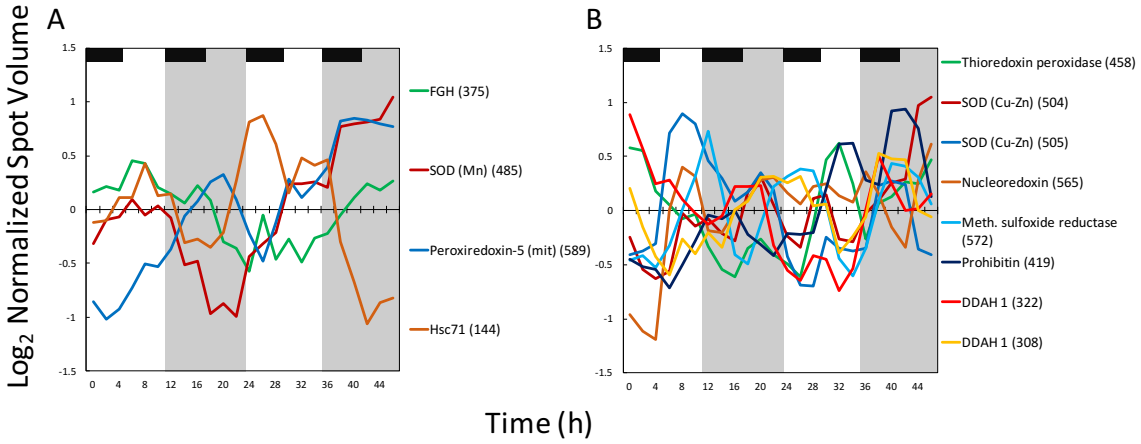

Figure 10. Moving average expression profiles across the 48 h time series for oxidative stress proteins. Simulated conditions at each time point are shown with high tide as black bar above and darkness as gray shading behind.

Anaerobic metabolism

Numerous studies have documented the shift in metabolic pathways seen in bivalve mussels following aerial emersion (Ahmad and Chaplin, 1984; Carroll and Wells, 1995; Connor and Gracey, 2012; Fields et al., 2014; Sadok et al., 1999; Widdows and Shick, 1985). Despite the well-documented anaerobic pathway in intertidal bivalves of accumulating opines to regenerate NAD^+ for continued glycolytic ATP formation, this study found that the abundance of D-octopine dehydrogenase (280) did not to follow low tide exposure (Fig. 11). The enzyme's low tide depletion suggests that it was not the most utilized pathway during aerial emersion. This is not unusual, partly because its role in fueling anaerobic metabolism in mussels may be limited to purely hypoxic or anoxic conditions or longer periods of aerial emersion, which may not have been the case in this study (Müller et al., 2012; Stefano et al., 2015). Mussels acclimated to a tidal regime in a

laboratory setting do not always utilize pathways that lead to opine accumulation (Demers and Guderley, 1994). This may be due to the efficiency of metabolic suppression in reducing energy demand or effective use of phosphagens to support basic metabolic processes (Kreutzer et al., 1989). Indeed, arginine kinase (299, 281) appeared to reach peak abundances during high tide, probably to support the regeneration of depleted phosphoarginine stores following aerial exposure (Ellington, 1983).

Some signs of anaerobic metabolism were visible in this study. Minor peaks of aminoadipic synthase (121) during low tide also support the finding that aminoadipate increased during low tide in a *M. californianus* time course study (Connor and Gracey, 2012). Propionyl-CoA carboxylase (121), which catalyzes the conversion between propionyl-CoA and methylmalonyl-CoA, also contributes to the well-documented anaerobic pathway for the accumulation of propionate in bivalves (Müller et al., 2012) (Fig. 11). While acyl-carnitine transferase was not identified in this study, Connor and Gracey (2012) found that propionylcarnitine accumulated during low tide in *M. californianus* gill tissue and the authors cite the potential protective role for this carnitine conjugate in ischemia/reperfusion injury (Micheletti et al., 1993). The low tide abundance of propionyl-CoA carboxylase in this study may reflect a diversion of methylmalonyl-CoA or the products of branched-chain amino acid (BCAA) metabolism toward the functional accumulation of a protective molecule.

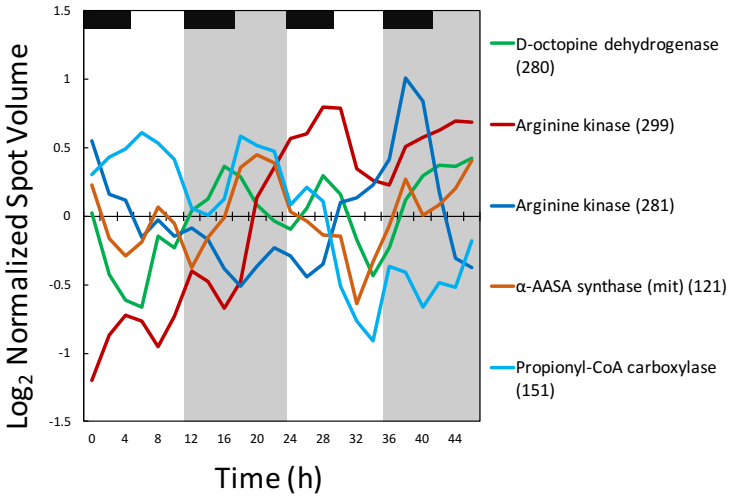

Figure 11. Moving average expression profiles across the 48 h time series for anerobic metabolism proteins. Simulated conditions at each time point are shown with high tide as black bar above and darkness as gray shading behind.

Recent studies have shown that many intertidal organisms are surprisingly capable of maintaining a degree of aerobic respiration during intermittent aerial exposure. Intertidal bivalves, including the clams *Mercenaria mercenaria* and oysters *C. virginica,* have shown very little accumulation of the typical anaerobic end products (L-alanine, succinate, and acetate) when exposed to periods of hypoxia lasting 18 h or less (Ivanina et al., 2016; Kurochkin et al., 2009). The limited evidence of oscillations in proteins from typical anaerobic pathways in this study may support a continuation of aerobic metabolism during aerial exposure. Particularly in a protected laboratory setting where desiccation stress is likely to be minimal, valve gaping during low tide could maintain enough available oxygen to continue a suppressed level of aerobic respiration. This is realistic as metabolic depression in bivalves may lower energetic requirements to as little

as 14% of the immersed requirements (Widdows and Shick, 1985). Furthermore, research on *C. gigas* responses to aerial exposure showed that, in contrast to research on fully hypoxic conditions, mitochondria retain full functional capacity for oxidative phosphorylation during typical low tide emersion, yet they show decreased capacity for ATP generation through ATP synthase (Dudognon et al., 2013). The decreased ATP synthase capacity may be evident in the fluctuations of F1 domain subunits seen in this time series, supporting the hypothesis that tidally acclimated mussels may anticipate and prevent the ATP-consuming reversal of this enzyme during potential hypoxic conditions (Brand, 2000; Rivera-Ingraham et al., 2013). These studies under normal cycles of aerial emersion suggest that tidally-acclimated *M. californianus* may be capable of retaining a functionally low level of aerobic respiration to supply the low metabolic demands of predictable tidal periods. The predictability of these tidal cycles also contrasts the proteomic evidence of anaerobic respiration following experimental aerial exposure and subsequent recovery in the salt marsh mussel *Geukensia demissia* after acclimation to subtidal conditions (Fields et al., 2014). Exposure to predictable tidal cycles may induce a different response or higher constitutive abundance of proteins to cope with tidal cycles than would be seen individuals that experience an acute episode of aerial emersion. It is also important to consider bouts of anaerobic metabolic depression are unlikely to be accompanied by protein synthesis, as hypoxia has been shown to induce translational arrest (Larade and Storey, 2002; Storey and Storey, 2004). Instead, post-translational modifications to existing proteins are utilized to redirect the flux of metabolites through anaerobic pathways, particularly at the "phosphoenolpyruvate branch point" shifting anaerobic metabolism from alanine to succinate formation (Brooks and Storey, 1997;

Russell and Storey, 1995; Storey, 1988). These studies may explain the weak signs of anaerobic metabolism seen in protein abundance changes during the tidal cycles in this study.

Protein turnover

The dynamics of protein turnover, including the timing of transcription, translation, and degradation, are a current focal point of circadian research (Atger et al., 2015; Gawron et al., 2014; Janich et al., 2015; Lück et al., 2014; Menet et al., 2012). In highly studied models such as mouse liver, this research has revealed a complex and dynamic system that regulates each step in the pathway to a functional protein (Eckel-Mahan et al., 2012; Eckel-Mahan et al., 2013; Patel et al., 2015). The addition of a tidal cycle to the typical model of circadian rhythms introduces a new level of complexity due to the drastic changes in the environment between high and low tide. Transcription and translation are typically suppressed during anoxia-induced metabolic depression, indicating an "economical" use of limited energy (Larade and Storey, 2007), while limited feeding cycles have been proposed as a metabolic gate determining cycles of tidal transcripts (Gracey et al., 2008). This is an interesting theory, as studies analyzing the energetic costs of circadian transcripts have shown that rhythmicity optimizes the energetic demands of producing transcripts and proteins that are significantly more costly than non-rhythmic ones, ensuring that they are synthesized only when necessary (Wang et al., 2015). In the context of this energy-optimization theory of circadian rhythms, tidal cycles and metabolic depression add another degree of complexity.

The process of transcriptional control is difficult to deduce in proteomics data. While rhythmic transcripts in *M. californianus* were detailed through similar tidal and light/dark cycles by Connor and Gracey (2011), the contribution of the proteome to determining transcriptional rhythms is complex and varied (Hershey et al., 2012). However, several proteins involved in transcription regulation, RNA processing, and mRNA localization showed rhythmic abundances in this time series. At the level of transcription regulation, a distinct high-tide cycle is visible in the abundance of upstream stimulating factor 1 (USF-1; 540), an important glucose-responsive transcription factor (Kietzmann et al., 2002) (Fig. 12). USF-1 is an E-box transcription factor, much like the clock proteins (e.g. BMAL and CLOCK), that has not previously been shown to exhibit cyclic abundance changes (Muñoz et al., 2002; Patel et al., 2012). USF-like factors have been found to bind E-box promoters such that circadian regulation of certain genes cannot occur (Muñoz et al., 2002). Furthermore, the binding of USF factors to glucose-regulatory elements may compete with binding by the hypoxia-inducible factor 1 (HIF-1) complex under low oxygen conditions (Kietzmann et al., 2002). In *M. galloprovincialis,* HIF-1α transcripts and proteins were shown to increase during short-term aerial emersion and degrade within one hour of reoxygenation (Giannetto et al., 2015). This competition between HIF-1 and USF-1 for similar promoters could indicate that high-tide cycling of USF-1 ensures a preference for glucose metabolism by HIF-1 hypoxic signaling during aerial exposure, which is supported by the observed depletion of glucose in *M. californianus* gill during low tide (Connor and Gracey, 2012). Short-term hypoxia in zebrafish *Danio rerio* has also shown that HIF-1α outcompetes the E-box promoter site binding activity of the clock protein PER1 (Egg et al., 2013). This overlap between the

hypoxic response and circadian rhythm could indicate a close connection between metabolic coordination under both changing light and oxygen conditions (Egg et al., 2013). With these environmental factors fluctuating regularly during circadian and tidal acclimation, HIF-1 may be a candidate regulator of a tidal response by co-opting shared components of the endogenous circadian clock.

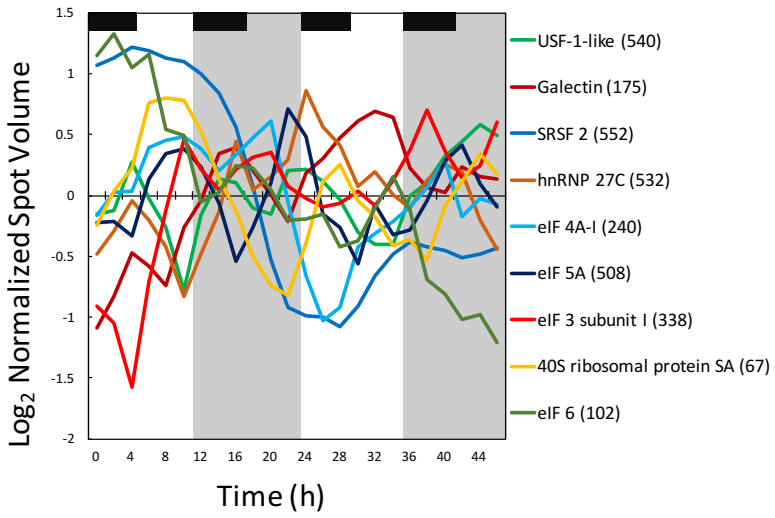

Figure 12. Moving average expression profiles across the 48 h time series for transcription and translation proteins. Simulated conditions at each time point are shown with high tide as black bar above and darkness as gray shading behind.

Following transcription, RNA undergoes processing before translation of mature mRNA can occur. In this study, two proteins involved in RNA splicing were identified: galectin (175), which peaked primarily during the evening high tides, and serine-arginine rich splicing factor 2 (SRSF2; 552), which tended to follow a circadian rhythm peaking prior to the day-night shift. The high-tide rhythm of binding, processing, and localizing

mRNA was also seen by the tidal rhythm of abundance in heterogeneous nuclear ribonucleoprotein 27C (hnRNP 27C; 532) (Fig. 12). This data suggests that RNA processing and localization responds in large part to the tidal cycle.

The timing of translation is vital in the coordination of rhythmic processes. While transcripts may exhibit clear cycles, the energetic costs of translation may dampen or eliminate the cycles of corresponding protein abundance (Liu et al., 2016; Wang et al., 2015). Rhythmic abundance changes reflect an important optimization strategy for the expression of energetically expensive proteins only when necessary (Wang et al., 2015). Robles et al. (2014) found that translation initiation and protein elongation elements showed a coordinated evening peak that matches peak activity and nutrient intake for the mice, as well as the synthesis time for 70% of the circadian proteins that were shown to be translationally regulated.

With the addition of a tidal cycle, the temporal availability of energy is further limited by the reduced duration of active metabolism. During low tide, *M. californianus* typically reduce their heart rate and enter metabolic depression (Connor and Gracey, 2012) while the availability of food determines the degree of metabolic activity during submersion (Thompson and Bayne, 1972). Despite the gill tissue being highly active and requiring protein synthesis at a rate of approximately 10% per day (Lyndon and Houlihan, 1998; McCarthy et al., 2016), metabolic depression triggers an arrest in transcription and translation (Larade and Storey, 2007; Storey and Storey, 2004). This was recently supported by a 25-fold increase in phosphorylation of eukaryotic initiation factor 2α (eIF2α) to reduce activity during hypoxia (Ivanina et al., 2016). These

competing influences of reduced timing for protein synthesis, limited feeding opportunity, and high rates of protein turnover complicate the role of circadian cycles alone in determining translation rates.

The abundances of translation complex proteins do suggest that translation occurs primarily in the evening on a circadian basis in *Mytilus* as well. Mature mRNA is recognized by complexes that include eIF4A (240), which peaked in abundance during the early night. Meanwhile, the preinitiation complex forms with other eIF proteins and the 40S ribosomal protein (Gawron et al., 2014), a process which was supported in this data by the matching cycles of eIF5A (508), eIF3 (338), and 40S ribosomal protein SA (67). Each of these factors showed primarily circadian rhythms peaking just prior to the day-night interphase. Transcription only proceeds with the joining of the 40S and 60S ribosomal subunits, which eIF6 regulates by preventing the premature association of these subunits (Gartmann et al., 2010, 6). In this study, eIF6 (102) was found to peak during the day several hours prior to the peak of eIF5A, eIF3, and 40S ribosomal proteins (Fig. 12). This indicates that translation appears to be carefully regulated to occur primarily during the transition into the evening high tide. Considering the importance of available energy to support protein synthesis and the scale of the increases in multiple metabolic processes seen in the evening, these results appear to agree with the evening peak of rhythmic translation found by Robles et al. (2014) in the mouse liver proteome.

Circadian timing of protein abundance may be dependent on the rates of protein degradation, particularly for the cyclical abundances of proteins with long half-lives (Lück et al., 2014). Protein abundance oscillations tend to show decreasing amplitudes as

half-lives extend beyond 1 h, and degradation models show that these proteins with translation peaks more than 6 h after the corresponding transcript are likely to show steady-state abundances (Lück et al., 2014). For this reason, statistical detection methods typically do not uncover circadian rhythmicity in long-lived proteins.

The introduction of a tidal cycle to studies of rhythmic degradation adds a new level of complexity. *Mytilus* species exhibit "protein sparing" by recycling between 38% and 90% of the protein breakdown products, with the rest used for energy metabolism (Hawkins, 1985). Gill tissue in particular shows a large mRNA pool, resulting in a high capacity for protein synthesis and ultimately leading to higher rates of protein synthesis than other tissues (McCarthy et al., 2016). Therefore, protein degradation products are an important contribution to this turnover (Hawkins, 1985). However, aerial emersion not only triggers translational arrest but also reduced protein degradation (Ivanina et al., 2016). Theoretically, this may concentrate the timing of degradation and synthesis to the intermittent high tide submersion periods.

In this study, signs of protein degradation were evident in components of the ubiquitin-proteasome and lysosomal protein degradation pathways, as well as the chaperoning of existing proteins during potentially stressful conditions. Molecular chaperones in the 70 kDa heat shock protein family appeared to peak during the daytime (144, 143) as well as low tide cycles (579), potentially to retain functional proteins during periods of lower activity and higher risk of stressful environmental conditions (Fig. 13A). Place et al. (2012) found that the cellular stress response was responsive to tidal cycles, with mussels inhabiting higher sites in the intertidal showing rapid responses in cellular

repair and degradation following re-immersion. At the day-night interphase, the lysosomal degradation proteins cathepsin L (96, 99, 105) showed prominent peaks, suggesting a high rate of degradation for extracellular components, proteins that accumulated damage over the daytime, or to liberate amino acids for the coordinated peak in energy metabolism (Stoka et al., 2016) (Fig. 13A). In the common periwinkle *Littorina littorea,* increased lysosomal autophagy in fasting individuals or during intermittent stress incites a protective regime of clearing damaged intracellular proteins and organelles (Moore et al., 2015). Decreased abundance of cathepsins during the evening submersion may also be a protective measure against the escape of lysosomal proteases into the cytoplasm during tidal cycles of lysosome membrane destabilization (Izagirre et al., 2008; Tremblay and Pellerin-Massicotte, 1997).

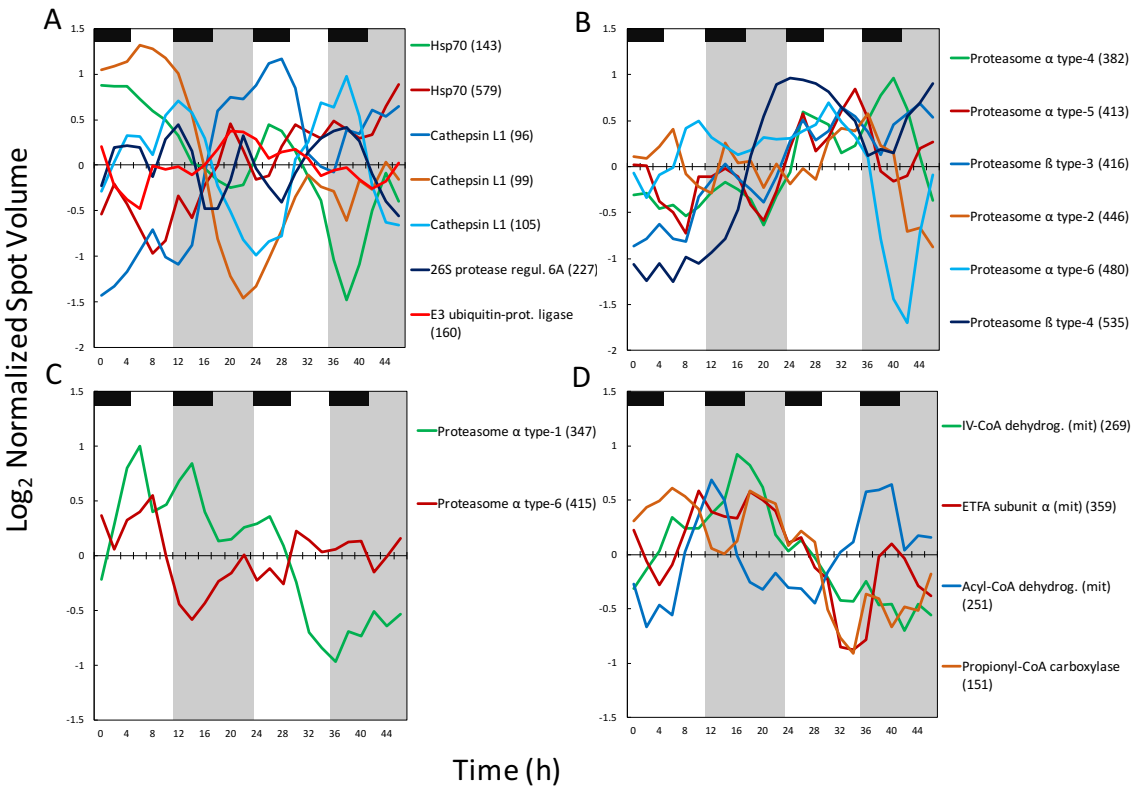

Figure 13. Moving average expression profiles across the 48 h time series for protein degradation. Simulated conditions at each time point are shown with high tide as black bar above and darkness as gray shading behind.

Ivanina et al. (2016) showed recently that 26S proteasome activity in intertidal mollusk gill tissue is suppressed during hypoxia and quickly restored during reoxygenation. This observation reinforces the role of molecular chaperones in maintaining functional protein pools during aerial emersion when available energy for protein degradation may be limited, with rapid restructuring following immersion (Ivanina et al., 2016). We found that the 26S proteasome regulatory subunit 6A (227) followed a high tide rhythm while other proteins involved in proteasomal degradation

followed a predominantly circadian cycle (Fig. 13A). Lück et al. (2014) produced a model by which the peak abundance of E3 ubiquitin ligase during the early morning would produce an overall 18 h phase for circadian proteins. In this study, JTK_Cycle identified a 28 h period and 1 h phase of ubiquitin-conjugating enzyme E2 (UBE2; 20), which acts to recruit E3 ligase, with a similar 28 h period and 0 h phase for E3 ubiquitin-protein ligase TRIM33 (160) (Fig. 13A). While both UBE2 and E3 ligase visibly contain high tide fluctuations, the JTK_Cycle output agrees with the timing of proteasomal degradation that Lück et al. (2014) predict may be responsible for the prominent 18 h phase enrichment for circadian proteins (Fig. 13C). Several proteasome α and ß subunits could contribute to this time course of degradation as there were multiple identified spots following a midday circadian rhythm (382, 413, 416, 446, 480, 535) (Fig. 13B) with two α subunits also showing visible high tide fluctuations as well (347, 415) (Fig. 13C).

Catabolism of BCAA (Val-Leu-Ile) in *M. californianus* gills was found in the Connor and Gracey (2012) metabolomics study during low tide. In this time course, this was supported by isovaleryl-CoA dehydrogenase (IVCDH; 269) showing partial synchrony with electron transport flavoprotein alpha (ETFA; 359), which is required for the IVCDH reaction (Fig. 13D). The mismatch between IVCDH and ETFA in the second evening can be associated with the transfer of electrons to ETFA from acyl-CoA dehydrogenase in fatty acid ß-oxidation (ACD; 251). Propionyl-CoA carboxylase (PCC; 151) is involved in the final steps of BCAA metabolism, and it followed a similar pattern of abundance as IVCDH (Fig. 13D). Amino acid catabolism during low tide is supported by observations that mussels tend to utilize this pathway when there is a low oxygen to nitrogen (O:N) ratio (Sadok et al., 1999).

The nitrogenous waste from protein catabolism is typically fixed as urea for excretion. Glutamate dehydrogenase (183) peaked during low tide, with ammonia being byproduct of its reaction. This ammonia is typically utilized in protein synthesis or detoxified as urea rather than accumulating in hemolymph during emersion (Sadok et al., 1999). Ammonia fixation into urea is partially accomplished by arginase (311), which peaked in concert with glutamate dehydrogenase, suggesting a highly responsive tidal cycle for the fixation and excretion of nitrogenous wastes (Fig. 14A). This is supported by the findings that free ammonia shows an exponential drop in accumulation with emersion duration in bivalve gills as well as stable ammonia efflux rates following re-immersion (Sadok et al., 1999), in part by ciliary beating to increase ammonia efflux into the surrounding water (Thomsen et al., 2016). Interestingly, the coordination of urea detoxification may be directed by the oscillations of post-translational modifications (PTMs) and the action of NAD^+-dependent deacylase sirtuin 5.

Evidence for post-translational regulation

The importance of PTMs for the alteration of protein activity has increasingly become a focus of studies on biochemical adaptation. Studies show that phosphorylation of pyruvate kinase (PK) and phosphenolpyruvate carboxykinase (PEPCK) are partially responsible for the metabolic shunt seen in mollusks in response to hypoxia (Russell and Storey, 1995; Storey, 1988). The importance of acetylation and phosphorylation for circadian regulation has also been demonstrated multiple times (Anderson and Hirschey, 2012; Kovacic and Somanathan, 2014; Masri et al., 2013; Mauvoisin et al., 2015; Rey

and Reddy, 2013b). In the circadian liver proteome, 67% of the rhythmic proteins were found to be phosphoproteins (Reddy et al., 2006), and rhythms of circadian acetylation are implicated in orchestrating mitochondrial metabolic pathways (Masri et al., 2013). Furthermore, in a study of the mouse liver proteome, the numerous proteins cycling with a small amplitude were found to be enriched for acetylation (Robles et al., 2014). The importance of PTMs to this study is visible in the results of a DAVID gene enrichment analysis of the 214 uniquely identified proteins in this study (Huang et al., 2009a; Huang et al., 2009b). This analysis confirmed that 51% of proteins may be acetylated and 50% phosphorylated, with 117 total proteins having the potential to show one or both of the modifications, making these the two most enriched functions in the rhythmic protein dataset.

Acylation

Two identified isoforms of the NAD^+-dependent deacylase sirtuin 5 (SIRT5) showed anticorrelated patterns of abundance, with one peaking during the middle of the night (356) and the other peaking during midday (349). This is the first documented occurrence of a cyclic abundance pattern of SIRT5. Sirtuin acylation works as a metabolic regulator that is highly responsive to cellular energy levels, with abundant metabolic substrates such as acetyl-CoA being incorporated in high levels of lysine acetylation that may alter enzyme activities (Anderson and Hirschey, 2012; Choudhary et al., 2009). The only known modification to SIRT5 is a mitochondrial transit cleavage site of 36 amino acids that determines the protein localization. The cleaved isoform is found exclusively in the mitochondria, which may explain the slightly lower molecular weight of SIRT5 (356) (about 1 kDa difference), while the uncleaved isoform may be

redistributed to the cytoplasm (Flick and Lüscher, 2012). The timing of the suspected cleavage of the SIRT5 transit site is matched by that of the mitochondrial-processing peptidase subunit ß (PMPC; 233), which may be responsible for cleaving the SIRT5 N-terminal transit peptide (Fig. 14A). Mitochondrial transit peptides were enriched in the dataset according to DAVID (Huang et al., 2009a; Huang et al., 2009b), with numerous other proteins matching the evening circadian cycle of PMPC (Fig. 14A). This agrees with the coordinated peak in metabolic processes in the evening and the day-night interphase enrichment for mitochondrial proteins found by Robles et al. (2014).

The peak abundance of the lower molecular weight isoform of SIRT5 appears to be coordinated with its well-documented influence over the urea cycle through the deglutarylation of the rate-limiting carbamoyl phosphate synthetase 1 (CPS1) (Tan et al., 2014) and desuccinylation of glutamate dehydrogenase (Weinert et al., 2013). SIRT5 deglutarylation increases the activity of CPS1, catalyzing the entry of ammonia into the urea cycle. In mice liver, Eckel-Mahan et al. (2012) showed that the urea cycle showed a clear, coordinated diurnal rhythm in multiple metabolites. The increased SIRT5 abundance in this study matched that of glutamate dehydrogenase (183) and was followed by peak abundances in arginase (311), which catalyzes the final step of urea formation in the cytosol (Fig. 14B). This suggests that the increase in SIRT5 is indeed deacylating CPS1 and glutamate dehydrogenase to increase ammonia detoxification. The time delay in arginase abundance changes is likely due to the delay between the mitochondrial and cytosolic portions of the urea cycle. This rhythmicity of SIRT5 and its role in regulating the rate-limiting enzyme in the urea cycle suggests that it coordinates the robust rhythms of ammonia detoxification (Reddy et al., 2006).

Protein acylation is closely linked to the cellular status as the acyl groups (acetyl-CoA, glutaryl-CoA, malonyl-CoA, succinyl-CoA, etc.) are integral to multiple metabolic pathways (Nishida et al., 2015). Higher concentrations of metabolites, such as glutaryl-CoA, tend to favor their non-enzymatic binding to substrates such as CPS1 and subsequently influence the protein's activity. The deacylating function of sirtuins, which is also tied to energy status through their NAD^+-dependent function (Peek et al., 2013), reverses the effects of the PTMs, making them ideal proteins to drive the rhythmic coordination of metabolic processes. In this study, SIRT5 only peaked during the late high tide to early low tide shift, which may correlate with the shift away from oxidative metabolism and therefore a reduction in the NAD^+/NADH ratio. Furthermore, as glutaryl-CoA is a known acyl group targeted by SIRT5, it is interesting to see that two enzymes involved in the degradation of lysine and subsequent production of glutaryl-CoA, α-aminoadipic semialdehyde synthase (121) and α-aminoadipic dehydrogenase (207), showed peaks prior to SIRT5 (Fig. 14B). This increased glutaryl-CoA may inhibit CPS1 at these times when α-aminoadipic dehydrogenase peak, which could result in the downstream effect of the visible decrease in arginase at these time points. The following increase in SIRT5 may be synchronized with lysine degradation to reverse the loss of ammonia detoxification with increased glutarylation. This presents an interesting link to the finding that lysine metabolites were regulated almost entirely by circadian rhythms (Eckel-Mahan et al., 2012). Eckel-Mahan et al. (2012) found that lysine pathway metabolites peaked in coordination at ZT 21, agreeing very closely with the 22 h phase and 24 h period calculated by JTK_Cycle for α-aminoadipic semialdehyde synthase (121) in this study. This pathway was only one of three found to show such highly regulated

circadian rhythmicity, with the other two being purine and nicotinamide pathways (Eckel-Mahan et al., 2012).

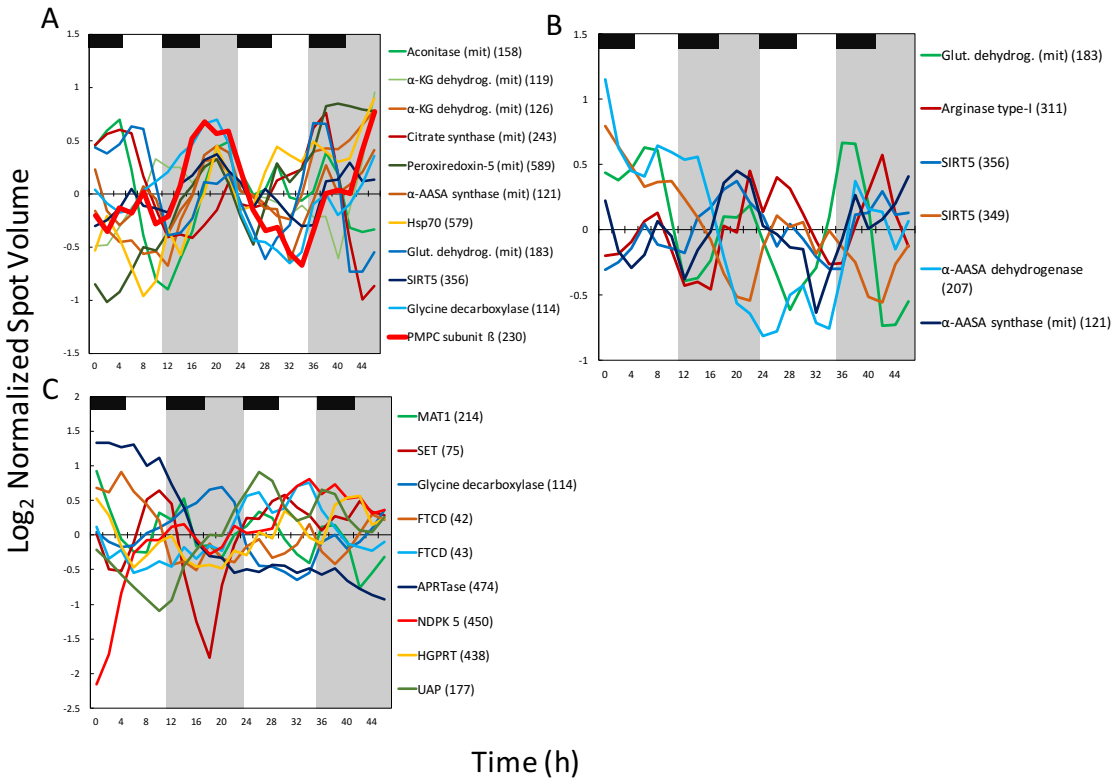

Figure 14. Moving average expression profiles across the 48 h time series for post-translational modification proteins. Simulated conditions at each time point are shown with high tide as black bar above and darkness as gray shading behind.

The increased concentration of acyl groups that are integral to numerous metabolic pathways presents a potential mechanism for complex orchestration of metabolism in *Mytilus*. For example, succinyl-CoA may provide a source over the day for the gradual non-enzymatic succinylation of lysine residues on a number of proteins (Park

et al., 2013; Weinert et al., 2013). Through sirtuin 5 (SIRT5) knockout studies, succinylation of lysine was found to be incredibly common, affecting roughly 70% of proteins involved in BCAA degradation, 80% of proteins involved in the TCA cycle, and 60% of proteins in fatty acid metabolism (Park et al., 2013). Furthermore, malonyl-CoA in the cytosol, another acyl group targeted by SIRT5 deacylation activity, is found to decrease glycolytic flux through the hypermalonylation of multiple enzymes seen in SIRT5 knockout mice (Nishida et al., 2015). While the stoichiometries and the interactions of these acyl group networks have yet to be uncovered, their importance to metabolic function and regulation by SIRT5 suggests that this enzyme is integral to controlling metabolic flux between fuel sources in both the cytosol and mitochondria (Nishida et al., 2015).

Methylation

Methylation is an important method of reversibly modifying RNA (Fustin et al., 2013), proteins (Dillon et al., 2005), and DNA (Maddocks et al., 2016) to augment the expression or activity of the substrate. One circadian sirtuin protein, SIRT1, has been shown to also influence circadian methylation patterns through the histone methyltransferase MLL1, which drives chromatin remodeling around clock genes and is active when acetylated (Tasselli and Chua, 2015). SIRT1 and MLL1 show anticorrelated influence over clock genes, with MLL1 methylating the genes when SIRT1 activity is reduced due to low NAD^+/NADH, and when NAD^+ levels climb SIRT1 activity drives the deacetylation of MLL1, decreasing its activity, as well as contributing to clock gene

chromatin remodeling (Tasselli and Chua, 2015). Thus, modification of clock genes is closely linked to the cellular energy status through the fluctuation of NAD^+/NADH.

The first requirement for methylation is the adenosine-dependent (with ATP as a donor) conversion of methionine to S-adenosylmethionine (SAM) by methionine adenosyltransferase (MAT, 214) (Fig. 14C). MAT showed a clear tidal pattern peaking during each high tide. The peak MAT abundance during high tide agrees with the finding that the downstream product after methylation, S-adenosylhomocysteine (SAH), was increased at high tide in *M. californianus*, suggesting that a high methylation potential (higher SAM/SAH ratio) exists during high tide (Connor and Gracey, 2012). Furthermore, we found MAT to be coordinated with the protein SET (75), a methyltransferase which transfers the methyl group from SAM to several possible lysine methylation sites on histones (Dillon et al., 2005). Following methylation, cells must restore both methionine and ATP as substrates for the MAT reaction that replenishes SAM. A recent study showed that these substrates are replenished using serine catabolism and the one-carbon metabolism cycle (Maddocks et al., 2016). This research tracked C^{13} labels to find that serine, in concert with the one-carbon cycle, is catabolized to fuel *de novo* purine synthesis to generate ATP as the necessary substrate for MAT to generate SAM. However, if cells were starved of methionine, the C^{13} is instead transferred as a methyl group to the one-carbon tetrahydrofolate (THF) to form meTHF, using the folate cycle of one-carbon metabolism to replenish methionine from homocysteine (Maddocks et al., 2016). Interestingly, this conversion of THF to meTHF can also be achieved by the glycine cleavage system, including glycine decarboxylase (114), which showed peak abundance in this study during the night. Alternatively,

formimidoyltransferase-cyclodeaminase (FTCD; 42, 43) directs a variant of THF toward the formation of meTHF and both isoforms peaked during the day (Fig. 14C). Between these two enzymes peaking during either the day or night, meTHF may be supplied to replenish methionine for MAT and the methyltransferase SET.

Maddocks et al. (2016) also note that the influence of de novo nucleotide synthesis for ATP to fuel methylation shows the importance of nucleotide synthesis for other sources besides DNA replication. Furthermore, the connection provides a novel view of methylation as an ATP-sensing pathway (Maddocks et al., 2016). This has important implications for methylation in restructuring the state of *Mytilus* gills for aerial emersion. Studies have noted that despite the metabolic depression seen in bivalves during low tide, there is still a continuation of both aerobic and anaerobic metabolism (Dudognon et al., 2013). Dudognon et al. (2013) found that the ATP-producing capacity of emersed *C. gigas* was approximately 31% lower than immersed individuals. The dependence of methylation on abundant ATP may explain the rhythmic decreases in MAT seen during low tide. Increased demand for ATP synthesis during high tide may be visible in the purine nucleotide synthesis proteins that were increased at these times, including posphoribosyl pyrophosphate synthetase 3 (PRPP synthetase 3; 274), adenosine phosphoribosyltransferase (APRT; 474), nucleoside diphosphate kinase 5 (450), and hypoxanthine phosphoribosyltransferase (HPRT; 438), as well as UDP-N-acetylhexosamine pyrophosphorylase (UAP; 177), which is involved in nucleotide sugar synthesis (Fig. 14C). While ATP demand may simply be the result of increased metabolism during feeding, it is interesting to consider methylation as a potent ATP-

sensing mechanism that modulates gene expression, translation, and protein function through tidal cycles.

Cytoskeleton and ciliary function

Dynamic equilibrium of the cytoskeleton ensures the structural responsiveness of cells to altered activity and environmental stress (Tomanek and Zuzow, 2010). Cytoskeletal components showed a diversity of timing regimes corresponding to tidal and light/dark regimes. A total of 38 spots were identified as actin or ß-actin isoforms with peak abundances scattered throughout the time course. Some isoforms (e.g. 283, 284, 360, 426) (Fig. 15A) showed a clear tidal cycle of low tide peaks while others (e.g. 184, 241, 597) followed high tide peaks (Fig. 15B). A large number of actin isoforms showed circadian rhythms with peaks during daylight (265, 549) or darkness (220, 291), but the majority corresponded with the day-night interphase (223, 233, 237, 258, 263, 272, 288, 601) (Fig. 15C). These frequent changes in the abundance of free actin reflect cycles of cytoskeletal restructuring along with environmental changes.

The regulation of actin cytoskeleton restructuring shows interesting dynamics. Cofilin (503), an actin-binding protein that accelerates the depolymerization of actin filaments (Elam et al., 2013), peaked strongly during each immersion cycle, with some overlap with actin-interacting protein 1 (147, 164), which may work in concert with cofilin to accelerate actin turnover (Lin et al., 2010) (Fig. 15D). Profilin (25), which promotes actin turnover and restructuring, showed peaks coinciding with the high- to low-tide shift (Rocher et al., 2015). Meanwhile, low tide aerial emersion ushered in

multiple actin-related proteins involved in bundling or stabilizing existing filaments, such as tropomyosin (71, 94), plastin (170), filamin-A (127, 574), actin-related protein 3 (577), and F-actin capping protein α-2 (335) (Feng and Walsh, 2004; Giganti et al., 2005; Rocher et al., 2015; Shinomiya and Shinomiya, 2012) (Fig. 15E). These coordinated interactions of actin-binding proteins suggest a highly regulated system of actin stabilization during aerial emersion followed by restructuring during submergence. Indeed, the rhythmic abundances of Rho-related proteins provide evidence for these cycles of maintenance and dynamism. A low-tide rhythm of Rho GTPase (453) supports the regulation of actin stress fiber assembly, while primarily high-tide peaks of Rho GDI (461, 471) act to inhibit Rho GTPase (Mounier and Arrigo, 2002) (Fig. 15F). This was further supported by the cyclic abundances of 26 isoforms of small heat shock proteins (sHsp24.1) (Fig. 16A-D). These sHsps have diverse chaperone functions during the cellular stress response, one of which is increased binding to F-actin when phosphorylated, serving to protect the filament from severing and breakage during stress and subsequently facilitate reorganization (Guilbert et al., 2015; Mounier and Arrigo, 2002). A diversity of sHsp cyclical patterns corresponded to tidal changes, with some peaking during low tide and others peaking prior to a tidal shift. However, their overall tidal distribution suggests that they play a consistent role in maintaining the rhythm of stabilization and reorganization of the actin cytoskeleton during regular cycles of emersion and immersion.

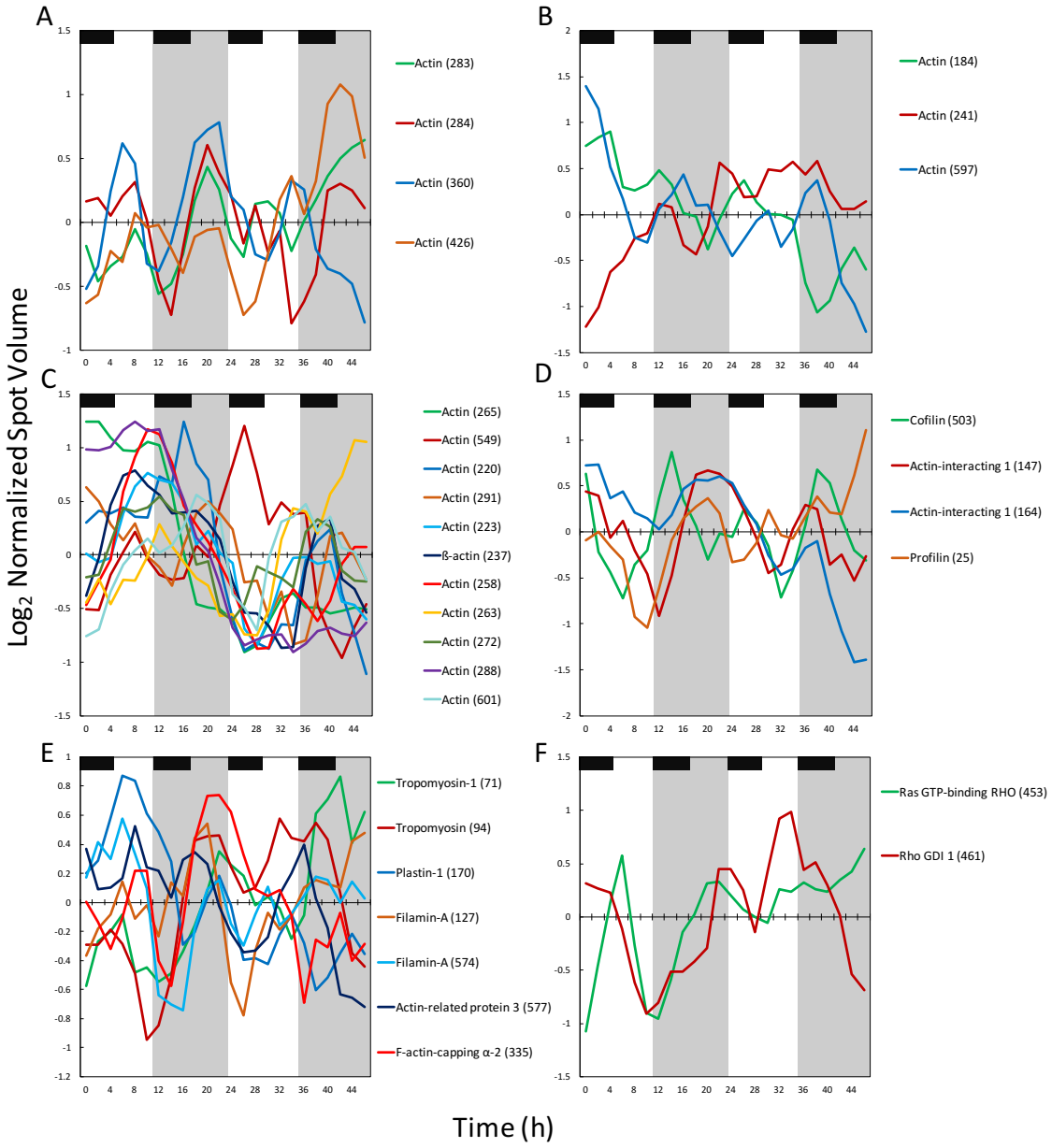

Figure 15. Moving average expression profiles across the 48 h time series for actin and actin-interacting proteins. Simulated conditions at each time point are shown with high tide as black bar above and darkness as gray shading behind.

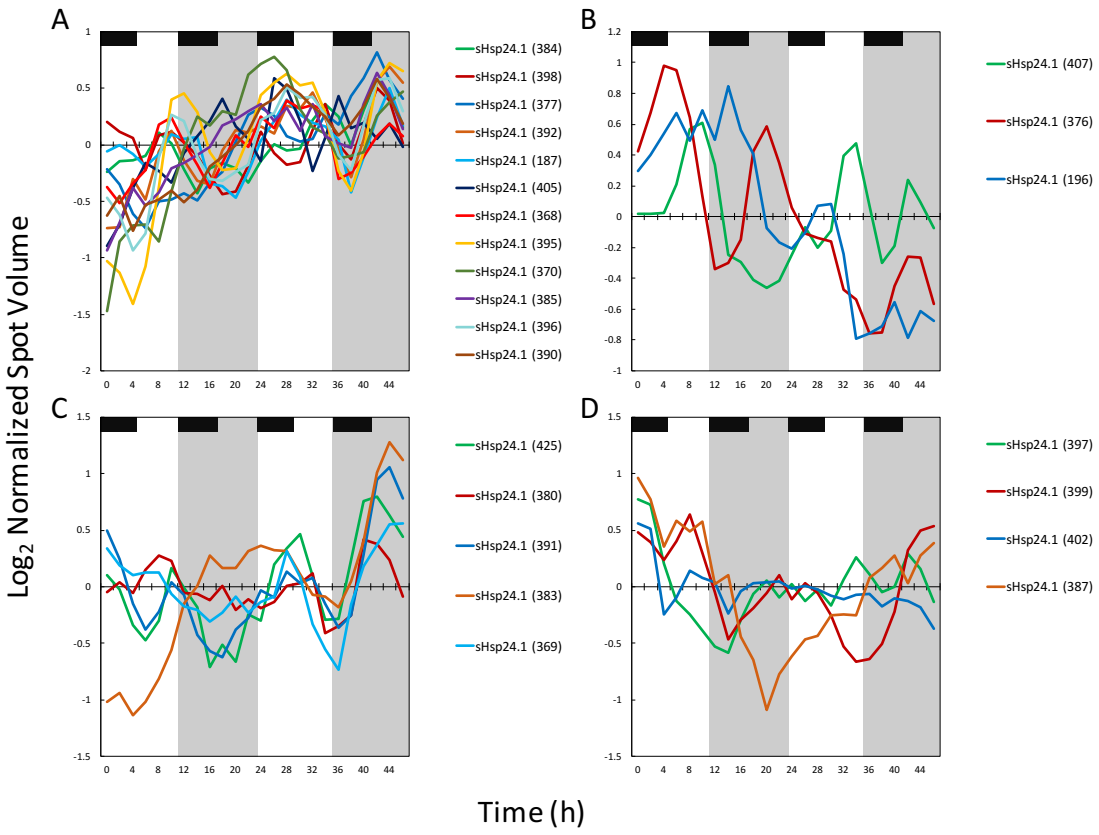

Figure 16. Moving average expression profiles across the 48 h time series for small heat shock proteins. Simulated conditions at each time point are shown with high tide as black bar above and darkness as gray shading behind.

Several other actin-binding proteins followed strong circadian rhythms, such as coactosin, which prevents F-actin depolymerization and may even accelerate polymerization (Hou et al., 2013). Coactosin showed two circadian isoforms peaking in the evening during high tide (570) and low tide (8). Likewise, another isoform of filamin-A (128) peaked during the nighttime low tide. Gelsolin, a Ca^{2+}-dependent regulator of actin polymerization and depolymerization, showed a circadian peak during the nighttime high tide (229) as well as a tidal cycle peaking at low tide (231) (Li et al., 2012) (Fig.

17A). Several structural proteins found in the extracellular matrix also showed tidal patterns. The predominantly low-tide cycle of heparin sulfate proteoglycan (312), fibulin-2 (536, 537), collagen 2 (188), and the clotting protein fibrinogen (388, 420) highlight their importance for stabilizing the elastic fibers and carbohydrates of the extracellular matrix (Fig. 17B). Like the intracellular cytoskeleton, aerial emersion appears to require abundant stabilizing factors to maintain extracellular integrity (Timpl et al., 2003). The combination of circadian and circatidal regulation of the dynamic cell structure may reflect the stresses imposed on gill tissue during tidal submersion and emergence as well as the sensitivity of the cytoskeleton to the rhythms of ROS accumulation and metabolic changes through daily light/dark cycles.

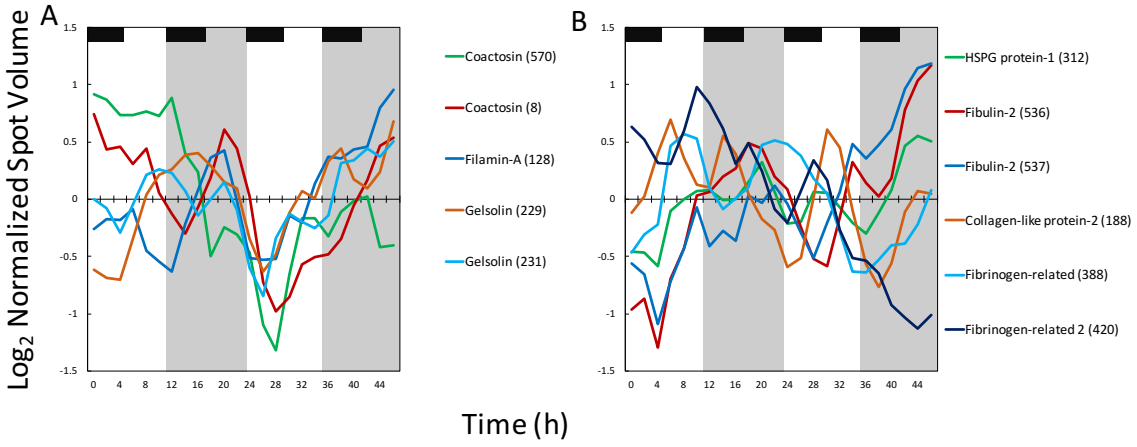

Figure 17. Moving average expression profiles across the 48 h time series for structural and actin-turnover proteins. Simulated conditions at each time point are shown with high tide as black bar above and darkness as gray shading behind.

Feeding activity

Many cytoskeletal proteins involved in ciliary function were also identified. These proteins play a vital role in the *Mytilus* gill tissue as ciliated cells require high metabolic activity to produce the flow of water across gill tissue for extraction of oxygen, food particle capture, and excretion of nitrogenous waste (Doeller et al., 1993; Thomsen et al., 2016). For some components, particularly dynein light chain proteins (28, 557) and radial spoke head protein 9 (331, 358), the abundances appeared more steady-state with broader gradual increases (Fig. 18A). However, tidal cycles could be seen in multiple structural components of cilia, including tektin-4 (211, 217, 225), the coiled-coil protein RIB43A-2 (226), intraflagellar transport protein 27 (587), radial spoke head protein 1 (65, 66), dynein intermediate chain proteins (133), and an uncharacterized C15orf26 protein with involvement in dynein arm assembly and proper cilia beating (Austin-Tse et al., 2013) (Fig. 18A). Many of these proteins, including tektin-4, a structural component of ciliary walls, tended to peak during tidal transitions (Amos, 2008; Fields et al., 2014) (Fig. 18B). The tidal cycle of changes to the cilia are supported by the abundance and turnover of α- and ß-tubulin, which represented 32 protein spots following various cycles of abundance changes that typically show peaks during either high or low tide (Fig. 19A-G). The restructuring of tubulin with tidal peaks was supported by the tidal patterns seen in multiple subunits of the cytoskeletal chaperone T-complex protein 1 (TCP1), peaking primarily during high tides (192, 200, 590) (Sternlicht et al., 1993) (Fig. 18C).

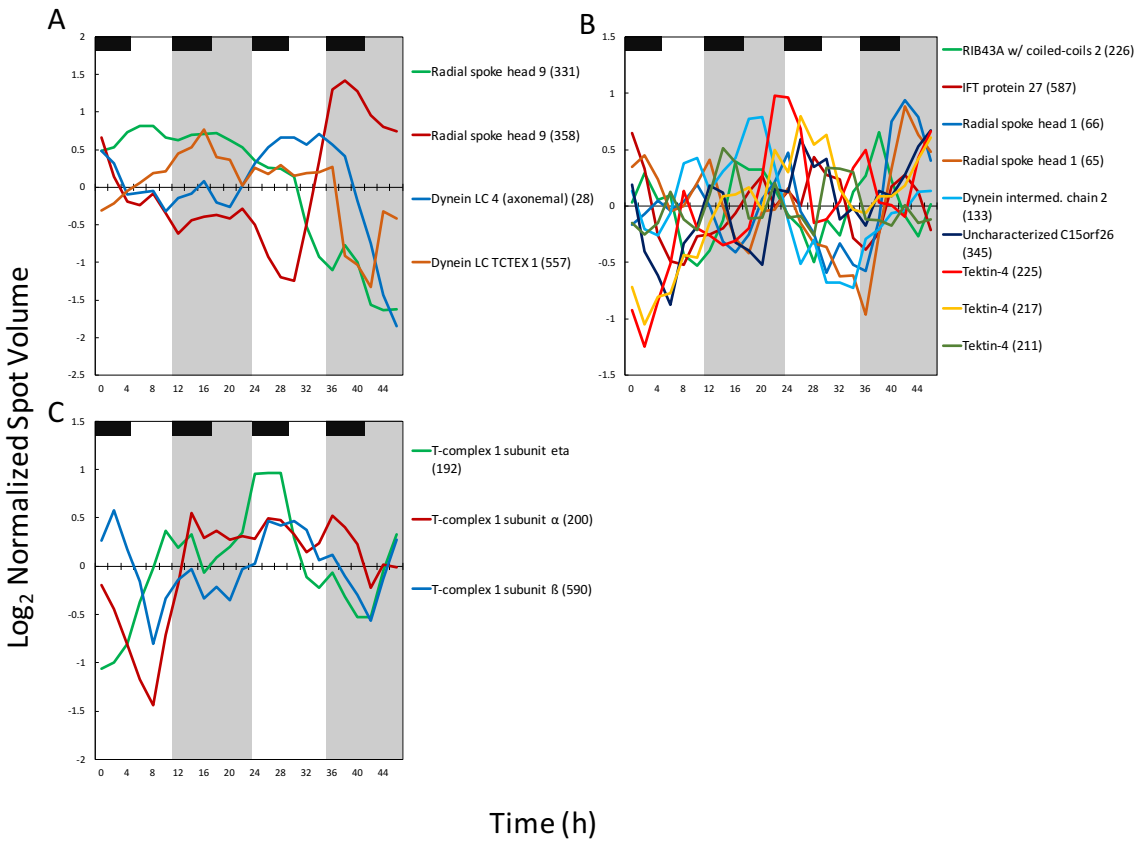

Figure 18. Moving average expression profiles across the 48 h time series for ciliary and tubulin-related proteins. Simulated conditions at each time point are shown with high tide as black bar above and darkness as gray shading behind.

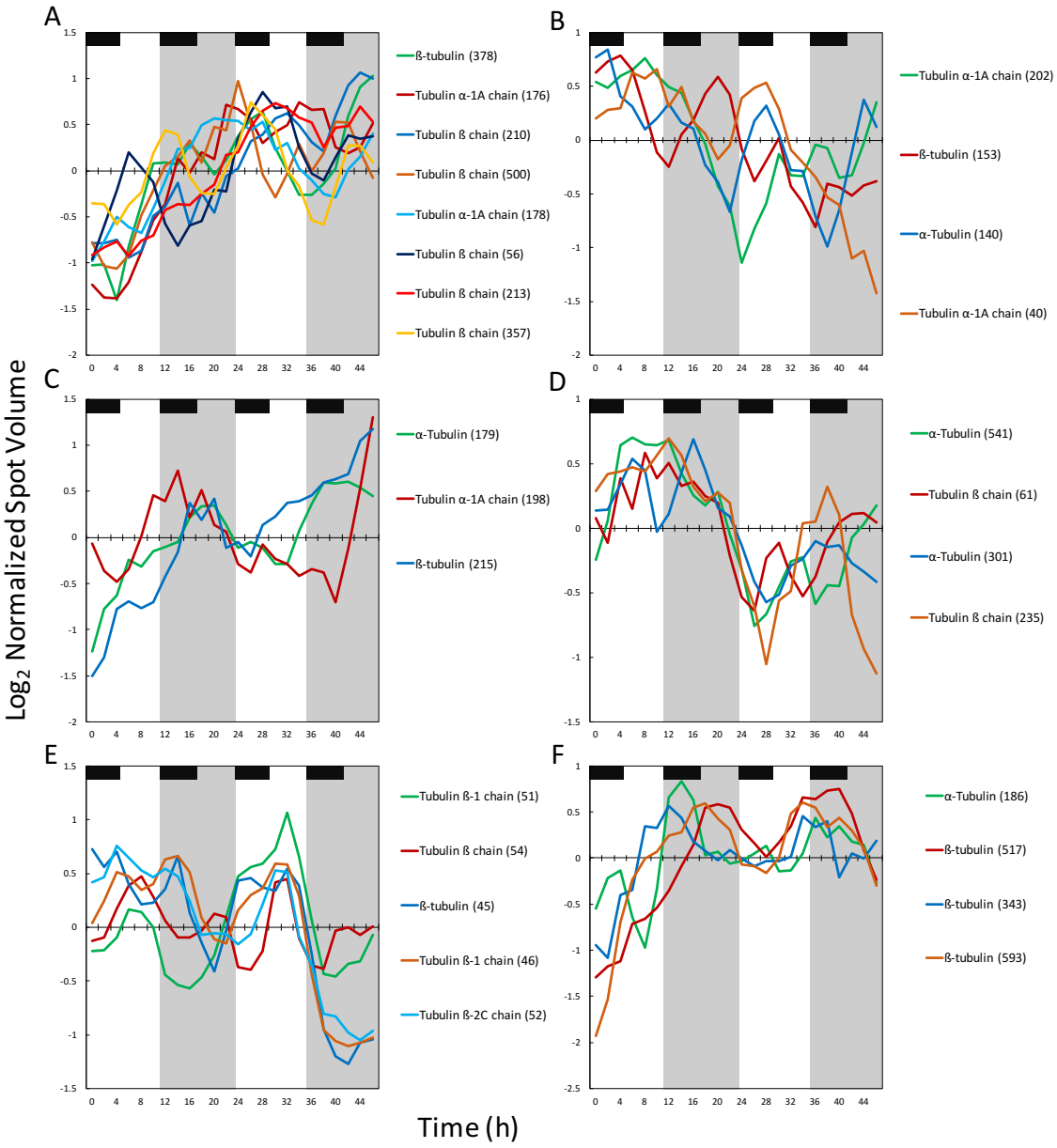

Figure 19. Moving average expression profiles across the 48 h time series for tubulin. Simulated conditions at each time point are shown with high tide as black bar above and darkness as gray shading behind.

Intracellular calcium has been shown to be a regulator of circadian rhythms (Báez-Ruiz and Díaz-Muñoz, 2011). Cytoplasmic calcium plays roles in entraining the circadian clock, regulation of clock gene expression, and signaling (Báez-Ruiz and Díaz-Muñoz, 2011). However, in *Mytilus* gill tissue there is a further influence of Ca^{2+} on cilia dynamics. Even a minor increase in Ca^{2+} at the axoneme of mussel gill cilia has been shown to induce ciliary arrest (Walter and Satir, 1978). The length of cilia has also been extended through the inhibition of Ca^{2+} release (Keeling et al., 2016). A signaling protein, complement C1q tumor necrosis factor-related protein 1 (C1QTNF1, 454), has been shown to elevate cytosolic Ca^{2+} concentration (Jeon et al., 2008) and showed peak abundance coordinated with low tide events, potentially showing a role for low-tide calcium signaling in the cessation of activity in gill cilia. However, in the gill tissue of the Pacific oyster *Crassostrea gigas*, aerial exposure was also found to increase the abundance of numerous ion transport and calcium binding proteins to potentially divert the Ca^{2+} signaling from activities such as proliferation and development (Zhang et al., 2015). This response could be supported by the increased abundances of the cAMP-regulated Ca^{2+}-binding protein calcyphosin (544) (Lefort et al., 1989) and EF-hand domain-containing protein (167) (Fig. 20).

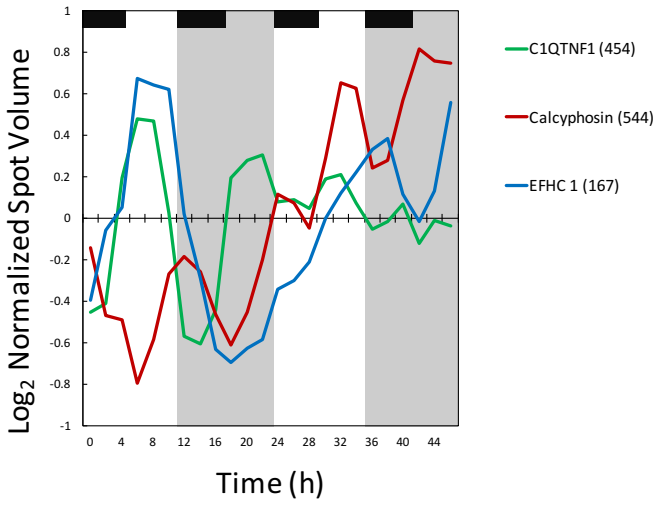

Figure 20. Moving average expression profiles across the 48 h time series for Ca2+-related proteins. Simulated conditions at each time point are shown with high tide as black bar above and darkness as gray shading behind.

Tubulin is also vital for intracellular transport, which is important for *Mytilus* gill tissue as specialized mucosal cells must secrete vesicles of acidified mucous rich in carbohydrate modifications to recognize, trap, and carry filtered particles along the ventral groove toward the mouth (Pales Espinosa et al., 2016; Riisgård et al., 2011; Rosa et al., 2015). Mucosal proteins that mature in the endoplasmic reticulum (ER) are released to the extracellular matrix, playing a vital role in both immune and food particle recognition, such as the protein galectin (175), which peaked during immersion (Pales Espinosa et al., 2016; Rosa et al., 2015). Immersion typically corresponded with peak abundances for ER chaperones that facilitate the folding and glycosylation of secreted proteins, including malectin B (604), calreticulin (50), translocon-associated protein subunit ß (591), calumenin (59), 78kDa glucose-related protein (592), protein disulfide

isomerase (201, 216), and Hsp90 (29, 30) (Hebert and Molinari, 2007) (Fig. 20A). In the mouse liver proteome, circadian proteins were enriched for protein processing in the ER during the night in nocturnally active mice, suggesting that tissues responsible for secretory processes follow highly controlled patterns of processing that correlate with activity rhythms (Robles et al., 2014).

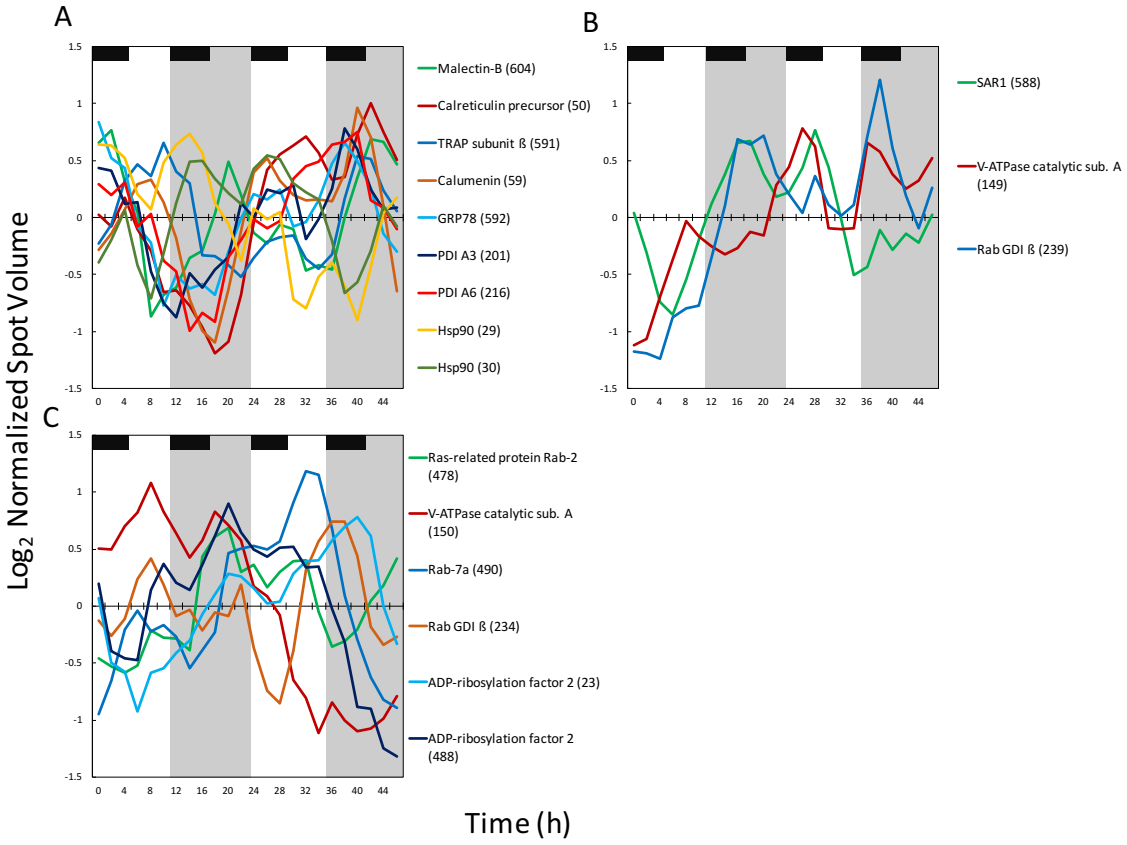

Figure 21. Moving average expression profiles across the 48 h time series for vesicular proteins. Simulated conditions at each time point are shown with high tide as black bar above and darkness as gray shading behind.

Robles et al. (2014) further found that proteins involved in ER and Golgi vesicle maturation followed similar nocturnal rhythms. Secreted proteins continue to mature within the exocytic vesicle transport process in the golgi apparatus. From the ER, vesicles are formed with the protein SAR1 (588), which peaked during high tide (Fig. 21B). However, vesicles are targeted to the Golgi and eventually secretion through the activity of Rab 2 (478), which peaked during low tide. Secretory vesicles must also undergo a decrease in pH, which is facilitated by the presence of V-type H^+ ATPases peaking during high tide (149) (Fig. 21B) and low tide (150) (Fig. 21C). The importance for altering the acidity of intracellular organelles has also been shown for the low-pH conditions of mucous vacuoles in bivalve endothelial cells (Rivera-Ingraham et al., 2016). Rab 7a (490), which targets endocytic vesicles for lysosomal degradation (Bhuin and Roy, 2014), was found to peak during low tide as well (Fig. 21C). Interestingly, two isoforms of Rab GDP dissociation inhibitor ß (GDI) peaked either during high tide (239) (Fig. 21B) or low tide (234) (Fig. 21C). As Rab GDI is required for recycling cytosolic Rab proteins following delivery of vesicles to acceptor membranes, their presence in coordination with SAR1, Rab2, and Rab7a support the evidence of vesicular trafficking during both high and low tide. Furthermore, once proteins are in the Golgi, ADP-ribosylation factors (ARF) recruit vesicle coatings required for transport within the Golgi or back to the ER (Lodish et al., 2000). In this study, ARF2 (23, 488) peaked primarily during low tide, suggesting a degree of vesicular transport in the retrograde direction (Fig. 21C).

The variability of these vesicular proteins may be indicative of the importance of the extracellular environment of the gill. During high tide, mucosal secretions ensure

efficient particle recognition, capture, and retention (Espinosa et al., 2010; Pales Espinosa et al., 2016) and protection from infection (Espinosa et al., 2010). During low tide, secretions may limit growth of microbiota (Antunes et al., 2010; Beck and Peatman, 2015), clean epithelial surfaces of particle residues (Pales Espinosa et al., 2016), or prevent desiccation (Davies and Hawkins, 1998). Recently, mucosal vacuoles have been found to concentrate superoxide radicals, suggesting that these secretions are conditioned to prevent the growth of microbiota (Rivera-Ingraham et al., 2016). These functions may explain the evidence of the secretory pathway during high tide as well as continued vesicle trafficking during low tide. Furthermore, the presence of retrograde trafficking proteins such as Rab7a may indicate some salvage of extracellular amino acids during aerial exposure (Pajor and Wright, 1987).

Immunity

Extracellular proteins involved in the innate immune system of bivalves were identified with peak abundances corresponding to tidal cycles. Among those peaking during high tide were several immune-related proteins, including apextrin (401, 443) and fibrinogen 2 (420). Meanwhile, immune-recognition C1q-domain-containing proteins showed isoforms peaking during high tide (19) as well as low tide (564) (Gerdol and Venier, 2015) (Fig. 22). The innate immune system of *Mytilus* is based on pathogen recognition via patterns on extracellular, intracellular, and circulating proteins (Venier et al., 2011). While anoxia has been shown to suppress immune function in *C. gigas*, natural tidal conditions are unlikely to present fully anoxic conditions (Dudognon et al., 2013).

C. gigas was shown to retain its hemocyte killing activity despite aerial exposure and decreased Po_2, though higher temperatures did significantly decrease killing ability (Allen and Burnett, 2008). For this reason, *M. californianus* experiencing tidal fluctuations may regularly utilize pathogen-recognizing proteins on the gill epithelium during high tide feeding cycles when they are likely to contact waterborne bacteria. However, during low tide the presence of circulating proteins with pathogen-recognition sequences are also vital to defenses despite suppressed cellular activity.

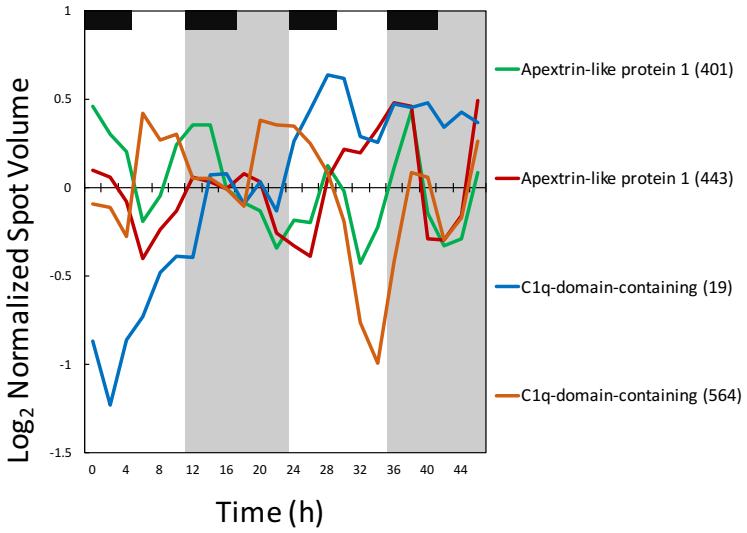

Figure 22. Moving average expression profiles across the 48 h time series for immune-related proteins. Simulated conditions at each time point are shown with high tide as black bar above and darkness as gray shading behind.

Proliferation

The influence of the tidal cycle on cell proliferation in bivalves has been an issue of speculation in multiple studies. In *Mytilus*, patterns of low tide cell proliferation have been seen in the gill tissue (Gracey et al., 2008) and the digestive epithelium (Zaldibar et al., 2004), suggesting that the activity of feeding and cell division are temporally separated in these tidally-acclimated mussels. In *C. gigas,* however, proteomic analysis of gill samples showed that aerial emersion may suppress DNA replication (Zhang et al., 2015). In this study, proteins involved in DNA repair and proliferation offer a mixed interpretation. Proliferating cell nuclear antigen (PCNA; 83), a common marker of proliferation (Maiorova and Odintsova, 2016), appears to follow a circadian cycle with a daytime low-tide peak, matched in part by DNA helicase (448) (Fig 23). However, another isoform of DNA helicase (460) corresponds to high tide cycles, perhaps reflecting a PTM to alter activity with the tides. A cycle of DNA repair by the protein RuvB (195, 212) appeared to peak primarily at night, though during low tide on the first day and high tide on the second day. Given the evidence of increased feeding, metabolic activity, and oxidative stress proteins around these evening times, it appears likely that DNA replication is temporally separated from peak activity, though on a daily scale rather than the tidal scale previously described in *Mytilus* (Gracey et al., 2008). Complexes I, II, and III in mitochondrial oxidative phosphorylation tend to be sources of ROS production when metabolic activity increases (Gottlieb and Bernstein, 2016). Due to the mutagenic consequences of ROS damaging DNA, temporal separation of oxidative metabolism from DNA replication has been well documented in the yeast metabolic cycle (Chen et al., 2007) and may be visible in this time course. The peak for RuvB, which

participates in an ATP-dependent helicase resolution of Holliday Junctions in DNA (Wyatt and West, 2014), may indicate that DNA repair is performed when stress is theoretically reduced and ATP is readily available.

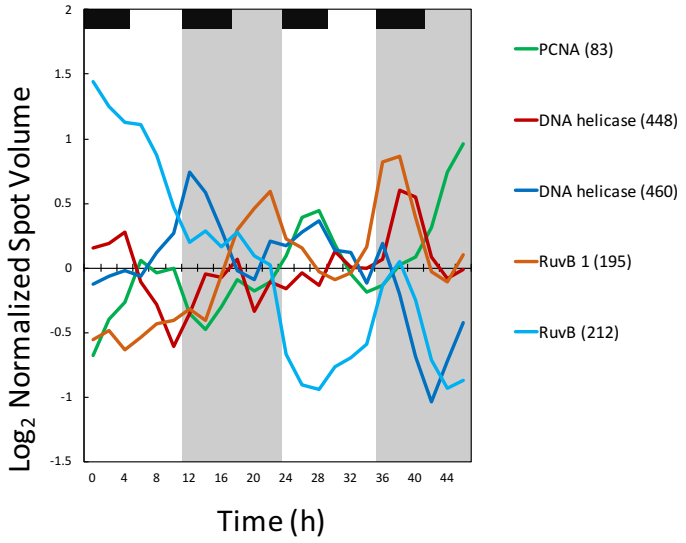

Figure 23. Moving average expression profiles across the 48 h time series for DNA replication and repair proteins. Simulated conditions at each time point are shown with high tide as black bar above and darkness as gray shading behind.

Signaling

Several proteins that have been documented in circadian regulation were identified in this study with cryptic results. One protein, dopamine-N-acetyltransferase (430), is an arylalkylamine N-acetyltransferase (AANAT) that is involved in the synthesis of melatonin from serotonin and has on occasion been dubbed the "timezyme" for its role in signaling circadian rhythms (Klein, 2007). AANAT has been found to increase its activity when dark-dependent phosphorylation stimulates a complex

formation with 14-3-3 proteins (100, 603), while cAMP signaling targets the complex for proteasomal degradation (Klein, 2007). In this study, dopamine-N-acetyltransferase and 14-3-3 isoforms showed similar overall trends, but the coordination and abundance changes do not clearly indicate a role in circadian cycling (Fig. 24). However, in *Mytilus* melatonin may act as a scavenger of ROS (Manchester et al., 2015) or dopamine-N-acetyltransferase may regulate the levels of serotonin and dopamine, which together stimulate and inhibit ciliary activity, respectively (Malanga, 1974; Stefano and Aiello, 1975). Another known circadian signaling protein found in this time course was the catalytic subunit of PP1-ß phosphatase (320). This protein has been shown to influence the nuclear localization of PER2 and thus guide light-resetting of the molecular clock (Schmutz et al., 2011). However, in this study the abundance pattern may indicate a more cryptic role in one of the many functions of PP1. For example, the frequent oscillations of PP1 tend to fall at the beginning or end of any high tide period (Fig. 24), which may support its role in dephosphorylating and activating eIF2 for translation, regulating actin dynamics and returning the cell to a basal state, and regulating energy expenditure (Ceulemans and Bollen, 2004).

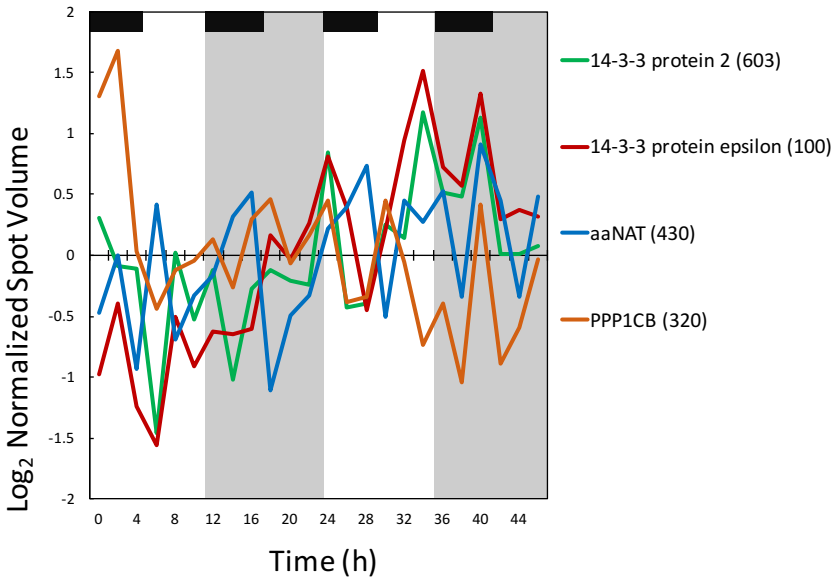

Figure 24. Mean expression profiles across the 48 h time series for potential circadian signaling proteins. Simulated conditions at each time point are shown with high tide as black bar above and darkness as gray shading behind.

Conclusions

This study is the first proteomic time-course analysis of rhythmic protein abundance changes in an organism experiencing a rhythmic environment in both light/dark and tidal cycles. Previous studies have determined the importance of these fluctuating conditions on the transcriptome (Connor and Gracey, 2011; Gracey et al., 2008) and the metabolome (Connor and Gracey, 2012), but proteomic studies are increasingly finding that post-transcriptional and post-translational mechanisms drive unique rhythms in the proteome (Atger et al., 2015; Mauvoisin et al., 2014; Robles et al., 2014). In this study, the circadian cycle appears to drive the dominant rhythms in the gill proteome of *M. californianus*. Energy metabolism in particular appears to pivot around

the darkness/high tide period in this study. Coordination is visible in carbohydrate metabolism at the night/day and low/high tide interphase, as seen in the abundance of glycolytic enzymes, PDH, and oxidative TCA cycle proteins. During immersion, a contribution of fatty acid oxidation becomes prominent, with electron flux from these fuel sources through succinate dehydrogenase and electron transfer flavoprotein matched to abundances of Complex III and ATP synthase. As the nighttime low tide sets in, a shift toward the PPP appears to take place, coordinated by the gluconeogenic enzyme F-1,6-BP and 6-phosphoglucolactonase. Daytime results in a general decrease in metabolic enzymes, with the exception of components that appear to direct metabolites toward the action of $NADP^+$-dependent isocitrate dehydrogenase, likely for scavenging ROS during the potential heat stress during the midday low tide.

The circadian rhythm of metabolic proteins was surprising, as restricted feeding and metabolic depression during tidal cycles were expected to exert a strong influence over these processes. The tidal cycle appeared to determine alterations to cytoskeletal components, some of which contribute to the function of cilia and may play a role in high-tide feeding activity. Cycling of the cytoskeleton was particularly apparent in actin-binding proteins that showed cycles of low tide stabilization of actin filaments with high tide depolymerization. Other functions under an apparent tidal influence included ER protein processing and vesicular trafficking, extracellular matrix and immune proteins, and proteostasis constituents involved in oxidative stress and chaperoning. In general, these functional categories tended to suggest that protein processing and exocytosis increases during high tides, with protective functions such as chaperones and immune proteins increasing in response to low tide aerial emersion.

While this study provides a broad overview of the changes in the soluble proteome over these cyclical environmental changes, there are some weaknesses to this approach. First, detection of rhythmic proteins using 2DGE tends to uncover more abundant proteins, which typically exhibit longer half-lives and therefore smaller amplitude rhythms (Lück and Westermark, 2015). This is likely the reason for core clock proteins going undetected in most large-scale proteomic studies despite their known oscillations. Furthermore, the typical mRNA half-life between 6 min and 50 h makes rhythmic transcripts far more detectable compared to proteins, which exhibit half-lives ranging from 1 h to 1,000 h (Lück et al., 2014). Differences between transcript and protein abundance were recently demonstrated in a sharp and immediate transcriptional response to unfolded protein stress while corresponding protein products showed a delayed, gradual increase to a new steady-state level (Cheng et al., 2016). The slower, deliberate rate of protein synthesis may result in less drastic fluctuations than the transcript level. The approach used in this study is also not optimized for the detection of PTMs. The importance of these modifications in determining the rhythmic state of cells is clear (Kovacic and Somanathan, 2014; Rey and Reddy, 2013b). While candidate proteins responsible for acylation, phosphorylation, and methylation provide clues as to the regulation of cellular processes, the methods used in this study primarily consider the altered abundances of identified proteins. Furthermore, the use of the gill tissue as a single entity compiles protein abundance regardless of cell types with diverse functions. At an even finer scale, the functional consequences of altered protein abundances may only be consequential depending on the sub-cellular localization (Boisvert et al., 2012; Lück and Westermark, 2015). The importance of rhythmic protein activity levels should

also be considered. A wide range of differential enzyme rate constants within a single metabolic pathway could mean that a single cycling protein could have profound impacts on the accumulation of metabolites (Lück and Westermark, 2015). Furthermore, due to the effects of gradual methionine oxidation over a long half-life, a steady-state amount of protein may exhibit rhythms in activity as older proteins are degraded and replaced with newly translated ones (Atger et al., 2015; Cui et al., 2011). Each of these factors may contribute to deviations between transcriptomics, proteomics, and metabolomics, such as the overall circadian peak in metabolic protein abundances seen in this study despite the strong tidal cycle of metabolites found by Connor and Gracey (2012).

Rhythmic protein abundance may be determined by constraints that are unique from those of transcripts and metabolites. The energetic cost of producing proteins far exceeds RNA, consuming as much as 50% of the cellular ATP (Liu et al., 2016). Traditionally, analyses of the energetic requirements of rhythmicity assume that translation into a final functional protein will occur, resulting in a cycle of predictive homeostasis that optimizes protein synthesis in anticipation of a known, regularly-occurring perturbation (Lück and Westermark, 2015; Wang et al., 2015). This predictive homeostasis is thought to limit the burden of reactive homeostasis, where a response is fully induced by the perturbation and damage has time to accumulate during slow protein synthesis (Lück and Westermark, 2015). However, the numerous regulatory steps leading to a functional protein add the potential for a combination of predictive and reactive homeostasis to play roles in rhythmic processes. For example, transcription cycles may be optimized to provide a pool of RNA for the option of rapid subsequent translation based on the needs of transient external conditions, thus adding an element of reactive

homeostasis to rhythmicity. The discovery of circadian miRNA, which may regulate the degradation or repression of mature mRNA, may be an example of this fine-scale regulation of protein translation (Wang et al., 2016). This would be accomplished by a molecular titration model, through which protein translation is repressed until mRNA exceeds a threshold of inhibitory miRNA, thus enacting a sharp, sensitive switch to protein production given a small increase in transcription (Mukherji et al., 2011). Additionally, researchers are continuously finding that the circadian rhythm itself appears to be a reactive mechanism. Several studies have found that beyond alterations to the period, phase, or amplitude of rhythmic components seen in a single experimental system there are increasingly more molecular species that show the capacity for novel oscillations given the right conditions, such as feeding times or nutrient types (Eckel-Mahan et al., 2013; Patel et al., 2015; Schunter et al., 2016).

The plasticity of these cycles leads to the question of how rhythms in protein abundance are regulated in this study, whether by external cues or endogenous cycles. We speculated that HIF-1 may play a role in driving a dynamic competition between transcription factors for gene promoter regions when aerial emersion is added to a light/dark cycle. Evidence of endogenous tidal rhythms is scarce. In *C. gigas*, studies found a free-running rhythm of circadian but not circatidal valve activity (Mat et al., 2014). More recently, the same researchers examined the contribution of the light-responsive cryptochrome 1 (*cry1*) in determining the circadian activity of *C. gigas.* They demonstrated the light-responsiveness by showing that *cry1* did oscillate under light/dark entrainment, but not in the absence of light. However, they also showed that *cry1* oscillated with a simulated tidal cycle in the absence of light (Mat et al., 2016, 1). This

suggests that rather than an endogenous circatidal cycle, acclimation to predictable tides may function by co-opting the circadian mechanisms to optimize responses to the addition of a tidal cycle.

This study provides evidence that a large portion of the soluble proteome in the gill tissue of *M. californianus* exhibits rhythmic abundance changes. In the absence of additional stressors, acclimation to a typical laboratory simulation of light/dark cycles and constant tidal cycles of emersion and immersion resulted in as much as 86% of the detectable proteins fluctuating over time. Patel et al. (2015) noted that the abundance of transcripts that have been found to oscillate, either regularly or under certain experimental manipulations, is a clear indication of the restraint necessary when interpreting results from differential gene expression studies using a limited number of time points. This reinforces the importance of establishing a familiarity with the baseline changes in organismal physiology in response to naturally fluctuating environments, specialized acclimation regimes, or even under constant conditions. Characterizing molecular variability, as in this study, is particularly important for comparative stress response studies (Dahlhoff, 2004; Logan et al., 2012) and biomonitoring programs (Izagirre et al., 2008; Luedeking and Koehler, 2004; Tremblay and Pellerin-Massicotte, 1997; Vidal-Liñán and Bellas, 2013) that often rely on the assumption of a static baseline.

Materials and methods

Collection, acclimation, and dissection

700 *Mytilus californianus* adults of 4-7 cm shell length were collected from Hazard Reef in Monaña de Oro State Park, Los Osos, CA (35°17'22.4"N, 120°52'58.4"W) in February 2015 and placed in a single layer in a tank in the tidal simulator at the California Polytechnic State University Pier in Avila Beach, CA for four weeks of acclimation. The computer-controlled conditions simulated 12:12 h light/dark cycles (lights on from 0600 to 1800) and square-wave 6:6 h high/low tidal cycles (high tides from 0600 to 1200 and 1800 to 0000) (Fig. 25). Full-spectrum lighting was provided by Orbit Marine LED lights (Current USA, Vista, CA, USA). Filtered seawater (Pentek ECP-1-10 1 µm filters, Pentair, Minneapolis, MN, USA) was cycled through the tank to provide natural seawater chemistry and a pump was programmed to provide a 15 mL dose of 1:10 Shellfish Diet 1800 (4 – 20 µm algal size; 40% *Isochrysis,* 15% *Pavlova*, 25% *Tetraselmis,* and 20% *Thalassiosira pseudonana*; Reed Mariculture, Inc., San Jose, CA) each hour during the 6 h high tide period to ensure a consistent feeding regime. The Shellfish Diet biomass composition is cited by the manufacturer as containing 45% protein, 14% lipid, 17% carbohydrate, and 22% ash (Reed Mariculture, Inc., San Jose, CA). Temperature was recorded for the duration of the acclimation and dissection period using a StowAway TidbiT TempLogger (Onset, Bourne, MA, USA). The acclimation temperatures showed an average of 16.10^{o}C with a range from 12.30^{o}C to 25.94^{o}C. However, the accuracy of these temperatures, particularly when exposed to the air, is likely a poor approximation of the temperature experienced by the mussels. A study comparing these temperature loggers to sensors within a live mussel found an average

error of up to 14^{o}C and cautioned against their use in estimating the temperature experienced by the organism (Fitzhenry et al., 2004). Therefore, these thermal maxima that were measured may never have been experienced by the mussels due to the thermal inertia or evaporative cooling of the organism and, in fact, the varying size or location of the mussels within the tank could result in slightly different body temperatures among individuals (Helmuth, 2002).

Gill tissue sampling was completed from 13-15 March 2015 beginning one hour into the daylight high tide condition at 0700. Gill tissue was dissected during continued acclimation conditions from six haphazardly selected individuals every two hours over a 48 h period from each treatment group and frozen at -80^{o} C (24 sampling time points, N = 6 per time point, 144 total gill tissue samples) (See Fig. 25 for acclimation and sampling design). Samples were then processed using the proteomic workflow outlined in Tomanek and Zuzow (2010) and detailed below. Unless otherwise stated, reagents were obtained from BioRad (Hercules, CA, USA) and Fisher Scientific (Pittsburg, PA, USA).

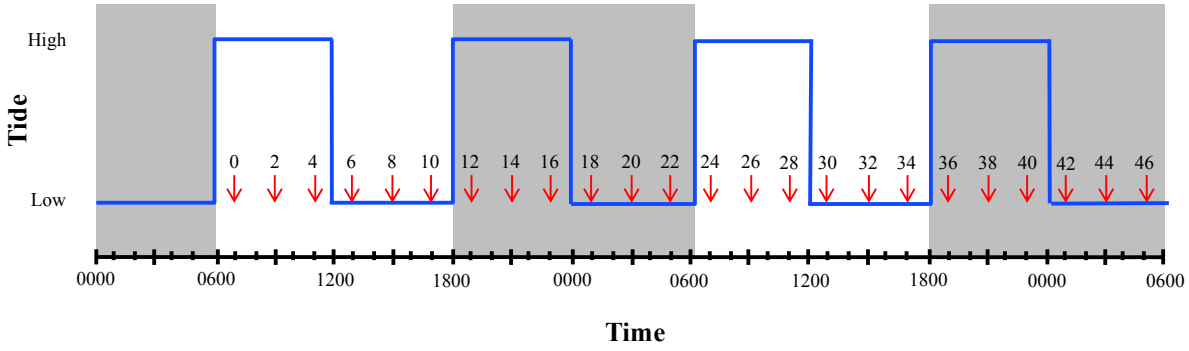

Figure 25. Acclimation and sampling conditions showing light/dark and tidal cycles with time of day on the horizontal axis. Blue line indicates high/low water level of the square wave tidal cycle. Grey background denotes darkness; white background is light. Sampling time points are shown as red arrows (N = 6 mussels per arrow), beginning with 0 h at 0700 and sampling every two hours to 46 h.

Homogenization

Approximately 0.3 g of gill tissue for each sample was weighed and homogenized in 1.2 mL of homogenization buffer (7M urea, 2M thiourea, 40mM Tris-HCl, 1%, amidosulfobetaine-14, 0.5% IPG buffer (GE Healthcare, Piscataway, NJ, USA), 40mM dithiothreitol) using ground-glass homogenizers and left for one hour at room temperature. To eliminate large cellular lysates, samples were centrifugation at 13,200 x G for 30 minutes at room temperature and the supernatant was retained. Each sample was separated into three separate aliquots, washed in 4X volume 10% trichloroacetic (TCA)/acetone, and stored overnight at -20°C to precipitate the proteins.

The next day, aliquots were centrifuged at 4°C for 15 minutes at 13,200 x G and the supernatant was discarded. Each protein pellet was washed with 100% acetone to remove any remaining TCA. After centrifugation at 4^{o}C for 15 min at 13,200 x G, the

acetone was quickly discarded and the protein pellet was resuspended in rehydration buffer (7M urea, 2 M thiourea, 2% cholamidopropyl-dimethylammonio-propanesulfonic acid, 2% nonyl phenoxylpolyethoxylethanol-40, 0.002% bromophenol blue, 0.5% IPG buffer (GE HealthCare), 100 mM dithioerythritol). The rehydrated protein aliquots were pooled and protein concentration was determined using a 2D Quant kit (GE HealthCare) following the manufacturer's instructions.

Gel electrophoresis

Using 11cm long immobilized pH gradient (IPG) strips ranging from pH 4-7 (ReadyStrip; BioRad, Hercules, CA, USA), we loaded 400 μg of protein to be separated by isoelectric point (pI) using a BioRad isoelectric focusing (IEF) cell using the following program: 5 h of passive rehydration, 12 h of active rehydration (50V), 500 V for 1 h, 1000 V for 1 h, and 8000 V for 2.5 h. After running, strips were frozen at -80^{o}C for at least one hour prior to separating proteins in the 2nd dimension.

For the 2nd dimension, IPG strips were incubated 15 minutes each in equilibration buffer (6 M urea, 50 mM Tris-HCl, pH 8.8, 30% glycerol, 2% SDS, 0.002% bromophenol blue) first with 65mM dithiothreitol and next with 135mM iodoacetamide. IPG strips were placed on top of 11.8% SDS-acrylamide gels, secured with 0.8% agarose, and run at 200V in a 12-gel BioRad Criterion Dodeca for 55 minutes in 10°C 1X running buffer (25 mM Tris base, 192 mM glycine, and 0.1% SDS). Gels were stained with Colloidal Coomassie Blue overnight and destained with repeated rinsing in Milli-Q water (Millipore, Billerica, MA, USA) for approximately 48 h. Destained gels were scanned to

.tif format with a predetermined tone correction on an Epson 1680 transparency scanner (Epson, Long Beach, CA, USA).

Gel image analysis

Digitized gel images were processed using Delta2D (version 4.3, Decodon, Greifswald, Germany). Gel images were warped to each other using a chained-group warping strategy and a fusion image was generated from the 144 gels to show the average spot volume for overlapping protein spots. This fusion image was used to generate spot boundaries and labels which were then transferred to all gel images. After background subtraction, spot volumes were normalized against the total spot volume of all proteins in the gel image and exported for statistical analysis.

Data analysis

The normalized spot volumes from every protein spot and sample gel were analyzed across all time points to test for rhythmic patterns of period length 4 – 28 h against a cosine waveform using JTK_Cycle algorithm v. 2.1 (Hughes et al., 2010) in R v. 3.2 (R Core Team, 2016). Further analysis was performed using the Bioconductor R package RAIN to detect rhythmic proteins with asymmetric rising and falling phases (Thaben and Westermark, 2014). RAIN was set to assess period lengths of 4 – 28 h and allow for rising and falling phases encompassing 30% and 70% of the total period length, respectively. For both statistical analyses, a threshold for significantly cycling proteins was set using the adaptive Benjamini-Hochberg method (Benjamini and Hochberg, 1995) false discovery rate of $q < 0.05$. Period and phase attributes of significant rhythms were identified by JTK_Cycle (Hughes et al., 2010).

Trypsin digestion

Proteins spots were excised from gels using a 2.0 mm diameter spot cutter (Manual Tissue Array Punches, Beecher Instruments, Inc., Sun Prairie, WI, USA). Spots of interest were shaken for 45 min at room temperature in destaining buffer (25mM ammonium bicarbonate (NH_4HCO_3)/50% acetonitrile) to remove Colloidal Coomassie Blue stain, dehydrated for 10 min in 100% acetonitrile, then proteins were digested with trypsin solution (40mM NH_4HCO_3, 10% acetonitrile, 4.3 μg/μL trypsin (MS Grade Trypsin Gold, Promega, Madison, WI)) overnight at 37°C. In the morning, spots were shaken for 1 h at room temperature in an analyte solution (2:1 0.1% TFA:Acetonitrile) to elute the peptides from the gel matrix. The leftover gel plugs were discarded. Analyte solution was concentrated in a new tube in a SpeedVac (Thermo Fisher Scientific, Waltham, MA, USA) for 1 h at 45°C. Dried peptides were resuspended in a TA-30 solution (70:30 0.1% TFA:Acetonitrile) and double-plated on a 600 μm Anchorchip 384 target plate (Bruker Daltonics Inc., Billerica MA, USA). After drying, a matrix solution (0.2mg/mL α-hydroxycyanocinnamic acid (HCCA) in acetonitrile, 0.1% trifluoroacetic acid (TFA)/acetonitrile) was added directly onto each plated protein and left to dry. For each sample, one of the two plated replicates was rinsed with ice cold HPLC H_2O to remove excess salts while the other replicate is untouched to preserve potentially water-soluble peptides. Peptide calibration standard (#206195, Bruker Daltonics Inc.) in matrix solution was plated for MS calibration.

Mass spectrometry

A matrix-assisted laser desorption ionization tandem time of flight (MALDI TOF/TOF) mass spectrometer (Ultraflex II, Bruker Daltonics Inc.) was used to generate

peptide mass fingerprints (PMFs) and peptide fragment fingerprints (PFFs) for plated proteins using a +1 charge state and a mass range of 900 – 3300 Da. FlexAnalysis (version 3.0, Bruker Daltonics Inc.) was used to detect peptide peaks with a SNAP peak detection algorithm using a signal-to-noise ratio threshold of 4 for MS and 5 for MS/MS). BioTools (version 2.2, Bruker Daltonics Inc.) and MASCOT search engine (version 2.2, Matrix Science Inc., Boston, MA, USA) were used to search sample spectra against databases with theoretical trypsin cleavage fragments, allowing a precursor ion tolerance of 500 ppm, fragment ion tolerance of 0.6 Da, and carbamidomethyl (C) and oxidation (M) variable sequence modifications. Databases used in the MASCOT search included the following: *Mytilus* protein (7,844 sequences), *Mytilus* EST (409,254 sequences), *Mytilus edulis* EST (447,720 sequence), Mollusca EST (1,147,871 sequences), and NCBI Metazoa (last update: April 2016; 9,560,026 sequences). A sequence match with a MOWSE score above a significance threshold ($p < 0.05$) and matching two or more peptide fragments were used as criteria for significant identifications. Sequence matches were run through NCBI Basic Local Alignment Search Tool (BLAST) to obtain protein identities based on sequence homology with previously annotated and reviewed entries. For some isoforms, the online ExPASy FindMod tool (Swiss Institute for Bioinformatics, Lausanne, Switzerland) was utilized to identify potential post-translational modifications based on mass changes to the sequence identity found in the PMF peak list. All identified proteins were also compared to putative human orthologs using NCBI tBLASTn to find enriched gene ontology (GO) categories in DAVID (Huang et al., 2009a; Huang et al., 2009b).

REFERENCES

2-D Quant Kit (80-6483-56) Product Information, GE Healthcare Bio-Sciences.

Abbott, A. (1999). A post-genomic challenge: learning to read patterns of protein synthesis. *Nature* 402, 715–720.

Abbott, D. P. and Haderlie, E. C. (1980). *Intertidal Invertebrates of California*. Stanford University Press.

Addison, J. A., Ort, B. S., Mesa, K. A. and Pogson, G. H. (2008). Range-wide genetic homogeneity in the California sea mussel (*Mytilus californianus*): a comparison of allozymes, nuclear DNA markers, and mitochondrial DNA sequences. *Molecular Ecology* 17, 4222–4232.

Aebersold, R. and Mann, M. (2003). Mass spectrometry-based proteomics. *Nature* 422, 198–207.

Ahmad, F. A. and Chaplin, A. E. (1984). Anaerobic metabolism of bivalve molluscs during exposure to air. *Biochemical Systematics and Ecology* 12, 85–88.

Allen, S. M. and Burnett, L. E. (2008). The effects of intertidal air exposure on the respiratory physiology and the killing activity of hemocytes in the pacific oyster, *Crassostrea gigas* (Thunberg). *Journal of Experimental Marine Biology and Ecology* 357, 165–171.

Altieri, A. H. (2006). Inducible variation in hypoxia tolerance across the intertidal-subtidal distribution of the blue mussel *Mytilus edulis*. *Marine Ecology Progress Series* 325, 295–300.

Amos, L. A. (2008). The tektin family of microtubule-stabilizing proteins. *Genome Biol* 9, 229.

Anderson, K. A. and Hirschey, M. D. (2012). Mitochondrial protein acetylation regulates metabolism. *Essays Biochem* 52.

Antunes, F., Hinzmann, M., Lopes-Lima, M., Machado, J. and Costa, P. M. da (2010). Association between environmental microbiota and indigenous bacteria found in hemolymph, extrapallial fluid and mucus of *Anodonta cygnea* (Linnaeus, 1758). *Microb Ecol* 60, 304–309.

AquaDect Musselmonitor®: a biological early warning system. *Musselmonitor®*.

Atger, F., Gobet, C., Marquis, J., Martin, E., Wang, J., Weger, B., Lefebvre, G., Descombes, P., Naef, F. and Gachon, F. (2015). Circadian and feeding rhythms differentially affect rhythmic mRNA transcription and translation in mouse liver. *PNAS* 112, E6579–E6588.

Austin-Tse, C., Halbritter, J., Zariwala, M. A., Gilberti, R. M., Gee, H. Y., Hellman, N., Pathak, N., Liu, Y., Panizzi, J. R., Patel-King, R. S., et al. (2013). Zebrafish ciliopathy screen plus human mutational analysis identifies C21orf59 and CCDC65 defects as causing primary ciliary dyskinesia. *Am. J. Hum. Genet.* 93, 672–686.

Aviram, R., Manella, G., Kopelman, N., Neufeld-Cohen, A., Zwighaft, Z., Elimelech, M., Adamovich, Y., Golik, M., Wang, C., Han, X., et al. (2016). Lipidomics analyses reveal temporal and spatial lipid organization and uncover daily oscillations in intracellular organelles. *Molecular Cell* 62, 636–648.

Báez-Ruiz, A. and Díaz-Muñoz, M. (2011). Chronic inhibition of endoplasmic reticulum calcium-release channels and calcium-ATPase lengthens the period of hepatic clock gene Per1. *Journal of Circadian Rhythms* 9, 6.

Ball, M. S. and Karuso, P. (2007). Mass spectral compatibility of four proteomics stains. *J. Proteome Res.* 6, 4313–4320.

Baltz, A. G., Munschauer, M., Schwanhäusser, B., Vasile, A., Murakawa, Y., Schueler, M., Youngs, N., Penfold-Brown, D., Drew, K., Milek, M., et al. (2012). The mRNA-bound proteome and its global occupancy profile on protein-coding transcripts. *Molecular Cell* 46, 674–690.

Bayne, B. L., Bayne, C. J., Carefoot, T. C. and Thompson, R. J. (1976). The physiological ecology of *Mytilus californianus* Conrad. 2. Adaptations to low oxygen tension and air exposure. *Oecologia* 22, 229–250.

Beck, B. H. and Peatman, E. (2015). *Mucosal Health in Aquaculture*. Academic Press.

Bell-Pedersen, D., Cassone, V. M., Earnest, D. J., Golden, S. S., Hardin, P. E., Thomas, T. L. and Zoran, M. J. (2005). Circadian rhythms from multiple oscillators: lessons from diverse organisms. *Nat Rev Genet* 6, 544–556.

Benedetti, M., Giuliani, M. E. and Regoli, F. (2015). Oxidative metabolism of chemical pollutants in marine organisms: molecular and biochemical biomarkers in environmental toxicology: Antioxidant responses in marine ecotoxicology. *Annals of the New York Academy of Sciences* 1340, 8–19.

Benjamini, Y. and Hochberg, Y. (1995). Controlling the false discovery rate: a practical and powerful approach to multiple testing. *Journal of the Royal Statistical Society. Series B (Methodological)* 57, 289–300.

Bernhardt, J. R. and Leslie, H. M. (2013). Resilience to climate change in coastal marine ecosystems. *Annual Review of Marine Science* 5, 371–392.

Berth, M., Moser, F. M., Kolbe, M. and Bernhardt, J. (2007). The state of the art in the analysis of two-dimensional gel electrophoresis images. *Appl Microbiol Biotechnol* 76, 1223–1243.

Bhuin, T. and Roy, J. K. (2014). Rab proteins: The key regulators of intracellular vesicle transport. *Experimental Cell Research* 328, 1–19.

Block, G. D. and Colwell, C. S. (2014). Molluskan Ocular Pacemakers: Lessons Learned. In *The Retina and Circadian Rhythms* (ed. Tosini, G.), Iuvone, P. M.), McMahon, D. G.), and Collin, S. P.), pp. 213–232. New York, NY: Springer New York.

Blumenthal, E. M., Block, G. D. and Eskin, A. (2001). Cellular and Molecular Analysis of Molluscan Circadian Pacemakers. In *Circadian Clocks* (ed. Takahashi, J. S.), Turek, F. W.), and Moore, R. Y.), pp. 371–400. Springer US.

Boisvert, F.-M., Ahmad, Y., Gierliński, M., Charrière, F., Lamont, D., Scott, M., Barton, G. and Lamond, A. I. (2012). A quantitative spatial proteomics analysis of proteome turnover in human cells. *Mol Cell Proteomics* 11, M111.011429.

Borthagaray, A. I. and Carranza, A. (2007). Mussels as ecosystem engineers: Their contribution to species richness in a rocky littoral community. *Acta Oecologica* 31, 243–250.

Brand, M. D. (2000). Uncoupling to survive? The role of mitochondrial inefficiency in ageing. *Experimental Gerontology* 35, 811–820.

Brooks, S. P. J. and Storey, K. B. (1997). Glycolytic controls in estivation and anoxia: A comparison of metabolic arrest in land and marine molluscs. *Comparative Biochemistry and Physiology Part A: Physiology* 118, 1103–1114.

Campos, A., Tedesco, S., Vasconcelos, V. and Cristobal, S. (2012). Proteomic research in bivalves: Towards the identification of molecular markers of aquatic pollution. *Journal of Proteomics* 75, 4346–4359.

Carl, C., Poole, A. J., Williams, M. R. and de Nys, R. (2012). Where to settle—settlement preferences of *Mytilus galloprovincialis* and choice of habitat at a micro spatial scale. *PLoS One* 7,.

Carroll, J. L. and Wells, R. M. G. (1995). Strategies of anaerobiosis in New Zealand infaunal bivalves: Adaptations to environmental and functional hypoxia. *New Zealand Journal of Marine and Freshwater Research* 29, 137–146.

Ceulemans, H. and Bollen, M. (2004). Functional diversity of protein phosphatase-1, a cellular economizer and reset button. *Physiological Reviews* 84, 1–39.

Chabot, C. C. and Watson III, W. H. (2014). Daily and Tidal Rhythms in Intertidal Marine Invertebrates. In *Annual, Lunar, and Tidal Clocks* (ed. Numata, H.) and Helm, B.), pp. 41–63. Springer Japan.

Chen, Z., Odstrcil, E. A., Tu, B. P. and McKnight, S. L. (2007). Restriction of DNA replication to the reductive phase of the metabolic cycle protects genome integrity. *Science* 316, 1916–1919.

Cheng, Z., Teo, G., Krueger, S., Rock, T. M., Koh, H. W., Choi, H. and Vogel, C. (2016). Differential dynamics of the mammalian mRNA and protein expression response to misfolding stress. *Molecular Systems Biology* 12, 855–855.

Choudhary, C., Kumar, C., Gnad, F., Nielsen, M. L., Rehman, M., Walther, T. C., Olsen, J. V. and Mann, M. (2009). Lysine acetylation targets protein complexes and co-regulates major cellular functions. *Science* 325, 834–840.

Chu, F.-L. E., Dupuy, J. L. and Webb, K. L. (1982). Polysaccharide composition of five algal species used as food for larvae of the American oyster, *Crassostrea virginica*. *Aquaculture* 29, 241–252.

Connor, K. M. and Gracey, A. Y. (2011). Circadian cycles are the dominant transcriptional rhythm in the intertidal mussel *Mytilus californianus*. *Proceedings of the National Academy of Sciences* 108, 16110–16115.

Connor, K. M. and Gracey, A. Y. (2012). High-resolution analysis of metabolic cycles in the intertidal mussel *Mytilus californianus*. *American Journal of Physiology - Regulatory, Integrative and Comparative Physiology* 302, R103–R111.

Cooke, J. P. (2004). Asymmetrical dimethylarginine. *Circulation* 109, 1813–1818.

Cui, Z. J., Han, Z. Q. and Li, Z. Y. (2011). Modulating protein activity and cellular function by methionine residue oxidation. *Amino Acids* 43, 505–517.

Dahlhoff, E. P. (2004). Biochemical indicators of stress and metabolism: applications for marine ecological studies. *Annual Review of Physiology* 66, 183–207.

Dahlhoff, E. and Menge, B. (1996). Influence of phytoplankton concentration and wave exposure on the ecophysiology of *Mytilus californianus*. *Mar Ecol Prog Ser* 144, 97–107.

Dahlhoff, E. P., Stillman, J. H. and Menge, B. A. (2002). Physiological community ecology: variation in metabolic activity of ecologically important rocky intertidal invertebrates along environmental gradients. *Integr. Comp. Biol.* 42, 862–871.

Davies, M. S. and Hawkins, S. J. (1998). Mucus from Marine Molluscs. In *Advances in Marine Biology*, pp. 1–71. Elsevier.

Dayton, P. K. (1971). Competition, Disturbance, and Community Organization: The Provision and Subsequent Utilization of Space in a Rocky Intertidal Community. *Ecological Monographs* 41, 351–389.

Deckard, A., Anafi, R. C., Hogenesch, J. B., Haase, S. B. and Harer, J. (2013). Design and analysis of large-scale biological rhythm studies: a comparison of algorithms for detecting periodic signals in biological data. *Bioinformatics* 29, 3174–3180.

de la Iglesia, H. O. and Johnson, C. H. (2013). Biological clocks: riding the tides. *Current Biology* 23, R921–R923.

Demers, A. and Guderley, H. (1994). Acclimatization to intertidal conditions modifies the physiological response to prolonged air exposure in *Mytilus edulis*. *Mar. Biol.* 118, 115–122.

Dillon, S. C., Zhang, X., Trievel, R. C. and Cheng, X. (2005). The SET-domain protein superfamily: protein lysine methyltransferases. *Genome Biol* 6, 227.

Doeller, J. E., Kraus, D. W., Shick, J. M. and Gnaiger, E. (1993). Heat flux, oxygen flux, and mitochondrial redox state as a function of oxygen availability and ciliary activity in excised gills of *Mytilus edulis*. *J. Exp. Zool.* 265, 1–8.

Dolmer, P. (2000). Algal concentration profiles above mussel beds. *Journal of Sea Research* 43, 113–119.

Dowd, W. W. (2012). Challenges for biological interpretation of environmental proteomics data in non-model organisms. *Integr. Comp. Biol.* 52, 705–720.

Dowd, W. W. and Somero, G. N. (2013). Behavior and survival of *Mytilus* congeners following episodes of elevated body temperature in air and seawater. *J Exp Biol* 216, 502–514.

Dowd, W. W., Felton, C. A., Heymann, H. M., Kost, L. E. and Somero, G. N. (2013). Food availability, more than body temperature, drives correlated shifts in ATP-generating and antioxidant enzyme capacities in a population of intertidal mussels (*Mytilus californianus*). *Journal of Experimental Marine Biology and Ecology* 449, 171–185.

Dudognon, T., Soudant, P., Seguineau, C., Quéré, C., Auffret, M. and Kraffe, E. (2013). Functional capacities of gill mitochondria in oyster *Crassostrea gigas* during an emersion/immersion tidal cycle. *Aquatic Living Resources* 26, 249–256.

Dunlap, J. C. (1999). Molecular bases for circadian clocks. *Cell* 96, 271–290.

Eckel-Mahan, K. L., Patel, V. R., Mohney, R. P., Vignola, K. S., Baldi, P. and Sassone-Corsi, P. (2012). Coordination of the transcriptome and metabolome by the circadian clock. *PNAS* 109, 5541–5546.

Eckel-Mahan, K. L., Patel, V. R., de Mateo, S., Orozco-Solis, R., Ceglia, N. J., Sahar, S., Dilag-Penilla, S. A., Dyar, K. A., Baldi, P. and Sassone-Corsi, P. (2013). Reprogramming of the circadian clock by nutritional challenge. *Cell* 155, 1464–1478.

Egg, M., Köblitz, L., Hirayama, J., Schwerte, T., Folterbauer, C., Kurz, A., Fiechtner, B., Möst, M., Salvenmoser, W., Sassone-Corsi, P., et al. (2013). Linking oxygen to

time: The bidirectional interaction between the hypoxic signaling pathway and the circadian clock. *Chronobiology International* 30, 510–529.

Elam, W. A., Kang, H. and De La Cruz, E. M. (2013). Biophysics of actin filament severing by cofilin. *FEBS Letters* 587, 1215–1219.

Ellington, W. R. (1983). The recovery from anaerobic metabolism in invertebrates. *J. Exp. Zool.* 228, 431–444.

Emerson, K. J., Bradshaw, W. E. and Holzapfel, C. M. (2008). Concordance of the circadian clock with the environment is necessary to maximize fitness in natural populations. *Evolution* 62, 979–983.

Espinosa, E. P., Hassan, D., Ward, J. E., Shumway, S. E. and Allam, B. (2010). Role of epicellular molecules in the selection of particles by the blue mussel, *Mytilus edulis*. *Biol Bull* 219, 50–60.

Espinosa, E. P., Cerrato, R. M., Wikfors, G. H. and Allam, B. (2016). Modeling food choice in the two suspension-feeding bivalves, *Crassostrea virginica* and *Mytilus edulis*. *Mar Biol* 163, 40.

Evans, T. G. (2015). Considerations for the use of transcriptomics in identifying the "genes that matter" for environmental adaptation. *Journal of Experimental Biology* 218, 1925–1935.

Feder, M. E. and Walser, J.-C. (2005). The biological limitations of transcriptomics in elucidating stress and stress responses. *Journal of Evolutionary Biology* 18, 901–910.

Feng, Y. and Walsh, C. A. (2004). The many faces of filamin: A versatile molecular scaffold for cell motility and signalling. *Nat Cell Biol* 6, 1034–1038.

Fields, P. A., Zuzow, M. J. and Tomanek, L. (2012). Proteomic responses of blue mussel (Mytilus) congeners to temperature acclimation. *Journal of Experimental Biology* 215, 1106–1116.

Fields, P. A., Eurich, C., Gao, W. L. and Cela, B. (2014). Changes in protein expression in the salt marsh mussel *Geukensia demissa*: evidence for a shift from anaerobic to aerobic metabolism during prolonged aerial exposure. *J Exp Biol* 217, 1601–1612.

Fitzgerald-Dehoog, L., Browning, J. and Allen, B. J. (2012). Food and heat stress in the california mussel: evidence for an energetic trade-off between survival and growth. *Biol Bull* 223, 205–216.

Fitzhenry, T., Halpin, P. M. and Helmuth, B. (2004). Testing the effects of wave exposure, site, and behavior on intertidal mussel body temperatures: applications and limits of temperature logger design. *Marine Biology* 145, 339–349.

Flick, F. and Lüscher, B. (2012). Regulation of sirtuin function by posttranslational modifications. *Front. Pharmacol.* 3, 29.

Fustin, J.-M., Doi, M., Yamaguchi, Y., Hida, H., Nishimura, S., Yoshida, M., Isagawa, T., Morioka, M. S., Kakeya, H., Manabe, I., et al. (2013). RNA-methylation-dependent RNA processing controls the speed of the circadian clock. *Cell* 155, 793–806.

Gaitán-Espitia, J. D., Quintero-Galvis, J. F., Mesas, A. and D'Elía, G. (2016). Mitogenomics of southern hemisphere blue mussels (Bivalvia: Pteriomorphia): Insights into the evolutionary characteristics of the *Mytilus edulis* complex. *Sci Rep* 6,.

Garcia-March, J. R., Jiménez, S., Sanchis, M. A., Monleon, S., Lees, J., Surge, D. and Tena-Medialdea, J. (2016). In situ biomonitoring shows seasonal patterns and environmentally mediated gaping activity in the bivalve, *Pinna nobilis*. *Mar Biol* 163, 1–12.

Gartmann, M., Blau, M., Armache, J.-P., Mielke, T., Topf, M. and Beckmann, R. (2010). Mechanism of eIF6-mediated Inhibition of Ribosomal Subunit Joining. *J. Biol. Chem.* 285, 14848–14851.

Gawron, D., Gevaert, K. and Van Damme, P. (2014). The proteome under translational control. *Proteomics* 14, 2647–2662.

Gerdol, M. and Venier, P. (2015). An updated molecular basis for mussel immunity. *Fish & Shellfish Immunology* 46, 17–38.

Giannetto, A., Maisano, M., Cappello, T., Oliva, S., Parrino, V., Natalotto, A., Marco, G. D., Barberi, C., Romeo, O., Mauceri, A., et al. (2015). Hypoxia-inducible factor α and HIF-prolyl hydroxylase characterization and gene expression in short-time air-exposed *Mytilus galloprovincialis*. *Mar Biotechnol* 17, 768–781.

Giganti, A., Plastino, J., Janji, B., Troys, M. V., Lentz, D., Ampe, C., Sykes, C. and Friederich, E. (2005). Actin-filament cross-linking protein T-plastin increases Arp2/3-mediated actin-based movement. *Journal of Cell Science* 118, 1255–1265.

Gnyubkin, V. F. (2010). The circadian rhythms of valve movements in the mussel *Mytilus galloprovincialis*. *Russ J Mar Biol* 36, 419–428.

Gomez, L., Paillard, M., Price, M., Chen, Q., Teixeira, G., Spiegel, S. and Lesnefsky, E. J. (2011). A novel role for mitochondrial sphingosine-1-phosphate produced by sphingosine kinase-2 in PTP-mediated cell survival during cardioprotection. *Basic Res Cardiol* 106, 1341–1353.

Gómez-Mendikute, A., Elizondo, M., Venier, P. and Cajaraville, M. P. (2005). Characterization of mussel gill cells in vivo and in vitro. *Cell Tissue Res* 321, 131–140.

Görg, A., Weiss, W. and Dunn, M. J. (2004). Current two-dimensional electrophoresis technology for proteomics. *Proteomics* 4, 3665–3685.

Görg, A., Drews, O., Lück, C., Weiland, F. and Weiss, W. (2009). 2-DE with IPGs. *ELECTROPHORESIS* 30, S122–S132.

Gosling, E. (2015). *Marine Bivalve Molluscs*. John Wiley & Sons.

Gottlieb, R. A. and Bernstein, D. (2016). Mitochondrial remodeling: Rearranging, recycling, and reprogramming. *Cell Calcium*.

Gracey, A. Y., Chaney, M. L., Boomhower, J. P., Tyburczy, W. R., Connor, K. and Somero, G. N. (2008). Rhythms of gene expression in a fluctuating intertidal environment. *Current Biology* 18, 1501–1507.

Guilbert, S. M., Varlet, A.-A., Fuchs, M., Lambert, H., Landry, J. and Lavoie, J. N. (2015). Regulation of Actin-Based Structure Dynamics by HspB Proteins and Partners. In *The Big Book on Small Heat Shock Proteins* (ed. Tanguay, R. M.) and Hightower, L. E.), pp. 435–456. Springer International Publishing.

Gutiérrez, J. L., Jones, C. G., Strayer, D. L. and Iribarne, O. O. (2003). Mollusks as ecosystem engineers: the role of shell production in aquatic habitats. *Oikos* 101, 79–90.

Hagger, J. A., Jones, M. B., Leonard, D. P., Owen, R. and Galloway, T. S. (2006). Biomarkers and integrated environmental risk assessment: Are there more questions than answers? *Integr Environ Assess Manag* 2, 312–329.

Halpin, P. M., Menge, B. A. and Hofmann, G. E. (2004). Experimental demonstration of plasticity in the heat shock response of the intertidal mussel *Mytilus californianus*. *Marine Ecology Progress Series* 276, 137–145.

Han, G., Zhang, S., Marshall, D. J., Ke, C. and Dong, Y. (2013). Metabolic energy sensors (AMPK and SIRT1), protein carbonylation and cardiac failure as biomarkers of thermal stress in an intertidal limpet: linking energetic allocation with environmental temperature during aerial emersion. *J Exp Biol* 216, 3273–3282.

Harbo, R. M. (1996). *Shells & Shellfish of the Pacific Northwest: A Field Guide*. Madiera Park, BC: Harbour Publishing.

Harley, C. D. G. (2008). Tidal dynamics, topographic orientation, and temperature-mediated mass mortalities on rocky shores. *Mar Ecol Prog Ser* 371, 37–46.

Harley, C. D. G., Randall Hughes, A., Hultgren, K. M., Miner, B. G., Sorte, C. J. B., Thornber, C. S., Rodriguez, L. F., Tomanek, L. and Williams, S. L. (2006). The impacts of climate change in coastal marine systems: Climate change in coastal marine systems. *Ecology Letters* 9, 228–241.

Hawkins, A. J. S. (1985). Relationships between the synthesis and breakdown of protein, dietary absorption and turnovers of nitrogen and carbon in the blue mussel, *Mytilus edulis* L. *Oecologia* 66, 42–49.

Hebert, D. N. and Molinari, M. (2007). In and out of the ER: protein folding, quality control, degradation, and related human diseases. *Physiological Reviews* 87, 1377–1408.

Helmuth, B. (2002). How do we measure the environment? Linking intertidal thermal physiology and ecology through biophysics. *Integr. Comp. Biol.* 42, 837–845.

Helmuth, B., Yamane, L., Lalwani, S., Matzelle, A., Tockstein, A. and Gao, N. (2011). Hidden signals of climate change in intertidal ecosystems: What (not) to expect when you are expecting. *Journal of Experimental Marine Biology and Ecology* 400, 191–199.

Hermes-Lima, M., Moreira, D. C., Rivera-Ingraham, G. A., Giraud-Billoud, M., Genaro-Mattos, T. C. and Campos, É. G. (2015). Preparation for oxidative stress under hypoxia and metabolic depression: Revisiting the proposal two decades later. *Free Radical Biology and Medicine* 89, 1122–1143.

Hershey, J. W. B., Sonenberg, N. and Mathews, M. B. (2012). Principles of translational control: an overview. *Cold Spring Harb Perspect Biol* 4, a011528.

Higgins, P. J. (1980). Effects of food availability on the valve movements and feeding behavior of juvenile *Crassostrea virginica* (Gmelin). I. Valve movements and periodic activity. *Journal of Experimental Marine Biology and Ecology* 229–244.

Hill, J. M., McQuaid, C. D. and Kaehler, S. (2008). Temporal and spatial variability in stable isotope ratios of SPM link to local hydrography and longer term SPM averages suggest heavy dependence of mussels on nearshore production. *Mar Biol* 154, 899–909.

Hou, X., Katahira, T., Ohashi, K., Mizuno, K., Sugiyama, S. and Nakamura, H. (2013). Coactosin accelerates cell dynamism by promoting actin polymerization. *Developmental Biology* 379, 53–63.

Hoyle, N. P. and O'Neill, J. S. (2015). Oxidation–reduction cycles of peroxiredoxin proteins and nontranscriptional aspects of timekeeping. *Biochemistry* 54, 184–193.

Huang, T.-C., Tu, J., Chow, T.-J. and Chen, T.-H. (1990). Circadian rhythm of the prokaryote *Synechococcus* sp. RF-1. *Plant Physiol.* 92, 531–533.

Huang, D. W., Sherman, B. T. and Lempicki, R. A. (2009a). Systematic and integrative analysis of large gene lists using DAVID bioinformatics resources. *Nat Protoc* 4, 44–57.

Huang, D. W., Sherman, B. T. and Lempicki, R. A. (2009b). Bioinformatics enrichment tools: paths toward the comprehensive functional analysis of large gene lists. *Nucleic Acids Res.* 37, 1–13.

Hughes, M. E., DiTacchio, L., Hayes, K. R., Vollmers, C., Pulivarthy, S., Baggs, J. E., Panda, S. and Hogenesch, J. B. (2009). Harmonics of circadian gene transcription in mammals. *PLOS Genet* 5, e1000442.

Hughes, M. E., Hogenesch, J. B. and Kornacker, K. (2010). JTK_CYCLE: an efficient nonparametric algorithm for detecting rhythmic components in genome-scale data sets. *J. Biol. Rhythms* 25, 372–380.

Hutchison, A. L., Maienschein-Cline, M., Chiang, A. H., Tabei, S. M. A., Gudjonson, H., Bahroos, N., Allada, R. and Dinner, A. R. (2015). Improved statistical methods enable greater sensitivity in rhythm detection for genome-wide data. *PLOS Comput Biol* 11, e1004094.

IPCC ed. (2015). *Climate Change 2014: Synthesis Report*. Geneva, Switzerland: Intergovernmental Panel on Climate Change.

Ivanina, A. V., Nesmelova, I., Leamy, L., Sokolov, E. P. and Sokolova, I. M. (2016). Intermittent hypoxia leads to functional reorganization of mitochondria and affects cellular bioenergetics in marine molluscs. *Journal of Experimental Biology* 219, 1659–1674.

Izagirre, U., Ramos, R. R. and Marigmez, I. (2008). Natural variability in size and membrane stability of lysosomes in mussel digestive cells: seasonal and tidal zonation. *Mar Ecol Prog Ser* 372, 105–117.

Jaafar, S. N. T., Coelho, A. V. and Sheehan, D. (2015). Redox proteomic analysis of *Mytilus edulis* gills: effects of the pharmaceutical diclofenac on a non-target organism. *Drug Test Anal* 7, 957–966.

Janich, P., Arpat, A. B., Castelo-Szekely, V., Lopes, M. and Gatfield, D. (2015). Ribosome profiling reveals the rhythmic liver translatome and circadian clock regulation by upstream open reading frames. *Genome Research* 25, 1848–1859.

Jeon, J. H., Kim, K., Kim, J. H., Baek, A., Cho, H., Lee, Y. H., Kim, J. W., Kim, D., Han, S. H., Lim, J.-S., et al. (2008). A novel adipokine CTRP1 stimulates aldosterone production. *FASEB J* 22, 1502–1511.

Jolley, C. C., Ode, K. L. and Ueda, H. R. (2012). A design principle for a posttranslational biochemical oscillator. *Cell Reports* 2, 938–950.

Jones, T. M., Durrant, J., Michaelides, E. B. and Green, M. P. (2015). Melatonin: a possible link between the presence of artificial light at night and reductions in biological fitness. *Phil. Trans. R. Soc. B* 370, 20140122.

Kaneko, M., Hernandez-Borsetti, N. and Cahill, G. M. (2006). Diversity of zebrafish peripheral oscillators revealed by luciferase reporting. *PNAS* 103, 14614–14619.

Keeling, J., Tsiokas, L. and Maskey, D. (2016). Cellular mechanisms of ciliary length control. *Cells* 5, 6.

Kietzmann, T., Krones-Herzig, A. and Jungermann, K. (2002). Signaling cross-talk between hypoxia and glucose via hypoxia-inducible factor 1 and glucose response elements. *Biochemical Pharmacology* 64, 903–911.

Kil, I. S., Ryu, K. W., Lee, S. K., Kim, J. Y., Chu, S. Y., Kim, J. H., Park, S. and Rhee, S. G. (2015). Circadian oscillation of sulfiredoxin in the mitochondria. *Molecular Cell* 59, 651–663.

Klein, D. C. (2007). Arylalkylamine N-acetyltransferase: "the Timezyme." *J. Biol. Chem.* 282, 4233–4237.

Klevecz, R. R., Bolen, J., Forrest, G. and Murray, D. B. (2004). A genomewide oscillation in transcription gates DNA replication and cell cycle. *PNAS* 101, 1200–1205.

Kojima, S., Sher-Chen, E. L. and Green, C. B. (2012). Circadian control of mRNA polyadenylation dynamics regulates rhythmic protein expression. *Genes Dev.* 26, 2724–2736.

Kojima, S., Gendreau, K. L., Sher-Chen, E. L., Gao, P. and Green, C. B. (2015). Changes in poly(A) tail length dynamics from the loss of the circadian deadenylase Nocturnin. *Scientific Reports* 5, 17059.

Kovacic, P. and Somanathan, R. (2014). Unifying effectors of circadian rhythm: Protein N-acetylation, phosphorylation, sulfation and other electrical effects. *Journal of Electrostatics* 72, 198–202.

Kreutzer, U., Siegmund, B. R. and Grieshaber, M. K. (1989). Parameters controlling opine formation during muscular activity and environmental hypoxia. *J Comp Physiol B* 159, 617–628.

Kurochkin, I. O., Ivanina, A. V., Eilers, S., Downs, C. A., May, L. A. and Sokolova, I. M. (2009). Cadmium affects metabolic responses to prolonged anoxia and reoxygenation in eastern oysters (*Crassostrea virginica*). *American Journal of Physiology - Regulatory, Integrative and Comparative Physiology* 297, R1262–R1272.

LaCourse, J. R. (1981). An anatomical and electrophysiological investigation of the visual organs of the mussel, *Mytilus edulis* L.

Larade, K. and Storey, K. B. (2002). Reversible suppression of protein synthesis in concert with polysome disaggregation during anoxia exposure in *Littorina littorea*. *Mol Cell Biochem* 232, 121–127.

Larade, K. and Storey, K. B. (2007). Arrest of transcription following anoxic exposure in a marine mollusc. *Mol Cell Biochem* 303, 243–249.

Lefort, A., Lecocq, R., Libert, F., Lamy, F., Swillens, S., Vassart, G. and Dumont, J. E. (1989). Cloning and sequencing of a calcium-binding protein regulated by cyclic AMP in the thyroid. *EMBO J* 8, 111–116.

Lesser, M. P. (2016). Climate change stressors cause metabolic depression in the blue mussel, *Mytilus edulis*, from the Gulf of Maine. *Limnol. Oceanogr.* 1–13.

Lesser, M. P., Bailey, M. A., Merselis, D. G. and Morrison, J. R. (2010). Physiological response of the blue mussel *Mytilus edulis* to differences in food and temperature in the Gulf of Maine. *Comparative Biochemistry and Physiology Part A: Molecular & Integrative Physiology* 156, 541–551.

Letendre, J., Chouquet, B., Manduzio, H., Marin, M., Bultelle, F., Leboulenger, F. and Durand, F. (2009). Tidal height influences the levels of enzymatic antioxidant defences in *Mytilus edulis*. *Marine Environmental Research* 67, 69–74.

Li, G. H., Arora, P. D., Chen, Y., McCulloch, C. A. and Liu, P. (2012). Multifunctional roles of gelsolin in health and diseases. *Med. Res. Rev.* 32, 999–1025.

Lin, M.-C., Galletta, B. J., Sept, D. and Cooper, J. A. (2010). Overlapping and distinct functions for cofilin, coronin and AIP1 in actin dynamics in vivo. *J Cell Sci* 123, 1329–1342.

Liu, Y., Beyer, A. and Aebersold, R. (2016). On the dependency of cellular protein levels on mRNA abundance. *Cell* 165, 535–550.

Livingston, R. J. (1976). Time as a Factor in Biomonitoring Estuarine Systems with Reference to Benthic Macrophytes and Epibenthic Fishes and Invertebrates. In *Biological Monitoring of Water and Effluent Quality* (ed. Cairns, J.), Dickson, K. L.), and Westlake, G. F.), pp. 212–223. West Conshohocken: ASTM International.

Lodish, H., Berk, A., Zipursky, S. L., Matsudaira, P., Baltimore, D. and Darnell, J. (2000). Molecular Mechanisms of Vesicular Traffic. In *Molecular Cell Biology*, p. W.H. Freeman and Company.

Logan, C. A., Kost, L. E. and Somero, G. N. (2012). Latitudinal differences in *Mytilus californianus* thermal physiology. *Mar Ecol Prog Ser* 450, 93–105.

Lovrić, J. (2011). *Introducing Proteomics: From Concepts to Sample Separation, Mass Spectrometry and Data Analysis*. John Wiley & Sons.

Lück, S. and Westermark, P. O. (2015). Circadian mRNA expression: insights from modeling and transcriptomics. *Cell. Mol. Life Sci.* 73, 497–521.

Lück, S., Thurley, K., Thaben, P. F. and Westermark, P. O. (2014). Rhythmic degradation explains and unifies circadian transcriptome and proteome data. *Cell Reports* 9, 741–751.

Luedeking, A. and Koehler, A. (2004). Regulation of expression of multixenobiotic resistance (MXR) genes by environmental factors in the blue mussel *Mytilus edulis*. *Aquatic Toxicology* 69, 1–10.

Lyndon, A. R. and Houlihan, D. F. (1998). Gill protein turnover: Costs of adaptation. *Comparative Biochemistry and Physiology Part A: Molecular & Integrative Physiology* 119, 27–34.

MacAllister, R. J., Parry, H., Kimoto, M., Ogawa, T., Russell, R. J., Hodson, H., Whitley, G. S. J. and Vallance, P. (1996). Regulation of nitric oxide synthesis by dimethylarginine dimethylaminohydrolase. *British Journal of Pharmacology* 119, 1533–1540.

Mack, G. A. and Wolfe, D. A. (1981). K-Sample Rank Tests for Umbrella Alternatives. *Journal of the American Statistical Association* 76, 175–181.

Maddocks, O. D. K., Labuschagne, C. F., Adams, P. D. and Vousden, K. H. (2016). Serine metabolism supports the methionine cycle and DNA/RNA methylation through de novo ATP synthesis in cancer cells. *Mol Cell* 61, 210–221.

Maiorova, M. A. and Odintsova, N. A. (2016). Proliferative potential of larval cells of the mussel *Mytilus trossulus* and their capacity to differentiate into myogenic cells in culture. *Russ J Mar Biol* 42, 281–285.

Malanga, C. J. (1974). Effects of dopamine on anaerobic metabolism and ciliary activity in bivalve gills. *Comparative and General Pharmacology* 5, 51–59.

Manchester, L. C., Coto-Montes, A., Boga, J. A., Andersen, L. P. H., Zhou, Z., Galano, A., Vriend, J., Tan, D.-X. and Reiter, R. J. (2015). Melatonin: an ancient molecule that makes oxygen metabolically tolerable. *Journal of Pineal Research* 59, 403–419.

Manoogian, E. N. C. and Panda, S. (2016). Circadian clock, nutrient quality, and eating pattern tune diurnal rhythms in the mitochondrial proteome. *PNAS* 113, 3127–3129.

Martelot, G. L., Canella, D., Symul, L., Migliavacca, E., Gilardi, F., Liechti, R., Martin, O., Harshman, K., Delorenzi, M., Desvergne, B., et al. (2012). Genome-wide RNA polymerase II profiles and RNA accumulation reveal kinetics of transcription and associated epigenetic changes during diurnal cycles. *PLOS Biol* 10, e1001442.

Masri, S., Patel, V. R., Eckel-Mahan, K. L., Peleg, S., Forne, I., Ladurner, A. G., Baldi, P., Imhof, A. and Sassone-Corsi, P. (2013). Circadian acetylome reveals regulation of mitochondrial metabolic pathways. *PNAS* 110, 3339–3344.

Mat, A. M., Massabuau, J.-C., Ciret, P. and Tran, D. (2012). Evidence for a plastic dual circadian rhythm in the oyster *Crassostrea gigas*. *Chronobiology International* 29, 857–867.

Mat, A. M., Massabuau, J.-C., Ciret, P. and Tran, D. (2014). Looking for the clock mechanism responsible for circatidal behavior in the oyster *Crassostrea gigas*. *Marine Biology* 161, 89–99.

Mat, A. M., Perrigault, M., Massabuau, J.-C. and Tran, D. (2016). Role and expression of cry1 in the adductor muscle of the oyster *Crassostrea gigas* during daily and tidal valve activity rhythms. *Chronobiol. Int.* 1–16.

Mata, J., Marguerat, S. and Bähler, J. (2005). Post-transcriptional control of gene expression: a genome-wide perspective. *Trends in Biochemical Sciences* 30, 506–514.

Mauvoisin, D., Wang, J., Jouffe, C., Martin, E., Atger, F., Waridel, P., Quadroni, M., Gachon, F. and Naef, F. (2014). Circadian clock-dependent and -independent rhythmic proteomes implement distinct diurnal functions in mouse liver. *PNAS* 111, 167–172.

Mauvoisin, D., Dayon, L., Gachon, F. and Kussmann, M. (2015). Proteomics and circadian rhythms: It's all about signaling! *Proteomics* 15, 310–317.

McCarthy, I. D., Nicholls, R., Malham, S. K. and Whiteley, N. M. (2016). Validation of the flooding dose technique to determine fractional rates of protein synthesis in a model bivalve species, the blue mussel (*Mytilus edulis* L.). *Comparative Biochemistry and Physiology Part A: Molecular & Integrative Physiology* 191, 166–173.

McClung, C. R. (2011). Circadian rhythms: lost in post-translation. *Current Biology* 21, R400–R402.

McDonagh, B., Tyther, R. and Sheehan, D. (2006). Redox proteomics in the mussel, *Mytilus edulis*. *Marine Environmental Research* 62, Supplement 1, S101–S104.

Menet, J. S., Rodriguez, J., Abruzzi, K. C. and Rosbash, M. (2012). Nascent-Seq reveals novel features of mouse circadian transcriptional regulation. *eLife* 1,.

Michel, P. E., Reymond, F., Arnaud, I. L., Josserand, J., Girault, H. H. and Rossier, J. S. (2003). Protein fractionation in a multicompartment device using Off-Gel™ isoelectric focusing. *ELECTROPHORESIS* 24, 3–11.

Micheletti, R., Paola, E. D. D., Schiavone, A., English, E., Benatti, P., Capasso, J. M., Anversa, P. and Bianchi, G. (1993). Propionyl-L-carnitine limits chronic ventricular dilation after myocardial infarction in rats. *American Journal of Physiology - Heart and Circulatory Physiology* 264, H1111–H1117.

Mislan, K. a. S., Helmuth, B. and Wethey, D. S. (2014). Geographical variation in climatic sensitivity of intertidal mussel zonation. *Global Ecology and Biogeography* 23, 744–756.

Moon, T. W. and Pritchard, A. W. (1970). Metabolic adaptations in vertically-separated populations of *Mytilus californianus* Conrad. *Journal of Experimental Marine Biology and Ecology* 5, 35–46.

Moore, M. N., Shaw, J. P., Ferrar Adams, D. R. and Viarengo, A. (2015). Anti-oxidative cellular protection effect of fasting-induced autophagy as a mechanism for hormesis. *Marine Environmental Research* 107, 35–44.

Morris, R. H., Abbott, D. P. and Haderlie, E. C. (1980). *Intertidal Invertebrates of California*. First Edition edition. Stanford, Calif: Stanford University Press.

Morton, B. (2008). The evolution of eyes in the Bivalvia: new insights. *American Malacological Bulletin* 26, 35–45.

Mounier, N. and Arrigo, A.-P. (2002). Actin cytoskeleton and small heat shock proteins: how do they interact? *Cell stress & chaperones* 7, 167.

Mukherji, S., Ebert, M. S., Zheng, G. X. Y., Tsang, J. S., Sharp, P. A. and van Oudenaarden, A. (2011). MicroRNAs can generate thresholds in target gene expression. *Nat Genet* 43, 854–859.

Müller, M., Mentel, M., Hellemond, J. J. van, Henze, K., Woehle, C., Gould, S. B., Yu, R.-Y., Giezen, M. van der, Tielens, A. G. M. and Martin, W. F. (2012). Biochemistry and evolution of anaerobic energy metabolism in eukaryotes. *Microbiol. Mol. Biol. Rev.* 76, 444–495.

Muñoz, E., Brewer, M. and Baler, R. (2002). Circadian transcription: Thinking outside the E-box. *Journal of Biological Chemistry* 277, 36009–36017.

Muñoz, J. L. P., Patiño, M. A. L., Hermosilla, C., Conde-Sieira, M., Soengas, J. L., Rocha, F. and Míguez, J. M. (2011). Melatonin in octopus (*Octopus vulgaris*). *J Comp Physiol A* 197, 789–797.

Nakahata, Y., Sahar, S., Astarita, G., Kaluzova, M. and Sassone-Corsi, P. (2009). Circadian control of the NAD+ salvage pathway by CLOCK-SIRT1. *Science* 324, 654–657.

Naylor, E. (2010). *Chronobiology of Marine Organisms*. Cambridge; New York: Cambridge University Press.

Neufeld-Cohen, A., Robles, M. S., Aviram, R., Manella, G., Adamovich, Y., Ladeuix, B., Nir, D., Rousso-Noori, L., Kuperman, Y., Golik, M., et al. (2016). Circadian control of oscillations in mitochondrial rate-limiting enzymes and nutrient utilization by PERIOD proteins. *Proceedings of the National Academy of Sciences* 113, E1673–E1682.

Nishida, Y., Rardin, M. J., Carrico, C., He, W., Sahu, A. K., Gut, P., Najjar, R., Fitch, M., Hellerstein, M., Gibson, B. W., et al. (2015). SIRT5 regulates both cytosolic and mitochondrial protein malonylation with glycolysis as a major target. *Molecular Cell* 59, 321–332.

Northrop, R. B. (2000). *Introduction to Dynamic Modeling of Neuro-Sensory Systems*. CRC Press.

Paine, R. T. (1974). Intertidal community structure. experimental studies on the relationship between a dominant competitor and its principal predator. *Oecologia* 15, 93–120.

Pairett, A. N. and Serb, J. M. (2013). De novo assembly and characterization of two transcriptomes reveal multiple light-mediated functions in the scallop eye (Bivalvia: Pectinidae). *PLOS ONE* 8, e69852.

Pajor, A. M. and Wright, S. H. (1987). l-Alanine uptake in brush border membrane vesicles from the gill of a marine bivalve. *J. Membrain Biol.* 96, 209–223.

Pales Espinosa, E., Koller, A. and Allam, B. (2016). Proteomic characterization of mucosal secretions in the eastern oyster, *Crassostrea virginica*. *Journal of Proteomics* 132, 63–76.

Palmer, J. D. (1996). Time, tide and the living clocks of marine organisms. *American Scientist* 84, 570–578.

Paranjpe, D. A. and Sharma, V. K. (2005). Evolution of temporal order in living organisms. *J Circadian Rhythms* 3, 7.

Park, J., Chen, Y., Tishkoff, D. X., Peng, C., Tan, M., Dai, L., Xie, Z., Zhang, Y., Zwaans, B. M. M., Skinner, M. E., et al. (2013). Sirt5-mediated lysine desuccinylation impacts diverse metabolic pathways. *Mol Cell* 50, 919–930.

Patel, V. R., Eckel-Mahan, K., Sassone-Corsi, P. and Baldi, P. (2012). CircadiOmics: integrating circadian genomics, transcriptomics, proteomics and metabolomics. *Nat Meth* 9, 772–773.

Patel, V. R., Ceglia, N., Zeller, M., Eckel-Mahan, K., Sassone-Corsi, P. and Baldi, P. (2015). The pervasiveness and plasticity of circadian oscillations: The coupled circadian-oscillators framework. *Bioinformatics* btv353.

Peek, C. B., Ramsey, K. M., Marcheva, B. and Bass, J. (2012). Nutrient sensing and the circadian clock. *Trends Endocrinol Metab* 23, 312–318.

Peek, C. B., Affinati, A. H., Ramsey, K. M., Kuo, H.-Y., Yu, W., Sena, L. A., Ilkayeva, O., Marcheva, B., Kobayashi, Y., Omura, C., et al. (2013). Circadian clock NAD+ cycle drives mitochondrial oxidative metabolism in mice. *Science* 342, 1243417.

Perkins, D. N., Pappin, D. J. C., Creasy, D. M. and Cottrell, J. S. (1999). Probability-based protein identification by searching sequence databases using mass spectrometry data. *Electrophoresis* 20, 3551–3567.

Petes, L. E., Menge, B. A. and Harris, A. L. (2008). Intertidal mussels exhibit energetic trade-offs between reproduction and stress resistance. *Ecological monographs* 78, 387–402.

Pittendrigh, C. S. (1993). Temporal organization: reflections of a Darwinian clock-watcher. *Annu. Rev. Physiol.* 55, 16–54.

Place, S. P., Menge, B. A. and Hofmann, G. E. (2012). Transcriptome profiles link environmental variation and physiological response of *Mytilus californianus* between Pacific tides. *Functional Ecology* 26, 144–155.

R Core Team (2016). *R: A Language and Environment for Statistical Computing*. Vienna, Austria: R Foundation for Statistical Computing.

Rabilloud, T. (1999). *Proteome Research: Two-Dimensional Gel Electrophoresis and Identification Methods*. Springer Science & Business Media.

Rabilloud, T. and Lelong, C. (2011). Two-dimensional gel electrophoresis in proteomics: A tutorial. *Journal of Proteomics* 74, 1829–1841.

Ramsey, K. M., Affinati, A. H., Peek, C. B., Marcheva, B., Hong, H.-K. and Bass, J. (2013). Circadian measurements of sirtuin biology. *Methods Mol Biol* 1077, 285–302.

Reddy, A. B. and Rey, G. (2014). Metabolic and nontranscriptional circadian clocks: Eukaryotes. *Annual Review of Biochemistry* 83, 165–189.

Reddy, A. B., Karp, N. A., Maywood, E. S., Sage, E. A., Deery, M., O'Neill, J. S., Wong, G. K. Y., Chesham, J., Odell, M., Lilley, K. S., et al. (2006). Circadian orchestration of the hepatic proteome. *Current Biology* 16, 1107–1115.

Refinetti, R., Cornélissen, G. and Halberg, F. (2007). Procedures for numerical analysis of circadian rhythms. *Biological Rhythm Research* 38, 275–325.

Reinke, H. and Gatfield, D. (2006). Genome-wide oscillation of transcription in yeast. *Trends in Biochemical Sciences* 31, 189–191.

Rey, G. and Reddy, A. B. (2013a). Protein acetylation links the circadian clock to mitochondrial function. *PNAS* 110, 3210–3211.

Rey, G. and Reddy, A. B. (2013b). Protein acetylation links the circadian clock to mitochondrial function. *PNAS* 110, 3210–3211.

Ricciardi, A. and Bourget, E. (1999). Global patterns of macroinvertebrate biomass in marine intertidal communities. *Marine Ecology Progress Series* 185, 21–35.

Righetti, P. G. and Bossi, A. (1997). Isoelectric focusing in immobilized pH gradients: recent analytical and preparative developments. *Analytical Biochemistry* 247, 1–10.

Riisgård, H. U., Kittner, C. and Seerup, D. F. (2003). Regulation of opening state and filtration rate in filter-feeding bivalves (*Cardium edule, Mytilus edulis, Mya arenaria*) in response to low algal concentration. *Journal of Experimental Marine Biology and Ecology* 284, 105–127.

Riisgård, H. U., Lassen, J. and Kittner, C. (2006). Valve-gape response times in mussels (*Mytilus edulis*)—effects of laboratory preceding-feeding conditions and in situ tidally induced variation in phytoplankton biomass. *Journal of Shellfish Research* 25, 901–911.

Riisgård, H. U., Egede, P. P. and Barreiro Saavedra, I. (2011). Feeding behaviour of the mussel, *Mytilus edulis*: new observations, with a minireview of current knowledge. *Journal of Marine Biology* 2011, e312459.

Riisgård, H. U., Pleissner, D., Lundgreen, K. and Larsen, P. S. (2013). Growth of mussels *Mytilus edulis* at algal (*Rhodomonas salina*) concentrations below and above saturation levels for reduced filtration rate. *Marine Biology Research* 9, 1005–1017.

Riisgård, H. U., Funch, P. and Larsen, P. S. (2014). The mussel filter–pump – present understanding, with a re-examination of gill preparations. *Acta Zool* 1–10.

Rivera-Ingraham, G. A., Rocchetta, I., Meyer, S. and Abele, D. (2013). Oxygen radical formation in anoxic transgression and anoxia-reoxygenation: Foe or phantom? Experiments with a hypoxia tolerant bivalve. *Marine Environmental Research* 92, 110–119.

Rivera-Ingraham, G. A., Rocchetta, I., Bickmeyer, U., Meyer, S. and Abele, D. (2016). Spatial compartmentalization of free radical formation and mitochondrial heterogeneity in bivalve gills revealed by live-imaging techniques. *Frontiers in Zoology* 13, 4.

Robles, M. S., Cox, J. and Mann, M. (2014). In-vivo quantitative proteomics reveals a key contribution of post-transcriptional mechanisms to the circadian regulation of liver metabolism. *PLoS Genetics* 10, e1004047.

Robson, A. A., Leaniz, C. G. D., Wilson, R. P. and Halsey, L. G. (2010a). Behavioural adaptations of mussels to varying levels of food availability and predation risk. *J. Mollus. Stud.* 76, 348–353.

Robson, A. A., Leaniz, C. G. de, Wilson, R. P. and Halsey, L. G. (2010b). Effect of anthropogenic feeding regimes on activity rhythms of laboratory mussels exposed to natural light. *Hydrobiologia* 655, 197–204.

Rocher, B., Bultelle, F., Chan, P., Foll, F., Letendre, J., Monsinjon, T., Olivier, S., Péden, R., Poret, A., Vaudry, D., et al. (2015). 2-DE mapping of the blue mussel gill proteome: the usual suspects revisited. *Proteomes* 3, 3–41.

Roenneberg, T. and Merrow, M. (2014). "What watch?...such much!" Complexity and evolution of circadian clocks. *Cell Tissue Res* 309, 3–9.

Rosa, M., Ward, J. E., Ouvrard, M., Holohan, B. A., Pales Espinosa, E., Shumway, S. E. and Allam, B. (2015). Examining the physiological plasticity of particle capture by the blue mussel, *Mytilus edulis* (L.): Confounding factors and potential artifacts with studies utilizing natural seston. *Journal of Experimental Marine Biology and Ecology* 473, 207–217.

Russell, E. L. and Storey, K. B. (1995). Regulation of enzymes of carbohydrate metabolism during anoxia in the salt marsh bivalve *Geukensia demissus*. *Physiological Zoology* 68, 567–582.

Sadok, S., Uglow, R. F. and Haswell, S. J. (1999). Some aspects of nitrogen metabolism in *Mytilus edulis*: effects of aerial exposure. *Marine Biology* 135, 297–305.

Salway, J. G. (2012). *Medical Biochemistry at a Glance*. John Wiley & Sons.

Saurel, C., Gascoigne, J. C., Palmer, M. R. and Kaiser, M. J. (2007). In situ mussel feeding behavior in relation to multiple environmental factors: Regulation through food concentration and tidal conditions. *Limnology and Oceanography* 52, 1919–1929.

Schick, S., Becker, K., Thakurela, S., Fournier, D., Hampel, M. H., Legewie, S. and Tiwari, V. K. (2016). Identifying novel transcriptional regulators with circadian expression. *Mol. Cell. Biol.* 36, 545–558.

Schmutz, I., Wendt, S., Schnell, A., Kramer, A., Mansuy, I. M. and Albrecht, U. (2011). Protein phosphatase 1 (PP1) is a post-translational regulator of the mammalian circadian clock. *PLoS One* 6,.

Schunter, C., Welch, M. J., Ryu, T., Zhang, H., Berumen, M. L., Nilsson, G. E., Munday, P. L. and Ravasi, T. (2016). Molecular signatures of transgenerational response to ocean acidification in a species of reef fish. *Nature Climate Change*.

Seed, R. and Suchanek, T. H. (1992). Population and community ecology of *Mytilus*. *The mussel Mytilus: ecology, physiology, genetics and culture* 25, 87–170.

Shaw, M. M. and Riederer, B. M. (2003). Sample preparation for two-dimensional gel electrophoresis. *Proteomics* 3, 1408–1417.

Shick, J. M., Gnaiger, E., Widdows, J., Bayne, B. L. and De Zwaan, A. (1986). Activity and metabolism in the mussel *Mytilus edulis* l. during intertidal hypoxia and aerobic recovery. *Physiological Zoology* 59, 627–642.

Shields, J. L., Barnes, P. and Heath, D. D. (2008). Growth and survival differences among native, introduced and hybrid blue mussels (*Mytilus* spp.): genotype, environment and interaction effects. *Mar Biol* 154, 919–928.

Shinomiya, H. and Shinomiya, H. (2012). Plastin family of actin-bundling proteins: its functions in leukocytes, neurons, intestines, and cancer, plastin family of actin-bundling proteins: its functions in leukocytes, neurons, intestines, and cancer. *International Journal of Cell Biology* 2012, 2012, e213492.

Smith, J. R., Fong, P. and Ambrose, R. F. (2006). Dramatic declines in mussel bed community diversity: response to climate change? *Ecology* 87, 1153–1161.

Smith, L. M., Kelleher, N. L. and Proteomics, T. C. for T. D. (2013). Proteoform: a single term describing protein complexity. *Nat Meth* 10, 186–187.

Somero, G. N., Beers, J. M., Chan, F., Hill, T. M., Klinger, T. and Litvin, S. Y. (2016). What changes in the carbonate system, oxygen, and temperature portend for the northeastern pacific ocean: a physiological perspective. *BioScience* 66, 14–26.

Stal, L. J. and Krumbein, W. E. (1985). Nitrogenase activity in the non-heterocystous cyanobacterium *Oscillatoria* sp. grown under alternating light-dark cycles. *Arch. Microbiol.* 143, 67–71.

State of California (2016). Mussel Watch Program. *State Water Resources Control Board*.

Stefano, G. B. and Aiello, E. (1975). Histofluorescent localization of serotonin and dopamine in the nervous system and gill of *Mytilus edulis* (bivalvia). *Biological Bulletin* 148, 141.

Stefano, G. B., Mantione, K. J., Casares, F. M. and Kream, R. M. (2015). Anaerobically functioning mitochondria: evolutionary perspective on modulation of energy metabolism in *Mytilus edulis*. *Inv Surv J* 12, 22–28.

Sternlicht, H., Farr, G. W., Sternlicht, M. L., Driscoll, J. K., Willison, K. and Yaffe, M. B. (1993). The T-complex polypeptide 1 complex is a chaperonin for tubulin and actin in vivo. *PNAS* 90, 9422–9426.

Stoka, V., Turk, V. and Turk, B. (2016). Lysosomal cathepsins and their regulation in aging and neurodegeneration. *Ageing Research Reviews*.

Storey, K. B. (1988). Suspended animation: the molecular basis of metabolic depression. *Can. J. Zool.* 66, 124–132.

Storey, K. B. and Storey, J. M. (2004). Metabolic rate depression in animals: transcriptional and translational controls. *Biological Reviews* 79, 207–233.

Storey, J. D. and Tibshirani, R. (2003). Statistical significance for genomewide studies. *PNAS* 100, 9440–9445.

St-Pierre, J., Brand, M. D. and Boutilier, R. G. (2000). Mitochondria as ATP consumers: Cellular treason in anoxia. *PNAS* 97, 8670–8674.

Strub, G. M., Paillard, M., Liang, J., Gomez, L., Allegood, J. C., Hait, N. C., Maceyka, M., Price, M. M., Chen, Q., Simpson, D. C., et al. (2011). Sphingosine-1-phosphate produced by sphingosine kinase 2 in mitochondria interacts with prohibitin 2 to regulate complex IV assembly and respiration. *FASEB J* 25, 600–612.

Suchanek, T. H. (1981). The role of disturbance in the evolution of life history strategies in the intertidal mussels *Mytilus edulis* and *Mytilus californianus*. *Oecologia* 50, 143–152.

Suckau, D., Resemann, A., Schuerenberg, M., Hufnagel, P., Franzen, J. and Holle, A. (2003). A novel MALDI LIFT-TOF/TOF mass spectrometer for proteomics. *Anal Bioanal Chem* 376, 952–965.

Tagliarolo, M., Clavier, J., Chauvaud, L., Koken, M. and Grall, J. (2012). Metabolism in blue mussel: intertidal and subtidal beds compared. *Aquat Biol* 17, 167–180.

Tan, M., Peng, C., Anderson, K. A., Chhoy, P., Xie, Z., Dai, L., Park, J. S., Chen, Y., Huang, H., Zhang, Y., et al. (2014). Lysine glutarylation is a protein post-translational modification regulated by SIRT5. *Cell Metab* 19, 605–617.

Tasselli, L. and Chua, K. F. (2015). Methylation gets into rhythm with NAD+-SIRT1. *Nature Structural & Molecular Biology* 22, 275–277.

Tessmar-Raible, K., Raible, F. and Arboleda, E. (2011). Another place, another timer: Marine species and the rhythms of life. *BioEssays* 33, 165–172.

Thaben, P. F. and Westermark, P. al O. (2014). Detecting rhythms in time series with RAIN. *Journal of biological rhythms* 748730414553029.

Thompson, R. J. and Bayne, B. L. (1972). Active metabolism associated with feeding in the mussel *Mytilus edulis* L. *Journal of Experimental Marine Biology and Ecology* 9, 111–124.

Thomsen, J., Himmerkus, N., Holland, N., Sartoris, F. J., Bleich, M. and Tresguerres, M. (2016). Ammonia excretion in mytilid mussels is facilitated by ciliary beating. *The Journal of Experimental Biology* 219, 2300–2310.

Thuaud, F., Ribeiro, N., Nebigil, C. G. and Désaubry, L. (2013). Prohibitin ligands in cell death and survival: mode of action and therapeutic potential. *Chemistry & Biology* 20, 316–331.

Timpl, R., Sasaki, T., Kostka, G. and Chu, M.-L. (2003). Fibulins: a versatile family of extracellular matrix proteins. *Nat Rev Mol Cell Biol* 4, 479–489.

Todgham, A. E. and Stillman, J. H. (2013). Physiological responses to shifts in multiple environmental stressors: relevance in a changing world. *Integr. Comp. Biol.* 53, 539–544.

Tomanek, L. (2008). The Importance of Physiological Limits in Determining Biogeographical Range Shifts due to Global Climate Change: The Heat-Shock Response. *Physiological and Biochemical Zoology* 81, 709–717.

Tomanek, L. (2011). Environmental proteomics: changes in the proteome of marine organisms in response to environmental stress, pollutants, infection, symbiosis, and development. *Annual Review of Marine Science* 3, 373–399.

Tomanek, L. (2012). Environmental proteomics of the mussel *Mytilus*: implications for tolerance to stress and change in limits of biogeographic ranges in response to climate change. *Integrative and Comparative Biology* 52, 648–664.

Tomanek, L. (2014). Proteomics to study adaptations in marine organisms to environmental stress. *Journal of Proteomics* 105, 92–106.

Tomanek, L. (2015). Proteomic responses to environmentally induced oxidative stress. *Journal of Experimental Biology* 218, 1867–1879.

Tomanek, L. and Zuzow, M. J. (2010). The proteomic response of the mussel congeners *Mytilus galloprovincialis* and *M. trossulus* to acute heat stress: implications for thermal tolerance limits and metabolic costs of thermal stress. *J Exp Biol* 213, 3559–3574.

Tomanek, L., Zuzow, M. J., Hitt, L., Serafini, L. and Valenzuela, J. J. (2012). Proteomics of hyposaline stress in blue mussel congeners (genus *Mytilus*): implications for biogeographic range limits in response to climate change. *Journal of Experimental Biology* 215, 3905–3916.

Tran, D., Nadau, A., Durrieu, G., Ciret, P., Parisot, J.-P. and Massabuau, J.-C. (2011). Field chronobiology of a molluscan bivalve: how the moon and sun cycles interact to drive oyster activity rhythms. *Chronobiology International: The Journal of Biological & Medical Rhythm Research* 28, 307–317.

Tran, D., Ciutat, A., Mat, A., Massabuau, J.-C., Hégaret, H., Lambert, C., Le Goic, N. and Soudant, P. (2015). The toxic dinoflagellate *Alexandrium minutum* disrupts daily rhythmic activities at gene transcription, physiological and behavioral levels in the oyster *Crassostrea gigas*. *Aquatic Toxicology* 158, 41–49.

Tremblay, R. and Pellerin-Massicotte, J. (1997). Effect of the tidal cycle on lysosomal membrane stability in the digestive gland of *Mya arenaria* and *Mytilus edulis* L. *Comparative Biochemistry and Physiology Part A: Physiology* 117, 99–104.

Venier, P., Varotto, L., Rosani, U., Millino, C., Celegato, B., Bernante, F., Lanfranchi, G., Novoa, B., Roch, P., Figueras, A., et al. (2011). Insights into the innate immunity of the Mediterranean mussel *Mytilus galloprovincialis*. *BMC Genomics* 12, 69.

Vidal-Liñán, L. and Bellas, J. (2013). Practical procedures for selected biomarkers in mussels, *Mytilus galloprovincialis* — Implications for marine pollution monitoring. *Science of The Total Environment* 461–462, 56–64.

Wallach, T., Schellenberg, K., Maier, B., Kalathur, R. K. R., Porras, P., Wanker, E. E., Futschik, M. E. and Kramer, A. (2013). Dynamic circadian protein–protein interaction networks predict temporal organization of cellular functions. *PLoS Genetics* 9, e1003398.

Walsh, C. T., Garneau-Tsodikova, S. and Gatto, G. J. (2005). Protein posttranslational modifications: the chemistry of proteome diversifications. *Angewandte Chemie International Edition* 44, 7342–7372.

Walter, M. F. and Satir, P. (1978). Calcium control of ciliary arrest in mussel gill cells. *J Cell Biol* 79, 110–120.

Wang, G.-Z., Hickey, S. L., Shi, L., Huang, H.-C., Nakashe, P., Koike, N., Tu, B. P., Takahashi, J. S. and Konopka, G. (2015). Cycling transcriptional networks optimize energy utilization on a genome scale. *Cell Reports* 13, 1868–1880.

Wang, H., Fan, Z., Zhao, M., Li, J., Lu, M., Liu, W., Ying, H., Liu, M. and Yan, J. (2016). Oscillating primary transcripts harbor miRNAs with circadian functions. *Scientific Reports* 6, 21598.

Weinert, B. T., Schölz, C., Wagner, S. A., Iesmantavicius, V., Su, D., Daniel, J. A. and Choudhary, C. (2013). Lysine succinylation is a frequently occurring modification in prokaryotes and eukaryotes and extensively overlaps with acetylation. *Cell Reports* 4, 842–851.

Weist, S., Eravci, M., Broedel, O., Fuxius, S., Eravci, S. and Baumgartner, A. (2008). Results and reliability of protein quantification for two-dimensional gel electrophoresis strongly depend on the type of protein sample and the method employed. *Proteomics* 8, 3389–3396.

Widdows, J. and Shick, J. M. (1985). Physiological responses of *Mytilus edulis* and *Cardium edule* to aerial exposure. *Marine Biology* 85, 217–232.

Wilkens, L. A. (2008). Primary inhibition by light: a unique property of bivalve photoreceptors. *American Malacological Bulletin* 26, 101–109.

Williams, B. G. and Pilditch, C. A. (1997). The entrainment of persistent tidal rhythmicity in a filter-feeding bivalve using cycles of food availability. *J. Biol. Rhythms* 12, 173–181.

Wyatt, H. D. M. and West, S. C. (2014). Holliday junction resolvases. *Cold Spring Harbor Perspectives in Biology* 6, a023192–a023192.

Yerushalmi, S. and Green, R. M. (2009). Evidence for the adaptive significance of circadian rhythms. *Ecology Letters* 12, 970–981.

Zaldibar, B., Cancio, I. and Marigómez, I. (2004). Circatidal variation in epithelial cell proliferation in the mussel digestive gland and stomach. *Cell and Tissue Research* 318, 395–402.

Zantke, J., Ishikawa-Fujiwara, T., Arboleda, E., Lohs, C., Schipany, K., Hallay, N., Straw, A. D., Todo, T. and Tessmar-Raible, K. (2013). Circadian and circalunar clock interactions in a marine annelid. *Cell Reports* 5, 99–113.

Zhang, L., Hastings, M. H., Green, E. W., Tauber, E., Sladek, M., Webster, S. G., Kyriacou, C. P. and Wilcockson, D. C. (2013). Dissociation of circadian and circatidal timekeeping in the marine crustacean *Eurydice pulchra*. *Current Biology* 23, 1863–1873.

Zhang, Y., Sun, J., Mu, H., Li, J., Zhang, Y., Xu, F., Xiang, Z., Qian, P.-Y., Qiu, J.-W. and Yu, Z. (2015). Proteomic basis of stress responses in the gills of the Pacific oyster *Crassostrea gigas*. *Journal of Proteome Research* 14, 304–317.

Table S1. List of identified proteins with significance in either JTK_Cycle or RAIN, predicted and estimated molecular weight (kDa) and isoelectric point (pI) from Delta2D or Expasy Protein Parameters, GenBank ID and NCBI accession number, and MASCOT protein ID score, peptide matches, and sequence coverage.

Spot ID	Protein ID	JTK_CYCLE	RAIN	MW (kDa) Predicted	pI Predicted	MW (kDa) Estimated	pI Estimated	GenBank ID	MOWSE Score	Peptide Matches	Sequence Coverage (%)
4	DAZ-associated protein 1	✓		10.00	6.61	46.13	6.44	gi|762085281|XP_011424949.1	149	3	8
5	Dynein light chain roadblock type 2	✓	✓	9.00	6.52	10.65	6.82	gi|762131349|XP_011448840.1	95	2	15
8	Coactosin	✓	✓	16.00	5.47	16.03	5.00	gi|919026004|XP_013396773.1	220	4	12
10	40S ribosomal protein S16		✓	14.00	5.46	16.77	10.14	gi|762135008|XP_011450742.1	56	2	14
11	Cystatin-B		✓	12.00	5.26	10.57	5.50	gi|762101260|XP_011433103.1	105	3	24
19	C1q-domain-containing protein		✓	19.00	6.85	18.74	8.39	gi|301598996|CBH31055.1	180	3	14
20	Ubiquitin-conjugating enzyme E2 variant 2	✓	✓	17.00	6.91	16.29	7.72	gi|762140796|XP_011453574.1	158	4	12
22	C1q-domain-containing protein	✓	✓	16.00	6.84	18.74	8.39	gi|301598996|CBH31055.1	240	4	19
23	ADP-ribosylation factor 2	✓	✓	18.00	6.60	15.03	6.60	gi|821400624|XP_012390507.1	125	4	10
24	Uncharacterized protein LOC105330279		✓	14.00	6.73	14.01	6.19	gi|762072409|XP_0 11430197.1	116	4	29
25	Profilin	✓	✓	12.00	6.79	14.69	6.27	gi|124106325|P18320.2	91	2	9
28	Dynein light chain 4, axonemal	✓	✓	9.00	5.69	11.99	5.52	gi|524871308|XP_005092427.1	94	3	6
29	Heat shock protein 90		✓	92.00	5.12	92.26	4.76	gi|919097451|XP_013385414.1	244	4	15
30	Heat shock protein 91		✓	91.00	5.05	92.26	4.76	gi|919097451|XP_013385414.1	183	4	15
35	Na/H exchange regulatory cofactor NHE-RF1	✓	✓	78.00	4.99	58.10	9.28	gi|1022762209|KZS08050.1	100	3	6
36	Na/H exchange regulatory cofactor NHE-RF1	✓	✓	77.00	5.03	58.10	9.28	gi|1022762209|KZS08050.1	184	5	13
37	Na/H exchange regulatory cofactor NHE-RF1	✓	✓	76.00	5.07	58.10	9.28	gi|1022762209|KZS08050.1	47	3	8
40	Tubulin α-1A chain	✓	✓	72.00	4.93	50.07	4.94	gi|762092848|XP_011428863.1	78	2	6
42	Formimidoyltransferase-cyclodeaminase		✓	72.00	4.97	60.15	4.96	gi|762106249|XP_011435709.1	73	3	13
43	Formimidoyltransferase-cyclodeaminase		✓	71.00	5.00	60.15	4.96	gi|762106249|XP_011435709.1	118	3	9
45	ß-tubulin	✓	✓	62.00	5.07	18.52	4.81	gi|34345524|AEM36060.1	124	2	15
46	Tubulin ß-1 chain	✓	✓	63.00	4.89	50.18	4.75	gi|936574177|XP_014219202.1	105	2	6
47	Prolyl hydroxylase ß subunit	✓	✓	63.00	4.67	55.06	4.53	gi|390979785|AFM30917.1	81	3	7
50	Calreticulin precursor		✓	62.00	4.54	48.16	4.53	gi|765826537|NP_001292262.1	101	3	13
51	Tubulin ß-1 chain	✓	✓	62.00	4.80	50.18	4.75	gi|936574177|XP_014219202.2	77	2	6
52	Tubulin ß-2C chain	✓	✓	60.00	4.93	25.86	4.95	gi|14124960|AAH08006.1	102	3	10
53	ATP synthase ß subunit	✓	✓	60.00	5.02	46.23	4.95	gi|46909261|AAT06148.1	228	6	18
54	Tubulin ß chain		✓	60.00	4.89	50.02	4.73	gi|291242757|XP_002741272.1	85	3	8
55	ATP synthase ß subunit	✓		59.00	5.09	46.23	4.95	gi|46909261|AAT06148.1	547	10	29
56	Tubulin ß chain	✓	✓	59.00	4.80	49.90	4.76	gi|762130794|XP_011448542.1	82	3	8
58	ATP synthase ß subunit	✓	✓	59.00	5.06	46.23	4.95	gi|46909261|AAT06148.1	336	6	18
59	Calumenin	✓	✓	57.00	4.60	38.24	4.60	gi|762104889|XP_011434992.1	99	2	1
61	Tubulin ß chain		✓	58.00	5.00	50.02	4.73	gi|291242757|XP_002741272.1	85	3	8
62	ATP synthase ß subunit	✓	✓	58.00	5.07	46.23	4.95	gi|46909261|AAT06148.1	468	9	26
64	Actin		✓	55.00	4.83	41.72	5.46	gi|5114428|AAD40314.1	188	4	12
65	Radial spoke head 1 homolog	✓	✓	54.00	4.55	35.09	4.59	gi|762085934|XP_011425286.1	268	4	16
66	Radial spoke head 1 homolog	✓	✓	54.00	4.59	35.09	5.59	gi|762085934|XP_011425286.1	350	5	22
67	40S ribosomal protein SA	✓	✓	53.00	4.69	33.50	5.24	gi|229891605|A3RLT6.1	226	3	20
71	Tropomyosin-1 isoform X1		✓	50.00	4.62	33.02	4.57	gi|762074188|XP_011437685.1	469	9	30
73	Actin		✓	47.00	5.02	41.72	5.46	gi|5114428|AAD40314.1	188	4	12
75	SET	✓	✓	48.00	4.26	28.09	4.34	gi|405963180|EKC28777.1	99	3	9
76	Immunoglobulin M heavy chain	✓	✓	48.00	4.47	10.14	5.06	gi|381354094|AFG25782.1	88	2	12
78	Translocon-associated protein subunit α		✓	47.00	4.52	31.61	4.47	gi|405976865|EKC41344.1	49	2	2
79	Tropomyosin	✓	✓	46.00	4.57	32.78	4.64	gi|66478635|Q25457.1	311	4	17
80	Annexin A7	✓	✓	47.00	4.30	34.80	4.35	gi|762118260|XP_011442013.1	60	2	9
83	Proliferating cell nuclear antigen-like		✓	42.00	4.55	28.70	4.59	gi|762125425|XP_011445738.1	201	5	18
94	Tropomyosin	✓	✓	40.00	4.75	28.72	4.65	gi|762074212|XP_011437792.1	107	4	22
96	Cathepsin L1	✓	✓	39.00	4.42	39.97	5.39	gi|762107740|XP_011436484.1	201	4	4
97	Tropomyosin isoform X14		✓	40.00	4.78	28.72	4.65	gi|762074212|XP_011437792.1	288	4	21
99	Cathepsin L1	✓	✓	38.00	4.44	39.97	5.39	gi|762107740|XP_011436484.1	121	4	21
100	14-3-3 protein ε		✓	37.00	4.77	27.30	4.80	gi|1020418362|XP_016128134.1	62	3	11
101	Elongation factor 1-ß	✓		35.00	4.59	24.01	4.50	gi|762130560|XP_011448419.1	134	3	11
102	Eukaryotic translation initiation factor 6	✓	✓	34.00	4.52	26.44	4.51	gi|919041535|XP_013404046.1	142	3	17
104	Elongation factor 1-ß		✓	33.00	4.52	24.01	4.50	gi|762130560|XP_011448419.1	143	3	11
105	Cathepsin L1	✓	✓	33.00	4.61	38.20	6.10	gi|762167480|XP_011422071.1	90	3	11
114	Glycine decarboxylase	✓	✓	94.00	6.34	114.19	6.39	gi|762104986|XP_011435044.1	78	4	4
118	Major vault protein	✓	✓	89.00	6.09	96.25	5.58	gi|76210059|XP_011432755.1	72	2	8
119	α-Ketoglutarate dehydrogenase (mit)		✓	91.00	6.61	114.36	6.37	gi|871275424|XP_012945931.1	80	4	2
121	α-aminoadipic semialdehyde synthase (mit)		✓	90.00	6.83	97.21	5.66	gi|762080937|XP_011419725.1	101	3	15
122	PIF	✓	✓	90.00	5.80	68.02	5.23	gi|762115345|XP_011440479.1	113	3	10
123	Major vault protein	✓	✓	89.00	5.86	31.74	5.45	gi|5714749|AAD48063.1	82	4	17
125	Aconitate hydratase (cytoplasmic)		✓	90.00	6.48	98.25	5.99	gi|762147902|XP_011411873.1	86	2	11
126	α-Ketoglutarate dehydrogenase (mit)	✓	✓	89.00	6.74	114.36	6.37	gi|871275424|XP_012945931.1	73	3	1
127	Filamin-A		✓	88.00	6.81	93.11	6.42	gi|762071767|XP_011426812.1	133	3	2
128	Filamin-A	✓	✓	89.00	6.78	93.11	6.42	gi|762071767|XP_011426812.1	77	3	2
131	Aconitate hydratase (mitochondrial)	✓	✓	87.00	6.73	84.60	6.84	gi|762118955|XP_011442376.1	224	4	4
133	Dynein intermediate chain 2, ciliary	✓	✓	86.00	6.24	87.37	5.55	gi|405951115|EKC19056.1	70	2	3
136	Aconitate hydratase (mitochondrial)		✓	83.00	6.76	84.60	6.84	gi|762118955|XP_011442376.1	396	8	7
137	Aconitate hydratase (mitochondrial)	✓	✓	83.00	6.87	84.60	6.84	gi|762118955|XP_011442376.1	194	3	3
139	PIF		✓	84.00	6.70	68.02	5.23	gi|762115345|XP_011440479.1	111	3	10
140	α-Tubulin	✓	✓	78.00	5.37	41.67	5.11	gi|302029718|ADK91434.1	29	2	5
141	Collagen-like protein-8		✓	78.00	5.32	24.25	5.11	gi|9065418369|AKS48186.1	97	2	9
143	Heat shock protein 70	✓	✓	77.00	5.45	71.60	6.44	gi|908501136|XP_013062306.1	129	2	2
144	Heat shock cognate 71	✓	✓	75.00	5.58	71.28	5.28	gi|76780612|CAH04109.1	260	6	10
146	Collagen-like protein-8	✓	✓	79.00	5.29	24.25	5.11	gi|9065418369|AKS48186.1	79	2	9
147	Actin-interacting protein 1	✓	✓	77.00	6.43	65.32	6.68	gi|762136518|XP_011451537.1	43	2	1
149	V-type proton ATPase catalytic subunit A	✓		78.00	5.82	69.25	5.33	gi|762160275|XP_011418350.1	88	2	1
150	V-type proton ATPase catalytic subunit A		✓	77.00	5.81	69.25	5.33	gi|762160275|XP_011418350.1	151	4	3
151	α-Propionyl-CoA carboxylase		✓	78.00	5.74	79.79	6.65	gi|206050|AAA88512.1	69	2	2
153	ß-tubulin	✓	✓	80.00	6.81	18.52	4.81	gi|34345524|AEM36060.1	123	2	15
156	E3 ubiquitin-protein ligase TRIM33		✓	77.00	6.78	85.09	8.51	gi|405950771|EKC18736.1	97	2	7
158	Aconitate hydratase (mitochondrial)	✓	✓	79.00	6.86	84.60	6.84	gi|762118955|XP_011442376.1	186	4	4
160	E3 ubiquitin-protein ligase TRIM33		✓	78.00	6.71	85.09	8.51	gi|405950771|EKC18736.1	81	3	3
161	Heat shock protein 70		✓	76.00	6.21	69.51	5.34	gi|62989584|CAE51348.1	159	3	8
162	Phenylalanine-tRNA ligase ß subunit		✓	75.00	6.37	65.61	6.03	gi|762131627|XP_011448986.1	104	3	3
164	Actin-interacting protein 1	✓		72.00	6.50	65.32	6.68	gi|762136518|XP_011451537.1	211	5	4
166	Long-chain fatty acyl-CoA ligase 1		✓	76.00	6.70	72.73	5.91	gi|762103124|XP_011434075.1	80	3	12
167	EF-hand domain-containing protein 1	✓	✓	75.00	6.65	74.34	6.23	gi|762138085|XP_011452353.1	221	5	7
169	Heterogeneous nuclear ribonucleoprotein L		✓	74.00	6.89	60.80	7.58	gi|762119243|XP_011442524.1	65	2	8
170	Plastin-1		✓	74.00	5.65	23.73	4.84	gi|762163377|XP_011419977.1	110	2	11
171	Non-neuronal cytoplasmic intermediate filament protein		✓	73.00	5.72	69.25	5.38	gi|405950795|EKC18758.1	121	3	5
173	Acyl-CoA oxidase 2 (peroxisomal)	✓	✓	73.00	6.80	74.75	7.23	gi|919063951|XP_013413582.1	51	3	2
174	Tubulin α-1A chain	✓	✓	74.00	5.79	50.07	4.94	gi|762092848|XP_011428863.1	59	2	6
175	Galectin		✓	72.00	5.19	63.28	4.99	gi|769748428|AJW60777.1	142	3	3
176	Tubulin α-1A chain		✓	72.00	5.87	50.07	4.94	gi|762092848|XP_011428863.1	68	2	6
177	UDP-N-acetylhexosamine pyrophosphorylase		✓	72.00	6.40	57.23	5.46	gi|762098431|XP_011431608.1	136	3	13
178	Tubulin α-1A chain	✓	✓	72.00	6.31	50.07	4.94	gi|762092848|XP_011428863.1	53	2	6
179	α-Tubulin	✓	✓	65.00	5.33	41.67	5.11	gi|302029718|ADK91434.4	142	2	8
181	T-complex protein 1 subunit α	✓	✓	70.00	6.60	59.89	6.17	gi|762090022|XP_011427374.1	82	4	6
182	Protein disulfide isomerase A3-like		✓	65.00	6.63	55.49	5.64	gi|762140057|XP_011453191.1	121	2	11
183	Glutamate dehydrogenase (mitochondrial)	✓		67.00	6.74	60.14	7.59	gi|871248375|XP_012940841.1	111	3	10
184	Actin	✓	✓	69.00	5.46	41.72	5.46	gi|5114428|AAD40314.1	188	4	12
186	α-Tubulin	✓		65.00	5.27	41.67	5.11	gi|302029718|ADK91434.1	134	6	20
187	Small heat shock protein 24.1		✓	65.00	5.74	28.52	5.61	gi|347545633|AEP02968.1	100	2	8

188	Collagen-like protein-2	✓	✓	67.00	5.85	50.10	7.10	gi|906541694|AKS48142.1	118	2	10
189	Actin	✓	✓	65.00	5.57	41.72	5.46	gi|5114428|AAD40314.1	148	3	10
190	Transketolase-like protein 2	✓	✓	69.00	6.86	67.55	6.62	gi|762090756|XP_011427761.1	97	2	8
191	Actin	✓		64.00	5.62	41.72	5.46	gi|5114428|AAD40314.1	98	2	7
192	T-complex protein 1 subunit eta-like	✓	✓	67.00	6.37	59.30	5.97	gi|762101230|XP_011433089.1	76	3	6
193	T-complex protein 1 subunit eta-like	✓	✓	66.00	6.49	59.30	5.97	gi|762101230|XP_011433089.1	112	3	6
195	RuvB 1		✓	65.00	6.42	50.19	5.80	gi|762149680|XP_011412783.1	152	3	21
196	Small heat shock protein 24.1		✓	66.00	6.05	28.52	5.61	gi|347545633|AEP02968.1	116	2	8
198	Tubulin α-1A chain		✓	66.00	6.32	50.07	4.94	gi|762092848|XP_011428863.1	76	2	6
199	Retrograde protein of 51 kDa-like	✓	✓	63.00	5.37	70.00	5.44	gi|762098694|XP_011431745.1	91	2	9
200	T-complex protein 1 subunit α		✓	66.00	6.59	59.89	6.17	gi|762090022|XP_011427374.1	91	2	2
201	Protein disulfide isomerase A3-like		✓	65.00	6.83	55.49	5.64	gi|762140057|XP_011453191.1	252	4	5
202	Tubulin α-1A chain		✓	65.00	6.39	50.07	4.94	gi|762092848|XP_011428863.1	99	2	6
203	Mitochondrial H+ ATPase α subunit	✓		61.00	6.90	59.64	8.92	gi|116008297|ABJ51956.1	259	3	5
204	α-Tubulin		✓	65.00	5.80	41.67	5.11	gi|302029718|ADK91434.1	89	3	11
205	Collagen-like protein-2	✓	✓	64.00	6.47	50.10	7.10	gi|906541694|AKS48142.1	93	2	4
206	Mitochondrial H+ ATPase α subunit	✓		62.00	6.73	59.64	8.92	gi|116008297|ABJ51956.1	92	2	11
207	α-aminoadipic semialdehyde dehydrogenase		✓	63.00	6.34	58.22	7.04	gi|762088534|XP_011426588.1	160	4	8
209	Aldehyde dehydrogenase (mit)		✓	63.00	6.05	16.94	7.85	gi|640788853|XP_008050245.1	193	4	26
210	Tubulin ß chain		✓	64.00	5.69	49.92	4.79	gi|765826404|NP_001292292.1	102	3	12
211	Tektin-4		✓	61.00	5.88	52.50	5.53	gi|762155969|XP_011416098.1	131	3	13
212	RuvB	✓	✓	63.00	6.42	50.19	5.80	gi|762149680|XP_011412783.1	65	2	4
213	Tubulin ß chain		✓	63.00	5.74	50.02	4.73	gi|291242757|XP_002741272.1	141	4	14
214	S-adenosylmethionine synthase isoform type-1	✓		62.00	6.79	45.31	6.32	gi|762123551|XP_011444759.1	101	2	11
215	ß-tubulin	✓	✓	61.00	5.19	18.52	4.81	gi|343455241|AEM36060.1	136	2	15
216	Protein disulfide isomerase A6-like		✓	62.00	5.77	47.44	5.14	gi|762126299|XP_011446200.1	151	4	15
217	Tektin-4		✓	61.00	5.97	52.50	5.53	gi|762155969|XP_011416098.1	111	3	13
220	Actin	✓		55.00	5.56	41.72	5.46	gi|5114428|AAD40314.1	214	4	12
221	Enolase	✓	✓	60.00	6.33	47.20	5.71	gi|762107263|XP_011436228.1	161	4	3
222	Phosphoglycerate kinase 1	✓	✓	58.00	6.66	43.00	7.59	gi|405963233|EKC28824.1	57	2	5
223	Actin		✓	61.00	5.82	41.72	5.46	gi|5114428|AAD40314.1	107	3	10
224	Cytochrome b-c1 complex subunit 2 (mitochondrial)	✓	✓	58.00	5.62	47.05	6.84	gi|957848481|XP_014674748.1	283	3	18
225	Tektin-4	✓		60.00	5.95	52.50	5.53	gi|762155969|XP_011416098.1	109	5	9
226	RIB43A-like with coiled-coils protein 2	✓	✓	59.00	6.52	45.41	6.09	gi|762123126|XP_011444532.1	84	3	4
227	26S protease regulatory subunit 6A-B		✓	60.00	5.42	47.98	5.08	gi|762138123|XP_011452372.1	137	3	12
228	Actin		✓	54.00	5.46	41.72	5.46	gi|5114428|AAD40314.1	245	5	18
229	Gelsolin	✓	✓	58.00	5.91	42.00	5.22	gi|41349563|CAF21863.1	77	3	20
230	Mitochondrial-processing peptidase subunit ß	✓	✓	59.00	5.97	53.00	6.48	gi|926615186|XP_013772662.1	95	2	8
231	Gelsolin		✓	57.00	6.26	41.91	5.44	gi|762074236|XP_011437904.1	244	6	9
233	Actin	✓		58.00	5.69	41.72	5.46	gi|5114428|AAD40314.1	213	4	13
234	Rab GDP dissociation inhibitor ß	✓	✓	59.00	6.21	50.01	5.57	gi|762090778|XP_011427772.1	144	4	5
235	Tubulin ß chain	✓	✓	59.00	5.41	50.02	4.73	gi|291242757|XP_002741272.1	85	3	8
237	ß-actin	✓	✓	58.00	5.79	20.16	5.15	gi|21540276|ACJ66626.1	65	2	14
238	Actin		✓	58.00	5.85	41.72	5.46	gi|5114428|AAD40314.1	125	4	13
239	Rab GDP dissociation inhibitor ß	✓	✓	58.00	6.33	50.01	5.57	gi|762090778|XP_011427772.1	74	2	15
240	Eukaryotic translation initiation factor 4A-I-like		✓	58.00	5.37	52.98	5.40	gi|919026190|XP_013396865.1	183	7	9
241	Actin		✓	58.00	5.82	41.72	5.46	gi|5114428|AAD40314.1	178	4	13
242	Pyruvate dehydrogenase E1 component subunit α	✓	✓	57.00	6.78	43.10	7.95	gi|762072718|XP_011431803.1	234	6	16
243	Citrate synthase (mitochondrial)		✓	56.00	6.88	49.41	6.47	gi|762091603|XP_011428205.1	95	2	3
244	Fumarylacetoacetase		✓	57.00	6.07	46.26	5.46	gi|762089599|XP_011427156.1	158	4	11
248	Pyruvate dehydrogenase E1 component subunit α		✓	57.00	6.22	43.10	7.95	gi|762072718|XP_011431803.1	218	4	13
249	NADP Isocitrate dehydrogenase		✓	57.00	6.34	50.46	6.77	gi|385268539|AFI56364.1	152	4	8
250	Actin	✓		56.00	6.01	41.72	5.46	gi|5114428|AAD40314.1	203	5	18
251	Medium-chain specific acyl-CoA dehydrogenase (mitochondrial)		✓	56.00	6.41	45.70	8.47	gi|762160932|XP_011418683.1	68	2	9
252	NADP Isocitrate dehydrogenase		✓	55.00	6.49	50.46	6.77	gi|385268539|AFI56364.1	227	6	15
253	Pyruvate dehydrogenase E1 component subunit α	✓	✓	56.00	6.77	31.55	6.01	gi|762101447|XP_011433204.1	136	3	8
254	Actin	✓	✓	55.00	5.74	41.72	5.46	gi|5114428|AAD40314.1	105	2	7
255	Actin		✓	53.00	5.95	41.72	5.46	gi|5114428|AAD40314.1	183	5	17
256	Actin	✓	✓	54.00	5.99	41.72	5.46	gi|5114428|AAD40314.1	196	4	13
257	NADP Isocitrate dehydrogenase	✓	✓	54.00	6.74	50.46	6.77	gi|385268539|AFI56364.1	39	2	3
258	Actin		✓	55.00	6.30	41.72	5.46	gi|5114428|AAD40314.1	29	2	7
259	NADP Isocitrate dehydrogenase	✓	✓	54.00	6.66	50.46	6.77	gi|385268539|AFI56364.1	258	6	15
260	NADP Isocitrate dehydrogenase	✓	✓	54.00	6.81	50.46	6.77	gi|385268539|AFI56364.1	124	4	9
261	ß-ureidopropionase	✓	✓	54.00	6.52	43.07	6.44	gi|762102257|XP_011433620.1	113	2	6
262	NADP Isocitrate dehydrogenase	✓	✓	54.00	6.86	50.46	6.77	gi|385268539|AFI56364.1	56	2	3
263	Actin		✓	55.00	6.26	41.72	5.46	gi|5114428|AAD40314.1	162	4	13
264	Actin		✓	53.00	6.10	41.72	5.46	gi|5114428|AAD40314.1	158	4	13
265	Actin	✓	✓	54.00	6.34	41.72	5.46	gi|5114428|AAD40314.1	108	3	10
266	Mitogen-activated protein kinase 1		✓	54.00	6.42	41.94	6.43	gi|762107124|XP_011436159.1	118	2	5
268	Actin	✓		52.00	6.23	41.72	5.46	gi|5114428|AAD40314.1	168	4	13
269	Isovaleryl-CoA dehydrogenase (mit)		✓	53.00	6.54	49.77	7.09	gi|762118977|XP_011442388.1	181	3	11
271	Actin	✓	✓	53.00	5.38	41.72	5.46	gi|5114428|AAD40314.1	196	3	9
272	Actin		✓	51.00	6.17	41.72	5.46	gi|5114428|AAD40314.1	120	5	18
273	Malate dehydrogenase	✓	✓	51.00	6.36	70.60	5.33	gi|405960257|EKC26198.1	142	4	15
274	Ribose-phosphate pyrophosphokinase 3 (mit)	✓		52.00	6.56	35.66	7.12	gi|405963876|EKC29408.1	76	2	6
277	Actin		✓	51.00	5.64	41.72	5.46	gi|5114428|AAD40314.1	111	4	13
278	Mannose-1-phosphate guanylyltransferase ß		✓	51.00	6.76	40.24	6.03	gi|762100405|XP_011432652.1	75	2	10
280	D-octopine dehydrogenase		✓	51.00	5.92	44.31	6.02	gi|399912965|AFP55365.1	121	3	13
281	Arginine kinase	✓	✓	50.00	6.80	39.38	8.84	gi|347450694|AEO94538.1	355	6	33
282	Mitogen-activated protein kinase 1	✓	✓	51.00	6.42	41.94	6.43	gi|762107124|XP_011436159.1	149	4	10
283	Actin	✓		51.00	5.40	41.72	5.46	gi|5114428|AAD40314.1	69	4	12
284	Actin		✓	50.00	5.46	41.72	5.46	gi|5114428|AAD40314.1	191	5	18
285	Tubulin α-1A chain		✓	50.00	6.07	50.07	4.94	gi|762092848|XP_011428863.1	114	2	6
286	NADP Isocitrate dehydrogenase		✓	50.00	6.66	50.46	6.77	gi|385268539|AFI56364.1	90	2	3
288	Actin	✓	✓	50.00	5.77	41.72	5.46	gi|5114428|AAD40314.1	88	3	10
289	Extrapallial protein precursor	✓	✓	47.00	5.27	26.90	5.24	gi|34304719|AAQ63463.1	91	2	11
290	Actin	✓	✓	49.00	5.49	41.72	5.46	gi|5114428|AAD40314.1	128	3	10
291	Actin		✓	49.00	5.56	41.72	5.46	gi|5114428|AAD40314.1	70	2	7
292	NAD Isocitrate dehydrogenase subunit α (mitochondrial)		✓	49.00	5.82	39.63	5.44	gi|762085542|XP_011425087.1	136	2	6
295	Arginine kinase		✓	49.00	6.82	39.38	8.84	gi|347450694|AEO94538.1	110	3	16
296	ATP-dependent (S)-NAD(P)H-hydrate dehydratase		✓	49.00	6.93	37.68	6.41	gi|390339986|XP_791028.3	122	3	15
297	Ribose-phosphate pyrophosphokinase 3 (mit)	✓	✓	49.00	6.88	35.66	7.12	gi|405963876|EKC29408.1	72	2	6
299	Arginine kinase		✓	49.00	6.70	39.38	8.84	gi|347450694|AEO94538.1	57	2	5
300	WD repeat-containing protein 5	✓	✓	48.00	6.55	38.10	5.95	gi|762170244|XP_011423544.1	135	5	10
301	α-Tubulin	✓	✓	49.00	6.13	10.81	4.80	gi|343455253|AEM36066.1	163	2	27
303	Actin		✓	49.00	6.01	41.72	5.46	gi|5114428|AAD40314.1	53	2	7
306	Actin		✓	48.00	5.50	41.72	5.46	gi|5114428|AAD40314.1	109	4	13
308	N(G), N(G)-deimethylarginine dimethylaminohydrolase 1		✓	48.00	6.44	33.91	6.07	gi|762159671|XP_011418031.1	279	4	5
309	Cytosolic malate dehydrogenase		✓	48.00	6.62	36.37	6.02	gi|73656269|AAZ79366.1	50	2	7
310	Fructose-1,6-bisphosphatase 1		✓	47.00	5.90	36.76	6.25	gi|762163253|XP_011419913.1	123	2	10
311	Arginase type-I	✓	✓	47.00	5.79	39.14	5.24	gi|328933188|AEB70965.1	244	4	18
312	Heparan sulfate proteoglycan-like protein-1	✓	✓	47.00	5.96	471.55	4.96	gi|906541676|AKS48136.1	119	2	16
315	Malate dehydrogenase precursor		✓	47.00	6.79	36.25	8.44	gi|6746611|AAF27650.1	67	2	10
316	Tubulin ß chain	✓	✓	47.00	6.06	49.90	4.76	gi|762130794|XP_011448542.1	65	3	8
317	Actin		✓	47.00	5.55	41.72	5.46	gi|5114428|AAD40314.1	81	3	10
319	Cytosolic malate dehydrogenase	✓	✓	46.00	6.29	36.37	6.02	gi|73656269|AAZ79366.1	122	2	4

320	Serine/threonine-protein phosphatase PP1-ß catalytic subunit	✓	✓	46.00	6.39	37.11	5.84	gi|919013689|XP_013391353.1	392	8	18
321	Cytosolic malate dehydrogenase		✓	46.00	6.52	36.37	6.02	gi|73656269|AAZ79366.1	127	2	7
322	N(G), N(G)-deimethylarginine dimethylaminohydrolase 1		✓	45.00	6.43	33.91	6.07	gi|762159671|XP_011418031.1	142	3	3
323	UDP-glucuronic acid decarboxylase 1		✓	46.00	6.47	34.96	6.07	gi|762138169|XP_011452397.1	248	4	16
324	Cytosolic malate dehydrogenase	✓	✓	46.00	6.65	36.37	6.02	gi|73656269|AAZ79366.1	93	2	7
325	Guanine nucleotide-binding protein subunit ß		✓	45.00	5.56	37.31	5.62	gi|762162094|XP_011419294.1	112	2	1
327	Guanine nucleotide-binding protein subunit ß	✓	✓	45.00	5.93	37.31	5.62	gi|762162094|XP_011419294.1	206	4	4
328	Trancriptional activator protein Pur-ß-B-like		✓	44.00	5.62	27.82	6.79	gi|762161734|XP_011419105.1	152	7	14
329	Malate dehydrogenase precursor		✓	44.00	6.78	36.25	8.44	gi|6746611|AAF27650.1	117	2	10
330	Guanine nucleotide-binding protein subunit ß	✓	✓	44.00	5.78	37.31	5.62	gi|762162094|XP_011419294.1	218	5	4
331	Radial spoke head protein 9 homolog		✓	44.00	6.15	31.36	5.32	gi|919082237|XP_013422186.1	164	3	16
335	F-actin-capping protein subunit α-2	✓	✓	44.00	6.34	32.66	5.18	gi|919061844|XP_013412571.1	60	2	9
336	Chloride intracellular channel protein 2	✓	✓	43.00	5.83	32.89	5.29	gi|762144218|XP_011455376.1	219	3	4
338	Eukaryotic translation initiation factor 3 subunit I	✓	✓	43.00	6.36	36.14	6.00	gi|762125838|XP_011445956.1	63	2	6
339	3-hydroxyanthranilate 3,4-dioxygenase	✓	✓	44.00	6.41	34.11	5.44	gi|762154170|XP_011415145.1	132	2	7
341	KEYSTONEin		✓	44.00	5.26	27.96	5.33	gi|426207677|AFY13478.1	106	2	6
342	Malate dehydrogenase precursor		✓	44.00	6.27	36.25	8.44	gi|6746611|AAF27650.1	135	2	10
343	ß-tubulin	✓		43.00	5.73	18.52	4.81	gi|343455241|AEM36060.1	110	2	15
344	Caspase 3/7-2		✓	43.00	6.12	35.13	5.62	gi|325516445|ADZ24781.1	86	2	13
345	Uncharacterized protein C15orf26 homolog		✓	43.00	6.48	32.62	6.02	gi|762158091|XP_011417213.1	181	4	17
347	Proteasome subunit α type-1		✓	42.00	5.48	30.92	5.41	gi|762113890|XP_011439711.1	201	4	19
349	Sirtuin 5		✓	43.00	6.66	35.11	7.07	gi|919022062|XP_013394893.1	217	6	20
350	Short-chain collagen C4-like		✓	42.00	5.44	31.15	8.56	gi|1005494340|XP_015749803.1	221	5	16
351	Short-chain collagen C4-like		✓	42.00	5.31	31.15	8.56	gi|1005494340|XP_015749803.1	245	5	16
352	Pyruvate dehydrogenase E1 component subunit ß		✓	42.00	5.58	24.12	5.51	gi|762137139|XP_011451859.1	214	5	30
354	Malate dehydrogenase precursor		✓	42.00	6.78	36.25	8.44	gi|6746611|AAF27650.1	156	4	23
355	2,4-dienoyl-CoA reductase (mit)	✓	✓	42.00	6.11	36.44	8.65	gi|405945552|EKC17379.1	54	2	7
356	Sirtuin 5	✓	✓	42.00	6.85	35.11	7.07	gi|919022062|XP_013394893.1	324	7	20
357	Tubulin ß chain		✓	40.00	5.56	50.02	4.73	gi|291242757|XP_002741272.1	93	3	8
358	Radial spoke head protein 9 homolog	✓	✓	43.00	6.15	30.99	5.20	gi|762133006|XP_011449700.1	92	2	5
359	Electron transfer flavoprotein subunit α (mit)	✓	✓	42.00	6.20	35.29	7.60	gi|762141795|XP_011454094.1	237	5	37
360	Actin	✓		42.00	5.77	41.72	5.46	gi|5114428|AAD40314.1	142	4	15
361	Malate dehydrogenase precursor		✓	42.00	6.79	36.25	8.44	gi|6746611|AAF27650.1	100	2	10
365	Dyp-type peroxidase (yfex)	✓	✓	40.00	6.32	39.57	5.96	gi|405978693|EKC43063.1	115	2	4
368	Small heat shock protein 24.1	✓	✓	40.00	5.71	28.52	5.61	gi|347545633|AEP02968.1	188	2	10
369	Small heat shock protein 24.1	✓	✓	39.00	5.93	28.52	5.61	gi|347545633|AEP02968.1	118	2	10
370	Small heat shock protein 24.1	✓	✓	40.00	5.83	28.52	5.61	gi|347545633|AEP02968.1	113	2	10
371	Short-chain collagen C4-like		✓	41.00	5.25	31.15	8.56	gi|1005494340|XP_015749803.1	51	2	6
372	Short-chain collagen C4-like		✓	41.00	5.42	31.15	8.56	gi|1005494340|XP_015749803.1	76	4	16
373	Uncharacterized protein LOC105336555		✓	40.00	6.53	26.60	5.49	gi|762112946|XP_011439220.1	197	8	17
375	S-formylglutathione hydrolase		✓	39.00	6.57	31.16	6.18	gi|405971478|EKC36313.1	164	4	18
376	Small heat shock protein 24.1	✓	✓	39.00	5.78	28.52	5.61	gi|347545633|AEP02968.1	186	2	10
377	Small heat shock protein 24.1		✓	37.00	6.00	28.52	5.61	gi|347545633|AEP02968.1	184	2	10
378	ß-tubulin		✓	39.00	5.27	18.52	4.81	gi|343455241|AEM36060.1	141	3	22
380	Small heat shock protein 24.1		✓	37.00	6.06	28.52	5.61	gi|347545633|AEP02968.1	207	2	10
381	Δ(3,5)-Δ(2,4)-dienoyl-CoA isomerase (mit)	✓	✓	38.00	6.86	33.38	9.01	gi|762158768|XP_011417573.1	81	3	10
382	Proteasome subunit α type-4		✓	38.00	6.36	28.58	5.91	gi|762162422|XP_011419473.1	109	2	9
383	Small heat shock protein 24.1		✓	38.00	5.28	28.52	5.61	gi|347545633|AEP02968.1	105	2	6
384	Small heat shock protein 24.1		✓	37.00	5.48	28.52	5.61	gi|347545633|AEP02968.1	193	2	10
385	Small heat shock protein 24.1		✓	37.00	5.83	28.52	5.61	gi|347545633|AEP02968.1	189	2	10
387	Small heat shock protein 24.1	✓	✓	38.00	6.45	28.52	5.61	gi|347545633|AEP02968.1	77	2	8
388	Fibrinogen-related protein		✓	39.00	6.81	30.15	5.71	gi|312270835|ADQ55814.1	67	3	10
390	Small heat shock protein 24.1		✓	37.00	5.86	28.52	5.61	gi|347545633|AEP02968.1	174	2	10
391	Small heat shock protein 24.1	✓	✓	38.00	5.30	28.52	5.61	gi|347545633|AEP02968.1	152	3	13
392	Small heat shock protein 24.1	✓		37.00	5.42	28.52	5.61	gi|347545633|AEP02968.1	240	3	14
395	Small heat shock protein 24.1		✓	37.00	5.59	28.52	5.61	gi|347545633|AEP02968.1	189	2	10
396	Small heat shock protein 24.1		✓	37.00	5.55	28.52	5.61	gi|347545633|AEP02968.1	218	3	14
397	Small heat shock protein 24.1		✓	37.00	5.70	28.52	5.61	gi|347545633|AEP02968.1	159	2	10
398	Small heat shock protein 24.1	✓	✓	36.00	5.77	28.52	5.61	gi|347545633|AEP02968.1	173	2	10
399	Small heat shock protein 24.1		✓	37.00	6.30	28.52	5.61	gi|347545633|AEP02968.1	199	3	14
400	Small heat shock protein 24.1		✓	37.00	6.67	28.52	5.61	gi|347545633|AEP02968.1	84	2	8
401	Apextrin-like protein 1	✓	✓	34.00	6.78	24.46	4.91	gi|891167089|AKQ70860.1	197	4	14
402	Small heat shock protein 24.1	✓	✓	37.00	5.91	28.52	5.61	gi|347545633|AEP02968.1	214	2	10
403	Small heat shock protein 24.1		✓	37.00	6.15	28.52	5.61	gi|347545633|AEP02968.1	114	2	10
405	Small heat shock protein 24.1	✓	✓	37.00	6.60	28.52	5.61	gi|347545633|AEP02968.1	102	2	10
407	Small heat shock protein 24.1		✓	36.00	5.33	28.52	5.61	gi|347545633|AEP02968.1	125	3	13
408	F-actin-capping protein subunit ß		✓	36.00	5.20	30.62	5.21	gi|926632224|XP_013781869.1	63	2	2
410	Uncharacterized protein LOC101857969	✓	✓	35.00	6.64	29.37	5.73	gi|524896868|XP_005104905.1	97	4	17
412	Peptidylprolyl cis-trans isomerase		✓	33.00	6.93	23.73	5.97	gi|762122623|XP_011444269.1	316	6	14
413	Proteasome subunit α type-5		✓	34.00	4.95	26.48	5.02	gi|762129467|XP_011447862.1	345	9	30
414	Apextrin-like protein		✓	36.00	5.85	24.39	8.42	gi|339785142|AEK10750.1	228	4	12
415	Proteasome subunit α type-6	✓		36.00	6.42	25.14	7.58	gi|762162644|XP_011419593.1	73	2	9
416	Proteasome subunit ß type-3		✓	35.00	5.37	23.11	5.01	gi|762091658|XP_011428234.1	220	6	25
418	Persulfide dioxygenase ETHE1 (mitochondrial)	✓	✓	34.00	6.19	35.04	9.13	gi|762094352|XP_011429655.1	202	7	17
419	Prohibitin-like		✓	34.00	5.62	29.80	5.62	gi|524879616|XP_005096482.1	353	7	27
420	Fibrinogen-related protein 2		✓	34.00	6.52	27.28	5.81	gi|319803013|DAA34037.1	102	3	8
422	Sperm-associated antigen 8-like	✓	✓	34.00	5.60	23.62	6.01	gi|762089292|XP_011426991.1	211	6	22
423	Apextrin-like protein 1	✓	✓	33.00	6.51	24.46	4.91	gi|891167089|AKQ70860.1	170	5	19
425	Small heat shock protein 24.1		✓	34.00	6.01	28.52	5.61	gi|347545633|AEP02968.1	130	2	10
426	Actin		✓	34.00	5.78	41.72	5.46	gi|5114428|AAD40314.1	73	2	6
427	L-xylulose reductase		✓	32.00	6.07	26.42	6.94	gi|919053033|XP_013408422.1	552	8	35
428	6-phosphoglucolactonase		✓	33.00	5.90	26.67	5.47	gi|762156115|XP_011416178.1	237	5	16
429	D-erythrulose reductase	✓	✓	33.00	6.63	25.94	7.67	gi|762144035|XP_011455281.1	73	2	8
430	Dopamine N-acetyltransferase		✓	33.00	6.33	24.69	5.85	gi|557761514|XP_005180475.1	151	5	20
431	Osteoclast-stimulating factor 1		✓	32.00	6.21	23.72	5.36	gi|919043872|XP_013405121.1	113	3	12
432	15-hydroxyprostaglandin dehydrogenase [NAD(+)]-like		✓	32.00	5.07	27.59	5.98	gi|762075986|XP_011445184.1	114	3	9
434	L-xylulose reductase		✓	32.00	5.86	26.42	6.94	gi|919053033|XP_013408422.1	294	4	20
435	Ubiquitin carboxyl-terminal hydrolase		✓	31.00	5.00	24.90	4.77	gi|762115659|XP_011440640.1	109	2	3
436	15-hydroxyprostaglandin dehydrogenase [NAD(+)]-like		✓	31.00	4.96	27.59	5.98	gi|762075986|XP_011445184.1	113	2	9
437	ATP synthase subunit d		✓	31.00	5.24	20.35	7.68	gi|524893715|XP_005103366.1	64	4	19
438	Hypoxanthine-guanine phosphoribosyltransferase		✓	32.00	6.02	25.32	5.37	gi|762136802|XP_011451683.1	79	3	8
439	DNA helicase		✓	31.00	4.90	219.91	4.78	gi|1011706141|WP_062551283.1	100	3	7
441	Peptidylprolyl cis-trans isomerase		✓	31.00	6.92	23.73	5.97	gi|762122623|XP_011444269.1	265	5	14
443	Apextrin-like protein 1	✓	✓	32.00	6.78	24.46	4.91	gi|891167089|AKQ70860.1	190	4	14
444	Calcium-dependent protein kinase isoform 2		✓	31.00	5.29	27.29	5.11	gi|405974628|EKC39257.1	102	3	13
445	Thiopurine S-methyltransferase		✓	30.00	5.73	38.67	8.37	gi|919008108|XP_013388872.1	134	3	13
446	Proteasome subunit α type-2	✓	✓	31.00	6.14	26.29	5.52	gi|762153684|XP_011414884.1	162	4	17
448	DNA helicase	✓	✓	31.00	5.40	219.91	4.78	gi|1011706141|WP_062551283.1	100	4	13
450	Nucleoside diphosphate kinase homolog 5	✓		31.00	6.21	24.10	6.22	gi|762132773|XP_011449580.1	113	3	15
451	Apextrin-like protein 1		✓	30.00	6.81	24.46	4.91	gi|891167089|AKQ70860.1	183	4	14
453	Ras GTP-binding protein RHO	✓	✓	29.00	6.24	21.69	5.64	gi|961068385|XP_014768529.1	162	5	12
454	Complement C1q tumor necrosis factor-related protein 1		✓	30.00	5.02	26.89	5.81	gi|584006153|XP_006798063.1	247	7	29
455	TSP-1 domain containing protein-1		✓	29.00	6.48	73.15	8.89	gi|919283007|ALA16017.1	153	3	10
456	Membrane-associated progesterone receptor component 1-like		✓	29.00	4.89	21.59	4.90	gi|762126808|XP_011446467.1	289	4	12
458	Thioredoxin peroxidase		✓	29.00	6.81	21.86	5.95	gi|306451460|ADM88874.1	442	9	21
459	Peptidylprolyl cis-trans isomerase	✓	✓	29.00	6.93	23.73	5.97	gi|762122623|XP_011444269.1	208	3	9

460	DNA helicase	✓		29.00	5.15	219.91	4.78	gi|1011706141|WP_062551283.1	216	6	21
461	Rho GDP-dissociation inhibitor 1	✓	✓	29.00	5.26	23.10	5.24	gi|762093558|XP_011429238.1	329	8	34
462	TSP-1 domain containing protein-1	✓	✓	29.00	5.97	73.15	8.89	gi|919283007|ALA16017.1	220	5	18
471	Rho GDP-dissociation inhibitor 1	✓		27.00	5.28	23.10	5.24	gi|762093558|XP_011429238.1	158	4	13
473	TSP-1 domain containing protein-1		✓	27.00	5.97	73.15	8.89	gi|919283007|ALA16017.1	234	5	24
474	Adenine phosphoribosyltransferase		✓	27.00	5.85	19.52	6.74	gi|762146952|XP_011456774.1	209	5	19
475	Nucleoside diphosphate kinase homolog 5		✓	27.00	5.90	24.10	6.22	gi|762132773|XP_011449580.1	153	3	15
476	Membrane-associated progesterone receptor component 1-like	✓	✓	27.00	4.96	21.59	4.90	gi|762126808|XP_011446467.1	231	4	12
478	Ras-related protein Rab-2	✓	✓	26.00	6.61	23.33	6.21	gi|762087002|XP_011425783.1	388	6	5
479	Peptidylprolyl isomerase A	✓	✓	26.00	6.26	22.05	5.77	gi|67294097|AIK22453.1	181	4	22
480	Proteasome subunit α type-6		✓	26.00	6.31	23.63	6.48	gi|973425559|ALX27214.1	72	3	14
483	Adenine phosphoribosyltransferase	✓	✓	26.00	5.85	19.52	6.74	gi|762146952|XP_011456774.1	120	2	8
485	Mn superoxide dismutase		✓	26.00	6.03	25.30	6.44	gi|402122769|AFQ32466.1	97	1	6
486	Mammalian ependymin-related protein 1-like	✓	✓	25.00	5.30	24.07	8.49	gi|919034350|XP_013400786.1	86	4	16
488	ADP-ribosylation factor 2		✓	25.00	6.24	15.03	6.60	gi|821400624|XP_012390507.1	88	3	10
490	Ras-related protein Rab-7a	✓	✓	24.00	5.96	23.05	5.39	gi|762070124|XP_011433497.1	295	5	21
494	TCTP	✓	✓	22.00	4.89	19.58	4.76	gi|359359687|AEV41412.1	200	5	30
500	Tubulin ß chain	✓	✓	20.00	4.82	50.02	4.73	gi|291242757|XP_002741272.1	99	4	14
501	UPF0587 protein v1g245604-like	✓	✓	19.00	6.16	17.99	5.30	gi|919043641|XP_013405038.1	115	3	6
502	Ferritin		✓	20.00	5.00	18.96	5.12	gi|343455265|AEM36072.1	44	2	14
503	Cofilin		✓	18.00	5.87	16.11	5.81	gi|291230460|XP_002735215.1	213	4	23
504	Cu-Zn superoxide dismutase	✓		18.00	6.01	15.87	5.84	gi|34481600|CAE46443.1	222	3	25
505	Cu-Zn superoxide dismutase	✓	✓	16.00	6.31	15.87	5.84	gi|34481600|CAE46443.1	318	3	25
506	ATP synthase δ chain	✓	✓	17.00	4.68	17.71	5.02	gi|126697378|ABO26646.1	193	3	21
508	Eukaryotic translation initiation factor 5A	✓	✓	17.00	5.67	17.10	5.30	gi|45594242|AAS68511.1	304	7	31
509	UPF0587 protein v1g245604-like	✓	✓	17.00	6.20	17.99	5.30	gi|919043641|XP_013405038.1	93	2	6
512	ATP synthase δ chain	✓	✓	16.00	4.65	17.71	5.02	gi|126697378|ABO26646.1	216	3	21
513	Serine/threonine-protein kinase kinX	✓	✓	16.00	4.82	49.11	4.34	gi|762151154|XP_011413554.1	198	3	10
514	Cytochrome b5	✓	✓	15.00	4.88	14.59	5.03	gi|765826424|NP_001292227.1	210	4	22
516	Fatty acid-binding protein homolog 6		✓	15.00	6.04	16.47	6.61	gi|762088820|XP_011426736.1	62	3	11
517	ß-tubulin		✓	14.00	4.94	18.52	4.81	gi|343455241|AEM36060.1	205	4	31
518	Fatty acid-binding protein homolog 5	✓	✓	15.00	5.97	21.17	7.76	gi|762076953|XP_011448183.1	50	2	10
519	ATP synthase δ chain	✓	✓	14.00	4.63	17.71	5.02	gi|126697378|ABO26646.1	223	3	21
522	40S ribosomal protein S12	✓	✓	12.00	5.92	14.90	5.79	gi|762145937|XP_011456257.1	190	3	25
525	Fatty acid-binding protein		✓	10.00	4.86	14.92	4.98	gi|762102277|XP_011433631.1	167	3	11
526	Dynein light chain roadblock-type 2	✓	✓	9.00	5.92	10.83	6.83	gi|591368966|XP_007059318.1	142	2	7
532	Heterogeneous nuclear ribonucleoprotein 27C	✓	✓	4.00	6.21	17.90	8.85	gi|751210710|XP_011158062.1	101	2	8
534	Major vault protein	✓	✓	89.00	5.96	96.25	5.58	gi|762100595|XP_011432755.1	162	3	3
535	Proteasome subunit ß type-4	✓	✓	28.00	5.58	28.64	5.80	gi|762158481|XP_011417423.1	201	5	33
536	Fibulin-2	✓	✓	95.00	5.66	71.18	5.28	gi|762094528|XP_011429747.1	149	2	11
537	Fibulin-2	✓	✓	95.00	5.70	71.18	5.28	gi|762094528|XP_011429747.1	109	2	11
538	Major vault protein	✓	✓	89.00	5.90	31.74	5.45	gi|5714749|AAD48063.1	130	4	17
539	Succinate dehydrogenase [ubiquinone] flavoprotein subunit (mitochondrial)		✓	77.00	5.95	73.04	6.04	gi|524896638|XP_005104791.1	174	4	4
540	USF-1-like		✓	30.00	5.47	24.68	5.27	gi|1005440749|XP_015757714.1	75	2	6
541	α-Tubulin		✓	26.00	5.42	10.81	4.80	gi|343455253|AEM36066.1	88	2	27
544	Calcyphosin		✓	22.00	5.35	21.37	5.07	gi|1020502561|XP_016090119.1	231	5	21
546	PIF	✓	✓	91.00	5.32	68.02	5.23	gi|762115345|XP_011440479.1	153	3	10
547	PIF	✓	✓	90.00	5.39	68.02	5.23	gi|762115345|XP_011440479.1	143	3	10
548	PIF-like		✓	89.00	5.49	68.02	5.23	gi|762115345|XP_011440479.1	133	3	10
549	Actin	✓	✓	89.00	5.57	41.72	5.46	gi|5114428|AAD40314.1	238	5	16
550	ß-actin	✓	✓	36.00	5.12	41.86	5.30	gi|341579620|AEK81538.1	84	3	6
551	Thiopurine S-methyltransferase		✓	29.00	5.60	38.67	8.37	gi|919008108|XP_013388872.1	161	4	17
552	Serine/arginine-rich splicing factor 2	✓	✓	30.00	5.58	21.70	11.51	gi|762149771|XP_011412825.1	74	2	5
553	PIF	✓	✓	90.00	5.68	68.02	5.23	gi|762115345|XP_011440479.1	174	3	11
554	PIF	✓	✓	89.00	5.65	68.02	5.23	gi|762115345|XP_011440479.1	107	3	10
557	Dynein light chain Tctex-type 1	✓	✓	11.00	4.98	12.48	4.97	gi|291221383|XP_002730697.1	93	3	18
559	Membrane-associated progesterone receptor component 1-like	✓	✓	28.00	4.82	21.59	4.90	gi|762126808|XP_011446467.1	73	2	7
560	Membrane-associated progesterone receptor component 1-like	✓	✓	26.00	4.89	21.59	4.90	gi|762126808|XP_011446467.1	201	4	12
564	C1q-domain-containing protein	✓	✓	15.00	6.41	18.74	8.39	gi|301598996|CBH31055.1	213	3	14
565	Nucleoredoxin	✓	✓	11.00	6.39	46.29	5.27	gi|919039793|XP_013403357.1	117	2	12
569	Coactosin		✓	18.00	5.49	16.03	5.00	gi|919026004|XP_013396773.1	195	3	10
570	Coactosin	✓	✓	17.00	5.49	16.03	5.00	gi|919026004|XP_013396773.1	148	3	10
571	UPF0587 protein v1g245604-like		✓	20.00	5.58	17.99	5.30	gi|919043641|XP_013405038.1	133	3	10
572	Methionine-R-sulfoxide reductase B2 (mitochondrial)	✓	✓	18.00	5.63	22.37	7.56	gi|762165226|XP_011420932.1	89	3	9
574	Filamin-A		✓	88.00	6.88	90.30	6.24	gi|762071775|XP_011426847.1	111	2	5
576	Ras-like protein 3 isoform X2		✓	24.00	6.57	21.69	7.59	gi|762144541|XP_011455539.1	62	2	7
577	Actin-related protein 3	✓		58.00	6.13	47.04	5.51	gi|524867514|XP_005090568.1	283	4	5
578	Major vault protein		✓	89.00	6.04	31.74	5.45	gi|5714749|AAD48063.1	143	5	22
579	Heat shock protein 70		✓	77.00	6.06	69.47	5.35	gi|76780606|CAH04106.1	46	2	10
580	Heat shock protein 70	✓	✓	77.00	6.10	69.51	5.34	gi|62989584|CAE51348.1	181	3	8
582	Collagen-like protein-2	✓	✓	66.00	6.13	50.10	7.10	gi|906541694|AKS48142.1	233	4	22
583	Dihydrolipoyl dehydrogenase (mitochondrial)	✓	✓	64.00	6.23	54.42	7.15	gi|524878388|XP_005095881.1	68	2	4
584	Amidase	✓	✓	63.00	6.21	59.08	5.93	gi|676439850|XP_009048985.1	102	3	9
585	Enolase		✓	61.00	6.17	47.20	5.71	gi|762107263|XP_011436228.1	93	5	3
586	Cell division cycle 42	✓	✓	24.00	6.77	19.16	5.45	gi|220979902|CAQ64775.1	58	2	12
587	Intraflagellar transport protein 27 homolog	✓	✓	26.00	6.77	21.12	5.56	gi|762158581|XP_011417472.1	96	2	10
588	GTP-binding protein SAR1-like		✓	25.00	6.70	21.72	6.30	gi|762125362|XP_011445703.1	359	7	21
589	Peroxiredoxin-5 (mitochondrial)		✓	20.00	6.65	19.69	8.19	gi|762144430|XP_011455482.1	65	2	13
590	T-complex protein 1 subunit ß		✓	70.00	6.03	57.45	6.03	gi|405972882|EKC37629.1	108	2	8
591	Translocon-associated protein subunit ß	✓	✓	30.00	5.65	20.80	6.75	gi|762087237|XP_011425903.1	177	3	15
592	78 kDa glucose-regulated protein		✓	78.00	5.15	73.14	4.88	gi|908455572|XP_013083694.1	199	5	26
593	ß-tubulin	✓	✓	61.00	5.13	18.52	4.81	gi|343455241|AEM36060.1	130	2	15
594	KEYSTONEin		✓	47.00	5.10	27.96	5.33	gi|426207677|AFY13478.1	144	3	10
597	Actin	✓	✓	27.00	4.49	41.72	5.46	gi|5114428|AAD40314.1	164	5	17
600	NADP Isocitrate dehydrogenase		✓	31.00	4.81	50.46	6.77	gi|385268539|AFI56364.1	152	6	14
601	Actin		✓	39.00	5.00	41.72	5.46	gi|5114428|AAD40314.1	85	4	14
602	PIF	✓	✓	91.00	5.27	68.02	5.23	gi|762115345|XP_011440479.1	93	3	10
603	14-3-3 protein 2		✓	38.00	5.07	28.81	4.87	gi|762115034|XP_011440318.1	85	3	6
604	Malectin-B			41.00	5.16	31.45	5.28	gi|762168159|XP_011422439.1	192	3	23
606	Membrane-associated progesterone receptor component 1-like			29.00	4.82	21.59	4.90	gi|762126808|XP_011446467.1	219	4	12